DECOMPOSING REPRESENTATION SPACE INTO INTERPRETABLE SUBSPACES WITH UNSUPERVISED LEARNING

Anonymous authors
Paper under double-blind review

ABSTRACT

Understanding internal representations of neural models is a core interest of mechanistic interpretability. Due to its large dimensionality, the representation space can encode various aspects about inputs. To what extent are different aspects organized and encoded in separate subspaces? Is it possible to find these "natural" subspaces in a purely unsupervised way? Somewhat surprisingly, we can indeed achieve this and find interpretable subspaces by a seemingly unrelated training objective. Our method, neighbor distance minimization (NDM), learns non-basis-aligned subspaces in an unsupervised manner. Qualitative analysis shows subspaces are interpretable in many cases, and encoded information in obtained subspaces tends to share the same abstract concept across different inputs, making such subspaces similar to "variables" used by the model. We also conduct quantitative experiments using known circuits in GPT-2; results show a strong connection between subspaces and circuit variables. We also provide evidence showing scalability to 2B models by finding separate subspaces mediating context and parametric knowledge routing.[1] Viewed more broadly, our findings offer a new perspective on understanding model internals and building circuits.

1 INTRODUCTION

Mechanistic Interpretability research aims to understand the internal mechanisms of neural networks. Unlike behavioral research, the community seeks deeper algorithmic descriptions or circuits of models. Insights from this kind of research can serve our purpose of building safer, more controllable, and more reliable AI systems (Bereska & Gavves, 2024), and making progress in other scientific fields by learning how data is modeled by these models (e.g. Futrell & Mahowald, 2025; Oota et al., 2023; Celeghin et al., 2023).

Researchers have made significant progress in this direction in recent years, uncovering circuits consisting of various types of basic units (or mediators (Mueller et al., 2024)), including components (attention heads and MLPs) of transformers (Wang et al., 2022; Hanna et al., 2023), sparse features obtained from Sparse Auto-Encoders (SAEs) or its variants (Cunningham et al., 2023; Bricken et al., 2023; Dunefsky et al., 2024; Ameisen et al., 2025), and subspaces (Geiger et al., 2024; Wu et al., 2023; Geiger et al., 2025). While providing valuable insights, they are limited in different ways. The information transferred between components is hard to understand, and researchers need to design specialized counterfactual data targeting certain aspect of the input to perform causal intervention, or use easy but much less reliable methods such as observing attention weights or projecting to vocabulary space. Sparse features provide a direct way to interpret (by reading from the inputs they activate on), but resulting circuits are input-dependent, in other words, specific for each input sequence, as different features are activated in different inputs. This approach also usually modifies the model's computation, replacing activations or MLPs with reconstruction from sparsity-encouraged new modules, in order to better analyze feature-to-feature interactions. Lastly, current subspace-based approaches require supervision from an abstract causal model specified by human. The abstract model represents a clear hypothesis of how the real model works, thus requiring anticipating possible mechanisms. We refer to Mueller et al. (2024) for a good summary of different mediators.

[1]Anonymous link for code and trained matrices `https://anonymous.4open.science/r/F48B/`

In this paper, we explore a new direction: unsupervised representation space decomposition. We show we can learn a partitioning of representation space by doing neighbor distance minimization (NDM) among subspace activations. We explain the intuition behind this training objective in terms of feature groups and mutual information and show that it looks for a partition such that subspaces are as independent as possible. Similar to Geiger et al. (2024), an orthogonal matrix is learned, which rotates and reflects the space before partitioning on the transformed basis. It captures the distributed nature of neural representations. While they aim to find the subspace for certain target variables by supervised learning, our method is unsupervised and makes use of "natural" structure inside the model. We first demonstrate the effectiveness of NDM in a toy setting, then move on to real language models. Somewhat surprisingly, we find that there is indeed meaningful inner structure of representation space in real-world models. We show that resulting subspaces are usually interpretable with InversionView (Huang et al., 2024b). We quantitatively test alignment between subspaces and variables in known circuits in GPT-2 Small using causal intervention. Moreover, we demonstrate its applicability on larger 2B models by showing that NDM finds separate subspaces mediating context knowledge and parametric knowledge.

Our method also points out a potential future direction: subspace circuits. Subspaces given by our method are suitable as new basic units for circuit analysis, as we can directly analyze model weights to understand, for example, which subspaces a certain attention head reads from and writes to. By building connections between subspaces across layers with model weights, we could construct *input-independent* circuits, as the space decomposition and model weights are input-independent. In these circuits, subspaces are like variables, each of which encapsulates a group of features it can take as values. Therefore, we believe our method and the possibilities it enables will benefit the interpretability community.

2 Motivation and Background

One of the key concepts in interpretability literature is superposition, which means a model can represent more features than its dimensionality by representing them as non-orthogonal directions. The phenomenon is well-illustrated in (Elhage et al., 2022), where they use a toy model as follows:

$$\boldsymbol{h} = \mathbf{W}\boldsymbol{x} \qquad\qquad \boldsymbol{x}' = \mathrm{ReLU}(\mathbf{W}^T\boldsymbol{h} + \boldsymbol{b}) \tag{1}$$

where $\boldsymbol{x}, \boldsymbol{x}' \in \mathbb{R}^z$, $\boldsymbol{h} \in \mathbb{R}^d$, $\mathbf{W} \in \mathbb{R}^{d\times z}$, $d < z$. The high-dimensional $\boldsymbol{x}$ is the ground truth feature vector, each entry x_i represents a "feature" and its value ranges in [0, 1], it is encoded in low-dimensional $\boldsymbol{h}$. The model output $\boldsymbol{x}'$ is trained to reconstruct $\boldsymbol{x}$. So each column in $\mathbf{W}$ corresponds to a direction in the lower-dimensional space that represents a feature x_i.

In this toy setting, (Elhage et al., 2022) found that **sparsity** is necessary to allow superposition to occur. In this paper, we argue that **mutual exclusiveness** could be a more fundamental condition. More specifically, for a group of features, if only one (or none) occurs at a time, they are said to be mutually exclusive, and can be represented with superposition without much loss of information. Although sparsity encourages mutual exclusiveness, they are different, since the former concept treats features uniformly while the latter emphasizes a non-uniform view under which some sets of features can be more dependent on each other.

If mutual exclusiveness holds, superposition works well; the only discrepancy between $\boldsymbol{x}$ and $\boldsymbol{x}'$ is because of small interference between almost orthogonal features. On the contrary, if multiple features are activated, they might cancel each other in certain directions, causing loss of information, so that reconstructed $\boldsymbol{x}'$ can be totally different from x (Fig. 5a and 5b in App.). In other words, *given two or more specific features*, if they often co-occur, superposing *these features* would not work well – incentivizing the model to represent them more orthogonally. On the other hand, if they are mutually exclusive (because the concepts they represent are mutually exclusive in the real world), the model would tend to make use of this fact and superpose their features.

Feature Groups and Subspaces It would be more interesting if we consider groups of mutually exclusive features. Features are mutually exclusive with features in the same group but independent of features in different groups. So each model activation $\boldsymbol{h}$ can result from multiple activating features, but each of them comes from a different group. As we discussed earlier, features in the same group tend to be superposed, while co-occurrence would encourage features from different groups to be more orthogonal. Therefore, in such an ideal case, each feature group can form a dedicated subspace, superposition happens inside the subspace, but subspaces are orthogonal to one another.

One might ask whether the mutual exclusiveness property is likely to happen in the real world. We think it is actually pervasive. For example, if the previous token is “the”, it cannot be any other tokens in the vocabulary; if the subject of a sentence is “Alice", it cannot be “Bob"; if the sum of two digits is 5, it cannot be simultaneously other numbers. In model’s processing, like an algorithm, it might have “variables” (like those searched by DAS (Geiger et al., 2024)) to encode certain aspects of information, and each variable can take only one value at a time, and each corresponds to a feature group, or a subspace. So we think such a mutual-exclusiveness property and group structure can be very common in the model, and there are “natural” partitions of orthogonal and interpretable subspaces. In the following section we show evidence in toy setting, and in Sec. 5, we show evidence in real neural language models. In addition, we find our notion of feature groups quite relevant to Multi-Dimensional Superposition Hypothesis (Engels et al., 2024), each feature group can be thought of as one multi-dimensional irreducible feature in this hypothesis, because of intra-group dependence and inter-group independence.

Toy Model of Intra-group Superposition In the toy setting (Elhage et al., 2022) where we have access to real features, we can straightforwardly verify superposition and orthogonality. We use the aforementioned toy model (Eq. 1). As a start, we set $z = 40$, $d = 12$, and features are split into two groups, 20 for each. When sampling $\boldsymbol{x}$, for each group, 0.25 of the time no feature is activated, 0.75 of the time one feature is randomly chosen and its value is sampled uniformly from [0, 1]. Features are equally important (not weighted when computing reconstruction loss).

After training, fraction of variance unexplained (FVU) is 0.059, and $\mathbf{W}^T\mathbf{W}$ is shown in Fig. 1a. We see that products of features coming from the same group are non-zero, while features in different groups are always orthogonal to each other. There are two orthogonal subspaces containing the two feature groups, respectively. Closer inspection of singular values shows that each feature group is encoded in 5-dimensional space. In App. C.1 we show different configurations of feature groups and the resulting $\mathbf{W}^T\mathbf{W}$. In sum, we can expect similar orthogonal subspaces when features follow the aforementioned group structure.

3 METHODOLOGY

If orthogonal structure exists, i.e., orthogonal partition of representation space such that each subspace contains one feature group, how can we find these subspaces? In toy setting, we can take all feature vectors from the same group, and then the subspace spanned by these is what we are looking for. But we aim to create a method that works for real-world models, i.e., without access to ground truth features $\boldsymbol{x}$ or projection $\mathbf{W}$. We need a method that only requires model activations $\boldsymbol{h}$. In this section, we describe our method, NDM, which finds the correct subspace given *only* model activations.

Intuition The intuition behind our method is illustrated in Fig. 1b. In a 3D space, assuming xy plane contains a group of 3 features (blue arrows), and z dimension contains another group of 2 features (orange arrows), so there are 2 subspaces orthogonal to each other and each contains a feature group. If intra-group mutual exclusiveness holds, data points will only lie in the pink planes, as each point is a sum of only one blue and one orange. Given the feature groups, the correct partition is thus (xy, z). If the 3D space is partitioned in this way, the data points’ projection on the xy subspace only lies on blue arrows, and similarly for the z subspace. Thus, given some data points, inside each subspace (consider their projection) points are concentrated on a few lines, and it is easy for each point to find another point in a close distance. However, if it is partitioned into xz and y, then the data points, after being projected to xz plane, cover the entire plane, causing larger distance between each point and their neighbor. In other words, the correct partition will make the distance to the nearest neighbor inside subspaces smaller, whereas incorrect partitions entail large distances because they arbitrarily combine features from different groups.

Optimization We define a *partition* as a tuple consisting of an orthogonal matrix $\mathbf{R}$ and a dimension configuration c (number of subspaces and their dimensionality). $\mathbf{R}$ rotates and reflects the space as

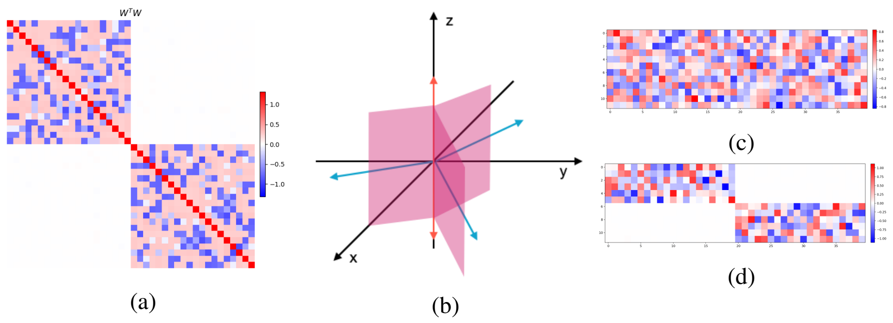

Figure 1: **(a)**: $\mathbf{W}^T\mathbf{W}$, $\mathbf{W} \in \mathbb{R}^{12\times 40}$ (Sec. 2). Each column of $\mathbf{W}$ is a feature direction, its first 20 columns belong to one feature group, the last 20 to the other. We can see the bottom left and top right parts are zero, which means feature vectors of different groups are orthogonal. **(b)**: Illustration for the intuition of our method (Sec. 3), correct partition can make data points easier to model. **(c) (d)**: **RW** before and after NDM training (Sec. 4). The final dimension configuration is $d_1 = 6, d_2 = 6$. The corresponding toy model is shown in (a). After training, the first subspace (first 6 coordinates) only depends on the first feature group (first 20 coordinates), and likewise for the other subspace.

needed (similar to (Geiger et al., 2024)), then the transformed space is partitioned on its standard basis (simply grouping coordinates) according to c. We optimize $\mathbf{R}$ as follows: given N model activations $[\boldsymbol{h_1} \cdots \boldsymbol{h_N}]$ where $\boldsymbol{h_n} \in \mathbb{R}^d$, and an orthogonal matrix to be trained $\mathbf{R} \in \mathbb{R}^{d\times d}$[2], dimension configuration $c = [d_1, \cdots, d_S]$, where S is the number of subspaces, $\sum_{s=0}^{S} d_s = d$, we do

$$[\hat{\boldsymbol{h}}_{\boldsymbol{1}} \cdots \hat{\boldsymbol{h}}_{\boldsymbol{n}}] = \mathbf{R}[\boldsymbol{h_1} \cdots \boldsymbol{h_n}], \qquad \hat{\boldsymbol{h}}_n = \begin{bmatrix} \hat{\boldsymbol{h}}_n^{(1)} \\ \vdots \\ \hat{\boldsymbol{h}}_n^{(S)} \end{bmatrix}, \quad \hat{\boldsymbol{h}}_n^{(s)} \in \mathbb{R}^{d_s} \tag{2}$$

$$n^* = \underset{\substack{m=1,\dots,N \\ m\neq n}}{\arg\min}\ \operatorname{dist}\left(\hat{\boldsymbol{h}}_n^{(s)}, \hat{\boldsymbol{h}}_m^{(s)}\right) \tag{3}$$

$$\min_{\mathbf{R}} \frac{1}{N} \sum_{s=1}^{S} \sum_{n=1}^{N} \operatorname{dist}\left(\hat{\boldsymbol{h}}_n^{(s)}, \hat{\boldsymbol{h}}_{n^*}^{(s)}\right) \qquad \text{s.t. } \mathbf{R}^\top\mathbf{R} = \mathbf{I} \tag{4}$$

where the function $\operatorname{dist}(\cdot)$ is the distance metric we can do experiment with. So we optimize the orthogonal matrix to minimize the distance with the nearest neighbor in subspaces.

Besides the aforementioned perspective in terms of feature superposition, there is also a heuristic interpretation of our method as **minimizing total correlation** between subspaces, which generalizes mutual information (MI)'s definition from two variables to multiple variables and measures the redundancy and dependence among them. Loosely speaking, neighbor distance reflects the entropy; our method reduces entropy in subspaces. Entropy of the whole space is invariant under orthogonal transformation; thus, total correlation is reduced (details in App. B.1). In other words, we look for a partition of representation space such that the resulting subspaces are as independent as possible, thus they are suitable to serve as the elementary units of interpretation. This MI/total correlation perspective justifies our method even when the previous feature group hypothesis does not strongly or strictly hold in real neural models.

Determining the Subspace Dimension Configuration However, there is still a question: how to find the correct dimension configuration (number of subspaces and their dimensions)? It is not differentiable and is unclear what is the appropriate objective to optimize for. In our method, we use MI to address this problem. The procedure is as follows: we start with a configuration of small

[2]Libraries like Pytorch (Paszke et al., 2019) contain parametrization to ensure orthogonality of matrix

and equal-sized subspaces and train the orthogonal matrix. We measure the MI between subspaces regularly during training using KSG estimator (Kraskov et al., 2004). If the MI[3] is higher than a threshold, we merge the two subspaces, so the nearest neighbor should be found in the joint subspace afterwards and keep training the orthogonal matrix. We stop training when we cannot find a pair of subspaces whose MI is above the threshold. This procedure is in line with our goal of reducing the dependency between subspaces, as we merge them if their MI is unavoidably high. We describe our method in detail in Algorithm 1 and App. B. We also experimented with other methods for determining the configuration, see App. G.4. In sum, NDM finds a partition containing both $\mathbf{R}$ and c.

4 EXPERIMENTS IN TOY MODELS

We first test our method in the toy model setting described in Sec.2, using a slightly different and less scalable version of Algorithm 1 (see details in App. C.2). We use Euclidean distance as the $\text{dist}(\cdot)$ in Eq. 3 and 4, because we find cosine similarity to perform worse in preliminary experiments. The toy model setting is an ideal testbed as we have access to the ground truth feature vectors and subspaces. As described, we rotate and reflect the hidden activations $\boldsymbol{h}$ from Eq.1, which results in $\hat{\boldsymbol{h}} = \mathbf{RW}\boldsymbol{x}$. Subspace activations, which are defined to be a continuous span of coordinates of $\hat{\boldsymbol{h}}$, should ideally result from only one feature group. Therefore, a good $\mathbf{R}$ means rows in $\mathbf{RW}$ corresponding to one subspace (subvectors of $\hat{\boldsymbol{h}}$) have nonzero values only at columns corresponding to one feature group (subvectors of $\boldsymbol{x}$). So, the important question is, can we find subspaces encoding each feature group by minimizing distances? Despite our argument before, this still sounds uncertain a priori, as we do not optimize $\mathbf{R}$ to associate subspaces with underlying groups but rather optimize the *indirect* objective of neighbor distance, as we want to avoid using $\mathbf{W}$ and $\boldsymbol{x}$. Somewhat beyond our expectation, the answer is yes, we find good subspaces by using NDM.

The result is shown in Fig. 1d. We initialize $\mathbf{R}$ as an identity matrix, and the $\mathbf{RW}$ after training is almost perfect. We present more experiments in Fig. 9-12 in App. C.2, where numbers of features and groups vary. The results overall show a strong performance of NDM, we are able to find the subspace partition close to the ground truth in all cases. In sum, in the toy setting where there exist orthogonal subspaces dedicated to each group, we indeed can find these subspaces by NDM.

5 EXPERIMENTS IN LANGUAGE MODELS

The key question is NDM's applicability to real-world neural models. Unlike the toy setting, we do not know ground-truth features, so we design new ways to do evaluation. In this section, we denote residual stream activations as $\boldsymbol{h}^{l,\{mid,post\}}$, where l is the layer index (starting from 0), mid means after adding the attention sublayer's output, and $post$ means after adding the MLP sublayer's output.

5.1 QUANTITATIVE EVALUATION BASED ON GPT-2 CIRCUITS

The evaluation is based on subspace activation patching, or subspace interchange intervention (Geiger et al., 2024). The main intuition is that, when processing inputs, key intermediate results should ideally lie in a single subspace. For example, in an induction head circuit where the residual stream contains the previous token, the previous token should be placed in a single subspace, independent of which token it is from. Therefore, if we patch subspace activations with the value they take in sequences with different previous tokens, the effect should be concentrated on that correct subspace. We refer to the previous token as the target information, which is changed in the counterfactual input. Different target information should ideally be concentrated in different subspaces. We describe subspace patching in detail in App. D.1 and address potential concerns from (Makelov et al., 2023) in App. G.2. In sum, we aim to explore whether the high-level "variable" lies in the same subspace no matter what value it takes by measuring inequality or concentration of subspace patching effect.

Test Suite and Metric We construct a test suite, making use of known circuits in GPT2 Small. It consists of 5 tests. The first 4 tests are based on the IOI circuit (Wang et al., 2022), where we intervene on the following pieces of information respectively: (1) previous token information contained in

[3]In practice, we divide the mutual information value by the sum of the two subspaces' dimensions.

Method	test 1			test 2			test 3			test 4			test 5			**Avg**
	-	d_s	Var$_s$	-	d_s	Var$_s$	-	d_s	Var$_s$	-	d_s	Var$_s$	-	d_s	Var$_s$	
Identity	0.33	0.05	0.23	0.32	0.11	0.25	0.40	0.12	0.19	0.31	0.04	0.15	0.32	0.12	0.19	0.21
Random	0.36	0.10	0.11	0.36	0.16	0.16	0.32	0.11	0.12	0.33	0.10	0.12	0.39	0.16	0.18	0.21
PCA 1	0.43	0.42	0.37	0.46	0.22	0.52	0.50	0.30	0.51	0.38	0.22	0.36	0.35	0.24	0.36	0.38
PCA 2	0.66	0.56	0.39	0.26	0.19	0.24	0.28	0.19	0.29	0.40	0.20	0.19	0.40	0.26	0.27	0.32
Feature	0.60	0.44	0.60	0.61	0.41	0.67	0.73	0.39	0.54	0.74	0.31	0.54	0.71	0.56	0.61	0.56
NDM	0.89	0.89	0.90	0.71	0.72	0.83	0.63	0.70	0.38	0.50	0.55	0.79	0.72	0.67	0.78	**0.71**

Table 1: Results on GPT-2 Small test suite, higher is better. Test 1-5 measure the concentration of various target information in various places in GPT-2 Small (details in App. D.2) based on ground truth circuits (Wang et al., 2022; Hanna et al., 2023). Numbers are Gini coefficient over subspace patching effects ("-"), over effects normalized by subspace dimension ("d_s"), and over effects normalized by subspace variance ("Var$_s$"). Last column is the average values over the whole row. We compare NDM with 5 baselines. An identity matrix ("Identity"); a random orthogonal matrix ("Random"); PCA 1 and 2 are matrices composed of eigenvectors after applying PCA on activations. We use dimension configuration $[d_1, \ldots, d_S]$ of NDM result as the configuration for all baselines. $[d_1, \ldots, d_S]$ is sorted in descending order, eigenvectors can be sorted in either way according to eigenvalues, resulting in PCA 1 and 2 – meaning either that the smallest subspace receives the biggest ("PCA 1") or smallest ("PCA 2") directions of variance; and subspaces obtained by clustering SAE features ("Feature"), using a method adapted from (Engels et al., 2024)) (details are in App. F.2). Importantly, as shown in App. D.4, the degree of concentration of target information becomes satisfactory when Gini coefficient > 0.6.

layer 4 residual stream (2) subject position in layer 6 (3) subject position and (4) subject name in layer 8 residual stream. The last test is based on Greater-than circuit (Hanna et al., 2023): (5) information about the last two digits of the starting year in layer 9. We measure patching effect as the change in logit difference for IOI-based tests and change in valid answer probability for the Greater-than-based test. See more details in in App. D.2. We then quantify the inequality of patching effect using Gini coefficient. Though very unconventional in machine learning, we find Gini coefficient a suitable metric. Because we want to measure how strongly patching effect is focused on just one or a few subspaces, this notion is captured by Gini coefficient as it measures inequality or degree of concentration. If the target information is mainly encoded in one subspace, the patching effect for this one would be much higher than others, thus resulting in Gini coefficient close to 1. On the other hand, evenly distributed patching effect results in 0. In App. D.4 we show examples of patching effect distributions and their corresponding Gini coefficients, from which we conclude that the coefficient should be > 0.6 to be considered satisfactory (i.e., the effect is mainly concentrated in one subspace). We also calculate the Gini coefficient over patching effect normalized by dimension d_s and variance Var$_s$ of subspaces.

Results We apply NDM to find subspace partitions in GPT-2 Small (Radford et al., 2019), details are described in App. D.3. The results of NDM using the best hyperparameters are shown in Table 1, together with 5 baselines, which, like NDM, are unsupervised and purely computed from activations. *As we can see, NDM clearly outperform baselines*. Though there are a few cases where Gini coefficient is low for NDM, the overall average value shows a strong concentration of target information (0.71, significantly higher than 0.6). Figure 21, 28 and 29 show the qualitative examples of the subspaces obtained by NDM with the highest effect in Test 1, 2, 5 respectively (See later section for how to read them). In App. D.5 we show ablation studies, providing experimental data on how different factors affect final results. Meanwhile, the estimated MI between subspaces decreases significantly after training (Fig. 14), matching the explanation of NDM's training objective.

5.2 Qualitative Analysis of Obtained Subspaces in GPT-2

Preliminaries (Huang et al., 2024b) show that we can interpret activations in terms of their *preimage*, which is the set of inputs that are mapped to the same activation by the model. Simply speaking, to interpret an activation (a vector, called query activation) at a certain place in the model (e.g., layer 3 residual stream, called activation site), we find those inputs that, when fed into the model, would give rise to roughly the same activation at that activation site. Therefore, when query activation is observed by downstream components, any input in preimage could be the current input,

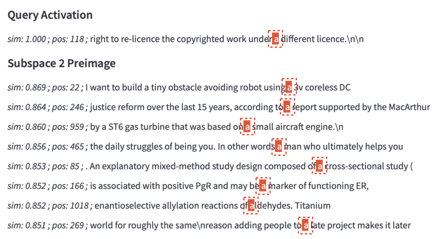

```
Query Activation

sim: 1.000 ; pos: 118 ; right to re-licence the copyrighted work under a different licence.\n\n

Subspace 2 Preimage

sim: 0.869 ; pos: 22 ; I want to build a tiny obstacle avoiding robot using a 3v coreless DC
sim: 0.864 ; pos: 246 ; justice reform over the last 15 years, according to a report supported by the MacArthur
sim: 0.860 ; pos: 959 ; by a ST6 gas turbine that was based on a small aircraft engine.\n
sim: 0.856 ; pos: 465 ; the daily struggles of being you. In other words a man who ultimately helps you
sim: 0.853 ; pos: 85 ; . An explanatory mixed-method study design composed of a cross-sectional study (
sim: 0.852 ; pos: 166 ; is associated with positive PgR and may be a marker of functioning ER,
sim: 0.852 ; pos: 1018 ; enantioselective allylation reactions of aldehydes. Titanium
sim: 0.851 ; pos: 269 ; world for roughly the same\nreason adding people to a late project makes it later
```

(a)

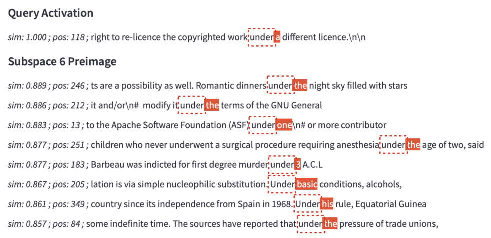

```
Query Activation

sim: 1.000 ; pos: 118 ; right to re-licence the copyrighted work under a different licence.\n\n

Subspace 6 Preimage

sim: 0.889 ; pos: 246 ; ts are a possibility as well. Romantic dinners under the night sky filled with stars
sim: 0.886 ; pos: 212 ; it and/or\n#  modify it under the terms of the GNU General
sim: 0.883 ; pos: 13 ; to the Apache Software Foundation (ASF) under one\n# or more contributor
sim: 0.877 ; pos: 251 ; children who never underwent a surgical procedure requiring anesthesia under the age of two, said
sim: 0.877 ; pos: 183 ; Barbeau was indicted for first degree murder under 3 A.C.L
sim: 0.867 ; pos: 205 ; lation is via simple nucleophilic substitution. Under basic conditions, alcohols,
sim: 0.861 ; pos: 349 ; country since its independence from Spain in 1968. Under his rule, Equatorial Guinea
sim: 0.857 ; pos: 84 ; some indefinite time. The sources have reported that under the pressure of trade unions,
```

(b)

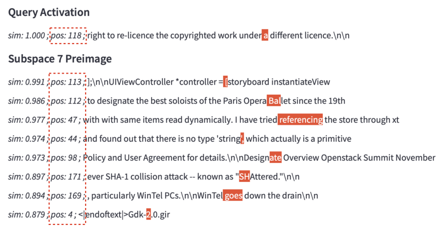

```
Query Activation

sim: 1.000 ; pos: 118 ; right to re-licence the copyrighted work under a different licence.\n\n

Subspace 7 Preimage

sim: 0.991 ; pos: 113 ; ];\n\nUIViewController *controller = [storyboard instantiateView
sim: 0.986 ; pos: 112 ; to designate the best soloists of the Paris Opera Ballet since the 19th
sim: 0.977 ; pos: 47 ; with with same items read dynamically. I have tried referencing the store through xt
sim: 0.974 ; pos: 44 ; and found out that there is no type 'string', which actually is a primitive
sim: 0.973 ; pos: 98 ; Policy and User Agreement for details.\n\nDesignate Overview Openstack Summit November
sim: 0.897 ; pos: 171 ; ever SHA-1 collision attack -- known as "SHAttered."\n\n
sim: 0.894 ; pos: 169 ; , particularly WinTel PCs.\n\nWinTel goes down the drain\n\n
sim: 0.879 ; pos: 4 ; <|endoftext|>Gdk-2.0.gir
```

(c)

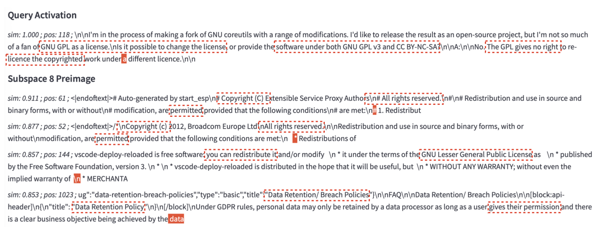

```
Query Activation

sim: 1.000 ; pos: 118 ; \n\nI'm in the process of making a fork of GNU coreutils with a range of modifications. I'd like to release the result as an open-source project, but I'm not so much
of a fan of GNU GPL as a license.\nIs it possible to change the license, or provide the software under both GNU GPL v3 and CC BY-NC-SA?\n\nA:\n\nNo. The GPL gives no right to re-
licence the copyrighted work under a different licence.\n\n

Subspace 8 Preimage

sim: 0.911 ; pos: 61 ; <|endoftext|># Auto-generated by start_esp\n# Copyright (C) Extensible Service Proxy Authors\n# All rights reserved.\n#\n# Redistribution and use in source and
binary forms, with or without\n# modification, are permitted provided that the following conditions\n# are met:\n# 1. Redistribut

sim: 0.877 ; pos: 52 ; <|endoftext|>/*\nCopyright (c) 2012, Broadcom Europe Ltd\nAll rights reserved.\n\nRedistribution and use in source and binary forms, with or
without\nmodification, are permitted provided that the following conditions are met:\n   * Redistributions of

sim: 0.857 ; pos: 144 ; vscode-deploy-reloaded is free software: you can redistribute it and/or modify   \n * it under the terms of the GNU Lesser General Public License as   \n * published
by the Free Software Foundation, version 3. \n * \n * vscode-deploy-reloaded is distributed in the hope that it will be useful, but  \n * WITHOUT ANY WARRANTY; without even the
implied warranty of  \n * MERCHANTA

sim: 0.853 ; pos: 1023 ; ug":"data-retention-breach-policies","type":"basic","title":"Data Retention/ Breach Policies"}\n\nFAQ\n\nData Retention/ Breach Policies\n\n[block:api-
header]\n{\n"title": "Data Retention Policy"\n}\n[/block]\nUnder GDPR rules, personal data may only be retained by a data processor as long as a user gives their permission and there
is a clear business objective being achieved by the data
```

(d)

Figure 2: Preimages of the subspace activation corresponding to the same token "a" in 4 different subspaces of the residual stream $\boldsymbol{h}^{4,post}$ in GPT-2 Small. Tokens highlighted with red background are those where the activations are taken from. Tokens highlighted with dashed boxes reflect the encoded information. These activations are projected into the subspaces and the first column "*sim*" is the similarity between this projection in the preimage and in the query activation. The second column "*pos*" is the position indices of the highlighted tokens. We are showing only the most recent part of the context and as well as 5 future tokens, the actual input sequences are much longer. Interpretation of encoded information: (a) current token "a". (b) the prior token "under". (c) current position, around 118. (d) the topic, the overall context is about licence/permission. In sum, we can see in different subspaces of the same layer, different aspects of the current context are encoded.

thus the commonality in preimage is the available information. In other words, query activation (any activation we want to interpret) "represents" the whole preimage.

Setting Instead of the whole space, we apply it to subspaces. (See discussion in App. G.1 for why it works better for subspaces). Instead of training decoders as in (Huang et al., 2024b), we collect around 1M model activations and conduct vector search among them to find preimages (see details in App. E.1). Though without a decoder the content of preimage is restricted by a fixed set of inputs (2000 sequences from MiniPile + 2000 IOI and greater-than sequences), it is easier to implement. We use cosine similarity to define the preimage, so it includes inputs whose corresponding activations are in a similar direction to the query activation. We set 0.85 as the threshold for preimages in most cases. For all qualitative results in the paper (including the web application), the subspace partition is given by the best configuration of NDM according to the test results from Sec. 5.1 (last row of Table 1).

Results In Fig. 2 we show 4 preimages corresponding to the same token at the same layer's residual stream. We see clearly that in this contextualized representation, different aspects of the context are encoded in different subspaces, i.e., the current token, position, prior token, the topic. NDM indeed decomposes the representation space in a meaningful way. Moreover, we also find that the function/interpretation of subspaces is *consistent*. For example, Fig. 2(a) shows subspace 2 encodes the current token, and we find it always encodes the current token. This is also true for the other 3 subspaces shown in the other 3 subfigures (See Fig. 20 to 23 in App.). Though being consistent, we also find that the meaning of subspaces can vary, depending on factors such as whether a certain pattern occurs or a certain mechanism is triggered. We provide an extensive discussion for the qualitative results in App. E.3. In sum, qualitative results show that most of the time, the preimages are interpretable, and we can find a high-level concept to summarize the encoded information in subspaces across inputs because of good consistency. Due to space limits we only present a very limited number of examples, we strongly recommend checking more in our web application[4].

[4]`https://subspace-partition.space` (No author identity information)

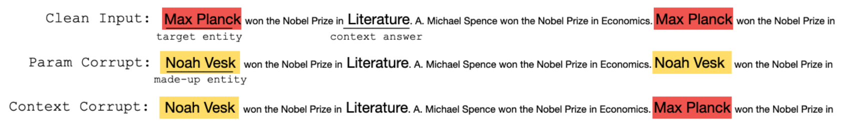
Clean Input: Max Planck won the Nobel Prize in Literature. A. Michael Spence won the Nobel Prize in Economics. Max Planck won the Nobel Prize in
target entity
context answer
Param Corrupt: Noah Vesk won the Nobel Prize in Literature. A. Michael Spence won the Nobel Prize in Economics. Noah Vesk won the Nobel Prize in
made-up entity
Context Corrupt: Noah Vesk won the Nobel Prize in Literature. A. Michael Spence won the Nobel Prize in Economics. Max Planck won the Nobel Prize in

Figure 3: Clean and counterfactual inputs used in knowledge conflict experiments. Patching with activation from `Param Corrupt` can cause the model to increase the probability of context answer, while patching with `Context Corrupt` can increase the probability of parametric answer.

5.3 Applicability to Larger Models

To test the applicability on larger models, we apply NDM on residual stream activations of Qwen2.5-1.5B (Qwen et al., 2025) and Gemma-2-2B (Team et al., 2024)[5]. As no very detailed ground-truth circuits are available for them, we design prompts that are likely to elicit separate mechanisms inside the model, and see if they are mediated by separate subspaces. This would constitute strong evidence that our partition is meaningful.

Setting We construct inputs that elicit knowledge conflicts: "Max Planck won the Nobel Prize in Literature. ... Max Planck won the Nobel Prize in". The model can either predict "Physics" (parametric answer) by using its parametric knowledge, or predict "Literature" (context answer) by copying the context knowledge. We refer "Max Planck" as target entity. We construct examples following this form with different target entities, using RAVEL dataset (Huang et al., 2024a). We do not use the dataset as the way it is designed, see App. D.6 for discussion and experimental details. To test whether a subspace plays a role in either of these two circuits quantitatively, we again use subspace patching and construct two types of counterfactual inputs (Fig. 3): 1) `Param Corrupt`: It aims to knock out the role of the parametric knowledge. We replace both occurrences of the target entity with a made-up entity, and other parts remain unchanged. Since the model does not have parametric knowledge for this made-up entity, the circuit for parametric knowledge is broken, while the circuit for context knowledge should not be affected much. 2) `Context Corrupt`: We replace only the first occurrence of the target entity with a made-up entity, other parts remain unchanged. This would presumably only break the context knowledge retrieval, as in the last sentence the target entity does not match any previous entity. We filter entities to ensure the model has parametric knowledge, and construct more than 500 prompts for both models, and measure the average patching effect over them. When patching, we patch *all* activations across token positions for a single subspace, since we do not know the underlying circuit, and our subspace partition is *uniform* across the entire sequence.

Results We show results in Fig. 4. We can see that NDM finds some subspaces that have non-trivial patching effect under one kind of counterfactual inputs, indicating they play a role in for only one mechanism. For example, in $\boldsymbol{h}^{11,mid}$ of Qwen2.5-1.5B, subspace 2 seems to do the heavy lifting for routing parametric knowledge, while subspace 10 is crucial in routing context knowledge. Both subspaces are part of the same representation space. In contrast, baselines (Fig. 18, 19 in App.) typically show correlated patching effects under two types of counterfactual inputs. Importantly, we need to be careful when interpreting these results since the detailed circuits are unknown, see caveats in App. D.6. Moreover, we also try to qualitatively interpret some important subspaces, subspace 2 and 6 for Qwen2.5-1.5B. We found that the two subspaces indeed encode parametric knowledge while being in different stages of knowledge routing. Subspace 2 encodes local knowledge (consistently focused on the current entity/n-gram), while subspace 6 encodes knowledge propagated from elsewhere by attention layers (could be about a previous entity). See details in App. E.4.

6 Discussions

Related Work The internal mechanisms of a model can be analyzed and described using various units at different levels, such as components (Wang et al., 2022; Hanna et al., 2023; Stolfo et al., 2023; Prakash et al., 2024; Yu & Ananiadou, 2024), sparse features (Cunningham et al., 2023; Bricken et al., 2023; Dunefsky et al., 2024; Ameisen et al., 2025), token positions (Haklay et al., 2025; Bakalova

[5]Both without post training

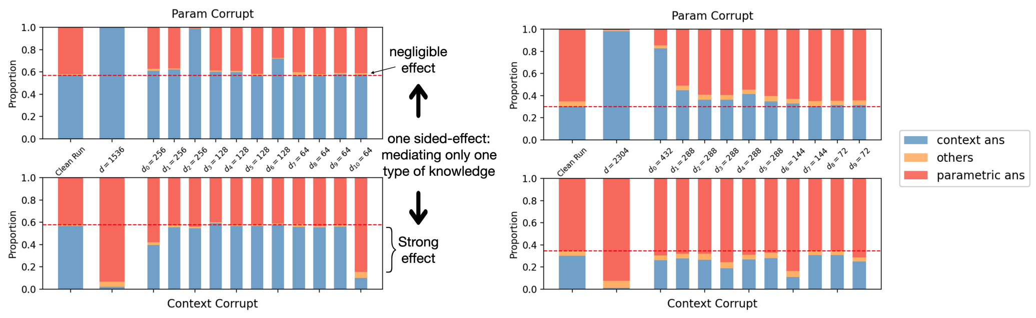

Figure 4: Subspace patching effect. **Left**: NDM partition on $\boldsymbol{h}^{11,mid}$ of Qwen2.5-1.5B. The model originally predicts the context answer around 60% of the time ("Clean Run"). If the entire space is patched by activations from `Param Corrupt`, the model always chooses the context answer ("d=1536"), and likewise for `Context Corrupt`. NDM finds subspaces that only mediate parametric knowledge routing ("$d_2 = 256$", context answer is 100% under `Param Corrupt` while parametric answer rate remains the same as clean run under `Context Corrupt`) or only mediate context knowledge routing ("$d_{10} = 64$"). See Fig. 18 in App. for baseline results. **Right**: NDM on $\boldsymbol{h}^{9,mid}$ of Gemma-2-2B. Similarly, some subspaces given by NDM have strong effect under one kind of counterfactual inputs but negligible effect under the other. See Fig. 19 in App. for baseline results.

et al., 2025), parameters (Braun et al., 2025; Bushnaq et al., 2025), and – most relevantly – subspaces. Interpretable and causally important non-neuron-basis-aligned multi-dimensional subspaces have been identified in many studies, though typically only those relevant to a specific sub-task or supporting certain arguments. For example, subspaces for gender bias (Bolukbasi et al., 2016; Belrose et al., 2023), linguistic concepts (Belrose et al., 2023; Guerner et al., 2023), greater-than and equality relationships (Wu et al., 2023; Geiger et al., 2024), estimation of current state (Shai et al., 2024), refusal behavior (Wollschläger et al., 2025), variables in abstract reasoning (Yang et al., 2025), days of the week, months, years (Engels et al., 2024; Clarke et al., 2024), and separate subspaces for digits of different significance in addition (Hu et al., 2025). Like the toy setting described in this paper, discussion of feature dependency leads to findings about interpretable subspaces (Engels et al., 2024; Clarke et al., 2024).

Future Directions and Limitations As we have shown, the resulting subspaces often align with meaningful "variables", representing groups of infinitely many features sharing a higher-level concept. We believe they are better fundamental units to build circuits. Unlike feature circuits where connections are specific to concrete features, circuits defined over such "variables" capture relationships at a more abstract, high-level, and input-independent level, offering greater potential for algorithm-like description (see more discussion in App. G.3).

Our current approach shows a promising direction, but we expect that even stronger results could be achieved using substantial computational resources and engineering efforts from industry. With more compute, applications to larger models or learning better subspace partition on 2B models can produce more interesting subspaces (Compute usage of this paper is in App. H). More experiments can be done to explore more fine-grained partitions, instead of start merging from subspaces of at least 32 dimension. It is very likely that the model uses intermediate variables that take value from a small set (e.g., sentiment), thus encoded in tiny subspaces. Moreover, as we interpret directions in subspaces by using cosine similarity to define preimages, we rely on the Linear Representation Hypothesis (Elhage et al., 2022; Park et al., 2023), which could be untrue in some cases (Csordás et al., 2024). Furthermore, as mentioned in App. E.3, we do not find clear interpretations for some small subspaces. Besides reasons mentioned before, it could be because the orthogonal matrices require more training, or because we assume strong orthogonality between meaningful subspaces, or some abstract variables used internally by the model may be hard to interpret on the basis of inputs.

7 Conclusion

In this paper, we present a novel way to decompose representation space into non-basis-aligned multi-dimensional subspaces by optimizing under an unsupervised objective, neighbor distance minimization. Our method uncovers interpretable and less dependent subspaces from only data distribution. Different from previous work, we aim to investigate and describe the whole space by studying each subspace. We present both quantitative and qualitative evidence supporting our claim that obtained subspaces are interpretable and consistent most of the time. On the other hand, we also highlight some limitations of the current version of the method, e.g., partition is not fine-grained enough. We believe many of them can be improved in the future. In sum, we believe our method can serve as a useful tool for the interpretability and, more broadly, machine learning community.

References

Emmanuel Ameisen, Jack Lindsey, Adam Pearce, Wes Gurnee, Nicholas L. Turner, Brian Chen, Craig Citro, David Abrahams, Shan Carter, Basil Hosmer, Jonathan Marcus, Michael Sklar, Adly Templeton, Trenton Bricken, Callum McDougall, Hoagy Cunningham, Thomas Henighan, Adam Jermyn, Andy Jones, Andrew Persic, Zhenyi Qi, T. Ben Thompson, Sam Zimmerman, Kelley Rivoire, Thomas Conerly, Chris Olah, and Joshua Batson. Circuit tracing: Revealing computational graphs in language models. *Transformer Circuits Thread*, 2025. URL `https://transformer-circuits.pub/2025/attribution-graphs/methods.html`.

Aleksandra Bakalova, Yana Veitsman, Xinting Huang, and Michael Hahn. Contextualize-then-aggregate: Circuits for in-context learning in gemma-2 2b. *arXiv preprint arXiv:2504.00132*, 2025.

Mohamed Ishmael Belghazi, Aristide Baratin, Sai Rajeshwar, Sherjil Ozair, Yoshua Bengio, Aaron Courville, and Devon Hjelm. Mutual information neural estimation. In *International conference on machine learning*, pp. 531–540. PMLR, 2018.

Nora Belrose, David Schneider-Joseph, Shauli Ravfogel, Ryan Cotterell, Edward Raff, and Stella Biderman. Leace: Perfect linear concept erasure in closed form. *Advances in Neural Information Processing Systems*, 36:66044–66063, 2023.

Leonard Bereska and Efstratios Gavves. Mechanistic interpretability for ai safety–a review. *arXiv preprint arXiv:2404.14082*, 2024.

Tolga Bolukbasi, Kai-Wei Chang, James Y Zou, Venkatesh Saligrama, and Adam T Kalai. Man is to computer programmer as woman is to homemaker? debiasing word embeddings. *Advances in neural information processing systems*, 29, 2016.

Dan Braun, Lucius Bushnaq, Stefan Heimersheim, Jake Mendel, and Lee Sharkey. Interpretability in parameter space: Minimizing mechanistic description length with attribution-based parameter decomposition. *arXiv preprint arXiv:2501.14926*, 2025.

Trenton Bricken, Adly Templeton, Joshua Batson, Brian Chen, Adam Jermyn, Tom Conerly, Nick Turner, Cem Anil, Carson Denison, Amanda Askell, Robert Lasenby, Yifan Wu, Shauna Kravec, Nicholas Schiefer, Tim Maxwell, Nicholas Joseph, Zac Hatfield-Dodds, Alex Tamkin, Karina Nguyen, Brayden McLean, Josiah E Burke, Tristan Hume, Shan Carter, Tom Henighan, and Christopher Olah. Towards monosemanticity: Decomposing language models with dictionary learning. *Transformer Circuits Thread*, 2023. https://transformer-circuits.pub/2023/monosemantic-features/index.html.

Lucius Bushnaq, Dan Braun, and Lee Sharkey. Stochastic parameter decomposition. *arXiv preprint arXiv:2506.20790*, 2025.

Alessia Celeghin, Alessio Borriero, Davide Orsenigo, Matteo Diano, Carlos Andrés Méndez Guerrero, Alan Perotti, Giovanni Petri, and Marco Tamietto. Convolutional neural networks for vision neuroscience: significance, developments, and outstanding issues. *Frontiers in Computational Neuroscience*, 17:1153572, 2023.

Matthew Clarke, hrdkbhatnagar, and Joseph Bloom. Compositionality and ambiguity: Latent co-occurrence and interpretable subspaces. *LESSWRONG*, 2024. URL `https://www.lesswrong.com/posts/WNoqEivcCSg8gJe5h/compositionality-and-ambiguity-latent-co-occurrence-and`.

Róbert Csordás, Christopher Potts, Christopher D Manning, and Atticus Geiger. Recurrent neural networks learn to store and generate sequences using non-linear representations. *arXiv preprint arXiv:2408.10920*, 2024.

Hoagy Cunningham, Aidan Ewart, Logan Riggs, Robert Huben, and Lee Sharkey. Sparse autoencoders find highly interpretable features in language models. *arXiv preprint arXiv:2309.08600*, 2023.

Matthijs Douze, Alexandr Guzhva, Chengqi Deng, Jeff Johnson, Gergely Szilvasy, Pierre-Emmanuel Mazaré, Maria Lomeli, Lucas Hosseini, and Hervé Jégou. The faiss library. 2024.

Jacob Dunefsky, Philippe Chlenski, and Neel Nanda. Transcoders find interpretable llm feature circuits. *Advances in Neural Information Processing Systems*, 37:24375–24410, 2024.

Nelson Elhage, Neel Nanda, Catherine Olsson, Tom Henighan, Nicholas Joseph, Ben Mann, Amanda Askell, Yuntao Bai, Anna Chen, Tom Conerly, Nova DasSarma, Dawn Drain, Deep Ganguli, Zac Hatfield-Dodds, Danny Hernandez, Andy Jones, Jackson Kernion, Liane Lovitt, Kamal Ndousse, Dario Amodei, Tom Brown, Jack Clark, Jared Kaplan, Sam McCandlish, and Chris Olah. A mathematical framework for transformer circuits. *Transformer Circuits Thread*, 2021. https://transformer-circuits.pub/2021/framework/index.html.

Nelson Elhage, Tristan Hume, Catherine Olsson, Nicholas Schiefer, Tom Henighan, Shauna Kravec, Zac Hatfield-Dodds, Robert Lasenby, Dawn Drain, Carol Chen, Roger Grosse, Sam McCandlish, Jared Kaplan, Dario Amodei, Martin Wattenberg, and Christopher Olah. Toy models of superposition. *Transformer Circuits Thread*, 2022. https://transformer-circuits.pub/2022/toy_model/index.html.

Joshua Engels, Eric J Michaud, Isaac Liao, Wes Gurnee, and Max Tegmark. Not all language model features are one-dimensionally linear. *arXiv preprint arXiv:2405.14860*, 2024.

Richard Futrell and Kyle Mahowald. How linguistics learned to stop worrying and love the language models. *arXiv preprint arXiv:2501.17047*, 2025.

Atticus Geiger, Zhengxuan Wu, Christopher Potts, Thomas Icard, and Noah Goodman. Finding alignments between interpretable causal variables and distributed neural representations. In *Causal Learning and Reasoning*, pp. 160–187. PMLR, 2024.

Atticus Geiger, Duligur Ibeling, Amir Zur, Maheep Chaudhary, Sonakshi Chauhan, Jing Huang, Aryaman Arora, Zhengxuan Wu, Noah Goodman, Christopher Potts, et al. Causal abstraction: A theoretical foundation for mechanistic interpretability. *Journal of Machine Learning Research*, 26 (83):1–64, 2025.

Ian Goodfellow, Jean Pouget-Abadie, Mehdi Mirza, Bing Xu, David Warde-Farley, Sherjil Ozair, Aaron Courville, and Yoshua Bengio. Generative adversarial networks. *Communications of the ACM*, 63(11):139–144, 2020.

Clément Guerner, Anej Svete, Tianyu Liu, Alexander Warstadt, and Ryan Cotterell. A geometric notion of causal probing. *arXiv preprint arXiv:2307.15054*, 2023.

Tal Haklay, Hadas Orgad, David Bau, Aaron Mueller, and Yonatan Belinkov. Position-aware automatic circuit discovery. *arXiv preprint arXiv:2502.04577*, 2025.

Michael Hanna, Ollie Liu, and Alexandre Variengien. How does gpt-2 compute greater-than?: Interpreting mathematical abilities in a pre-trained language model. *Advances in Neural Information Processing Systems*, 36:76033–76060, 2023.

Xinyan Hu, Kayo Yin, Michael I Jordan, Jacob Steinhardt, and Lijie Chen. Understanding in-context learning of addition via activation subspaces. *arXiv preprint arXiv:2505.05145*, 2025.

Jing Huang, Zhengxuan Wu, Christopher Potts, Mor Geva, and Atticus Geiger. Ravel: Evaluating interpretability methods on disentangling language model representations. *arXiv preprint arXiv:2402.17700*, 2024a.

Xinting Huang, Madhur Panwar, Navin Goyal, and Michael Hahn. Inversionview: a general-purpose method for reading information from neural activations. *Advances in Neural Information Processing Systems*, 37:137903–137964, 2024b.

Jean Kaddour. The minipile challenge for data-efficient language models. *arXiv preprint arXiv:2304.08442*, 2023.

L. F. Kozachenko and N. N. Leonenko. Sample estimate of the entropy of a random vector. *Probl. Pered. Inform.*, 23:9, 1987.

Alexander Kraskov, Harald Stögbauer, and Peter Grassberger. Estimating mutual information. *Physical Review E—Statistical, Nonlinear, and Soft Matter Physics*, 69(6):066138, 2004.

Aleksandar Makelov, Georg Lange, and Neel Nanda. Is this the subspace you are looking for? an interpretability illusion for subspace activation patching. *arXiv preprint arXiv:2311.17030*, 2023.

Aaron Mueller, Jannik Brinkmann, Millicent Li, Samuel Marks, Koyena Pal, Nikhil Prakash, Can Rager, Aruna Sankaranarayanan, Arnab Sen Sharma, Jiuding Sun, et al. The quest for the right mediator: A history, survey, and theoretical grounding of causal interpretability. *arXiv preprint arXiv:2408.01416*, 2024.

SubbaReddy Oota, Manish Gupta, and Mariya Toneva. Joint processing of linguistic properties in brains and language models. *Advances in Neural Information Processing Systems*, 36:18001–18014, 2023.

Kiho Park, Yo Joong Choe, and Victor Veitch. The linear representation hypothesis and the geometry of large language models. *arXiv preprint arXiv:2311.03658*, 2023.

Adam Paszke, Sam Gross, Francisco Massa, Adam Lerer, James Bradbury, Gregory Chanan, Trevor Killeen, Zeming Lin, Natalia Gimelshein, Luca Antiga, et al. Pytorch: An imperative style, high-performance deep learning library. *Advances in neural information processing systems*, 32, 2019.

Nikhil Prakash, Tamar Rott Shaham, Tal Haklay, Yonatan Belinkov, and David Bau. Fine-tuning enhances existing mechanisms: A case study on entity tracking. *arXiv preprint arXiv:2402.14811*, 2024.

Qwen, :, An Yang, Baosong Yang, Beichen Zhang, Binyuan Hui, Bo Zheng, Bowen Yu, Chengyuan Li, Dayiheng Liu, Fei Huang, Haoran Wei, Huan Lin, Jian Yang, Jianhong Tu, Jianwei Zhang, Jianxin Yang, Jiaxi Yang, Jingren Zhou, Junyang Lin, Kai Dang, Keming Lu, Keqin Bao, Kexin Yang, Le Yu, Mei Li, Mingfeng Xue, Pei Zhang, Qin Zhu, Rui Men, Runji Lin, Tianhao Li, Tianyi Tang, Tingyu Xia, Xingzhang Ren, Xuancheng Ren, Yang Fan, Yang Su, Yichang Zhang, Yu Wan, Yuqiong Liu, Zeyu Cui, Zhenru Zhang, and Zihan Qiu. Qwen2.5 technical report, 2025. URL `https://arxiv.org/abs/2412.15115`.

Alec Radford, Jeff Wu, Rewon Child, David Luan, Dario Amodei, and Ilya Sutskever. Language models are unsupervised multitask learners. 2019.

Adam Shai, Lucas Teixeira, Alexander Oldenziel, Sarah Marzen, and Paul Riechers. Transformers represent belief state geometry in their residual stream. *Advances in Neural Information Processing Systems*, 37:75012–75034, 2024.

Alessandro Stolfo, Yonatan Belinkov, and Mrinmaya Sachan. A mechanistic interpretation of arithmetic reasoning in language models using causal mediation analysis. *arXiv preprint arXiv:2305.15054*, 2023.

Milan Studenỳ and Jirina Vejnarová. The multiinformation function as a tool for measuring stochastic dependence. *Learning in graphical models*, pp. 261–297, 1998.

Gemma Team, Morgane Riviere, Shreya Pathak, Pier Giuseppe Sessa, Cassidy Hardin, Surya Bhupatiraju, Léonard Hussenot, Thomas Mesnard, Bobak Shahriari, Alexandre Ramé, Johan Ferret, Peter Liu, Pouya Tafti, Abe Friesen, Michelle Casbon, Sabela Ramos, Ravin Kumar, Charline Le Lan, Sammy Jerome, Anton Tsitsulin, Nino Vieillard, Piotr Stanczyk, Sertan Girgin, Nikola Momchev, Matt Hoffman, Shantanu Thakoor, Jean-Bastien Grill, Behnam Neyshabur, Olivier Bachem, Alanna Walton, Aliaksei Severyn, Alicia Parrish, Aliya Ahmad, Allen Hutchison, Alvin Abdagic, Amanda Carl, Amy Shen, Andy Brock, Andy Coenen, Anthony Laforge, Antonia Paterson, Ben Bastian, Bilal Piot, Bo Wu, Brandon Royal, Charlie Chen, Chintu Kumar, Chris Perry, Chris Welty, Christopher A. Choquette-Choo, Danila Sinopalnikov, David Weinberger, Dimple Vijaykumar, Dominika Rogozińska, Dustin Herbison, Elisa Bandy, Emma Wang, Eric Noland, Erica Moreira, Evan Senter, Evgenii Eltyshev, Francesco Visin, Gabriel Rasskin, Gary Wei, Glenn Cameron, Gus Martins, Hadi Hashemi, Hanna Klimczak-Plucińska, Harleen Batra, Harsh Dhand, Ivan Nardini, Jacinda Mein, Jack Zhou, James Svensson, Jeff Stanway, Jetha Chan, Jin Peng Zhou, Joana Carrasqueira, Joana Iljazi, Jocelyn Becker, Joe Fernandez, Joost van Amersfoort, Josh Gordon, Josh Lipschultz, Josh Newlan, Ju yeong Ji, Kareem Mohamed, Kartikeya Badola, Kat Black, Katie Millican, Keelin McDonell, Kelvin Nguyen, Kiranbir Sodhia, Kish Greene, Lars Lowe Sjoesund, Lauren Usui, Laurent Sifre, Lena Heuermann, Leticia Lago, Lilly McNealus, Livio Baldini Soares, Logan Kilpatrick, Lucas Dixon, Luciano Martins, Machel Reid, Manvinder Singh, Mark Iverson, Martin Görner, Mat Velloso, Mateo Wirth, Matt Davidow, Matt Miller, Matthew Rahtz, Matthew Watson, Meg Risdal, Mehran Kazemi, Michael Moynihan, Ming Zhang, Minsuk Kahng, Minwoo Park, Mofi Rahman, Mohit Khatwani, Natalie Dao, Nenshad Bardoliwalla, Nesh Devanathan, Neta Dumai, Nilay Chauhan, Oscar Wahltinez, Pankil Botarda, Parker Barnes, Paul Barham, Paul Michel, Pengchong Jin, Petko Georgiev, Phil Culliton, Pradeep Kuppala, Ramona Comanescu, Ramona Merhej, Reena Jana, Reza Ardeshir Rokni, Rishabh Agarwal, Ryan Mullins, Samaneh Saadat, Sara Mc Carthy, Sarah Cogan, Sarah Perrin, Sébastien M. R. Arnold, Sebastian Krause, Shengyang Dai, Shruti Garg, Shruti Sheth, Sue Ronstrom, Susan Chan, Timothy Jordan, Ting Yu, Tom Eccles, Tom Hennigan, Tomas Kocisky, Tulsee Doshi, Vihan Jain, Vikas Yadav, Vilobh Meshram, Vishal Dharmadhikari, Warren Barkley, Wei Wei, Wenming Ye, Woohyun Han, Woosuk Kwon, Xiang Xu, Zhe Shen, Zhitao Gong, Zichuan Wei, Victor Cotruta, Phoebe Kirk, Anand Rao, Minh Giang, Ludovic Peran, Tris Warkentin, Eli Collins, Joelle Barral, Zoubin Ghahramani, Raia Hadsell, D. Sculley, Jeanine Banks, Anca Dragan, Slav Petrov, Oriol Vinyals, Jeff Dean, Demis Hassabis, Koray Kavukcuoglu, Clement Farabet, Elena Buchatskaya, Sebastian Borgeaud, Noah Fiedel, Armand Joulin, Kathleen Kenealy, Robert Dadashi, and Alek Andreev. Gemma 2: Improving open language models at a practical size, 2024. URL `https://arxiv.org/abs/2408.00118`.

Kevin Wang, Alexandre Variengien, Arthur Conmy, Buck Shlegeris, and Jacob Steinhardt. Interpretability in the wild: a circuit for indirect object identification in gpt-2 small. *arXiv preprint arXiv:2211.00593*, 2022.

Satosi Watanabe. Information theoretical analysis of multivariate correlation. *IBM Journal of research and development*, 4(1):66–82, 1960.

Gail Weiss, Yoav Goldberg, and Eran Yahav. Thinking like transformers. In *International Conference on Machine Learning*, pp. 11080–11090. PMLR, 2021.

Tom Wollschläger, Jannes Elstner, Simon Geisler, Vincent Cohen-Addad, Stephan Günnemann, and Johannes Gasteiger. The geometry of refusal in large language models: Concept cones and representational independence. *arXiv preprint arXiv:2502.17420*, 2025.

Zhengxuan Wu, Atticus Geiger, Thomas Icard, Christopher Potts, and Noah Goodman. Interpretability at scale: Identifying causal mechanisms in alpaca. *Advances in neural information processing systems*, 36:78205–78226, 2023.

Yukang Yang, Declan Campbell, Kaixuan Huang, Mengdi Wang, Jonathan Cohen, and Taylor Webb. Emergent symbolic mechanisms support abstract reasoning in large language models. *arXiv preprint arXiv:2502.20332*, 2025.

Zeping Yu and Sophia Ananiadou. Interpreting arithmetic mechanism in large language models through comparative neuron analysis. *arXiv preprint arXiv:2409.14144*, 2024.

A Additional Figures For Motivation and Background

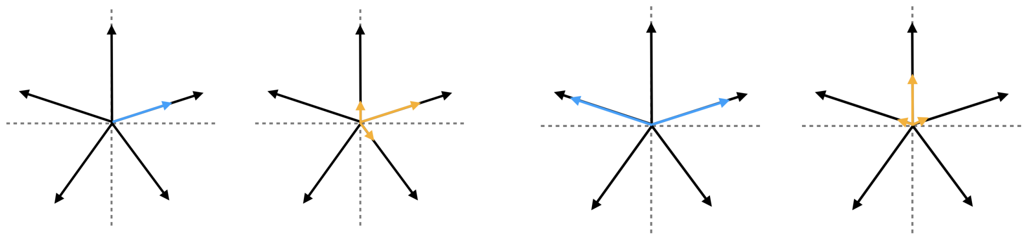

(a) Left: input features $\boldsymbol{x}$, blue arrow represents the only activating feature; Right: yellow arrows represent reconstructed features $\boldsymbol{x}'$

(b) Left: input features $\boldsymbol{x}$, two features are activated, their sum h is aligned with the y-axis; Right: reconstructed features $\boldsymbol{x}'$

Figure 5: Toy model representing 5 features in 2D space, each black arrow corresponds to a column in its weight matrix $\mathbf{W}$

B Methodology Details

B.1 Total correlation Perspective

The entropy of continuous random vector can be estimated based on the distance to kth-nearest neighbor (Kozachenko & Leonenko, 1987). Formally, given random samples $(\boldsymbol{x_1} \cdots \boldsymbol{x_N})$ of the random vector X, the entropy estimate $\hat{H}(X)$ is as follows

$$\hat{H}(X) = \frac{1}{N}\sum_{n=1}^{N} \log \epsilon(n) + \text{const.} \tag{5}$$

$\epsilon(n)$ is twice the distance from $\boldsymbol{x}_n$ to its kth neighbor, const. is a constant if N and k are fixed. Meanwhile, the total correlation (Watanabe, 1960) or multi-information (Studený & Vejnarová, 1998) is defined as

$$C(X_1, \dots, X_S) = \sum_{s=1}^{S} H(X_s) - H(X_1, \dots, X_S) \tag{6}$$

which generalizes mutual information's binary case to multiple random variables and measures the redundancy and dependence among them. Therefore, when we minimize the distances in Eq.4, the entropy of individual subspaces decreases[6], and because the last term of Eq.6 is constant as the entropy of the joint subspace is invariant under orthogonal transformation, we actually minimize the total correlation.

B.2 Algorithm Details

Here we supplement Sec. 3 and Algorithm 1 with some important details and explanations. The MI is measured by KSG estimator (Kraskov et al., 2004). We use the first algorithm presented in the paper (Estimator $I^{(1)}(X,Y)$) and normalize the variance of each subspace before estimation, by dividing subspace activations by the square root of the sum of the variance of each dimension in the subspace. Note that MI is invariant under this transformation in theory but it helps reduce errors in practice (Kraskov et al., 2004). We measure pair-wise MI for subspaces, and then divide them by the sum of dimensions of subspace pairs. We use subspace dimension as a very rough estimate of entropy, which forms the upper-bound of MI. So the intuition behind normalizing MI with dimensionality is to roughly estimate the ratio of entropy removed after the other variable is observed. We set a threshold for normalized MI, we select and sort all pairs whose normalized MI is above the threshold. We then iterate over these pairs, selecting pairs that do not intersect with selected pairs. For example, for

[6]In our preliminary experiments, we found including the $\log(\cdot)$ in Eq.5 as part of the training objective does not help.

Algorithm 1 NDM

```
Require: Activations Buffer B, $[\boldsymbol{h}_1, \cdots, \boldsymbol{h}_N]$, threshold $\tau$, initial configuration $c = [d_1, \ldots, d_S]$
  where $\sum_{s=1}^{S} d_s = d$, initial orthogonal matrix $R \leftarrow I$, batch size $b$, search steps $n$, block size $m$,
  merging start delay $p$, merging interval $t$, maximum update steps $K$.
  for $k = 1$ to K do
      $H_q \leftarrow$ B.pop($b$)                    ▷ a batch of activations, deleted after pop
      $\hat{H}_q \leftarrow RH_q$
      $H_{nearest} \leftarrow$ [[ ] For 1 to S]
      $D_{nearest} \leftarrow$ [[$\infty$ For 1 to b] For 1 to S ]
      Stop gradient tracking:
          for 1 to n do
              $H_k \leftarrow$ B.next()              ▷ a batch of size $m$, without being deleted from B
              $\hat{H}_k \leftarrow RH_k$
              for $s = 1$ to $S$ do
                  D = pair_wise_dist($\hat{H}_q^{(s)}$, $\hat{H}_k^{(s)}$)          ▷ $D \in \mathbb{R}^{b\times m}$
                  for $i = 1$ to $b$ do
                      if $\min(D[i]) < D_{nearest}[s][i]$ then
                          $D_{nearest}[s][i] \leftarrow \min(D[i])$
                          $H_{nearest}[s][i] \leftarrow H_k[\arg\min(D[i])]$
                      end if
                  end for
              end for
          end for
      $D_{nearest}$ = [ ]
      for $s = 1$ to $S$ do                          ▷ Start gradient tracking
          $\hat{H}_k \leftarrow RH_{nearest}[s]$
          d = dist($\hat{H}_q^{(s)}$, $\hat{H}_k^{(s)}$)                       ▷ $d \in \mathbb{R}^{b}$
          $D_{nearest}[s] = \frac{1}{b}\sum_b d$
      end for
      $f = \frac{1}{S}\sum_s D_{nearest}[s])$                                 ▷ Final loss
      update_(R, $\nabla_R f$ )   ▷ Gradient descent, orthogonality ensured by special parameterization
      if $k > p$ and $k \bmod t = 0$ then
          $I$ = mutual_info($R, c, B$)                                ▷ $I \in \mathbb{R}^{S\times S}$
          if any $\frac{I_{[s_1][s_2]}}{d_{s_1}+d_{s_2}} > \tau$ then
              Sort by $\frac{I_{[s_1][s_2]}}{d_{s_1}+d_{s_2}}$ and select top $S/8$ non-intersecting pairs $> \tau$
              Update configuration c (and R if necessary, to keep the correspondence between c and
  sub-matrices of R)
          else
              break
          end if
      end if
  end for
  return R, c
```

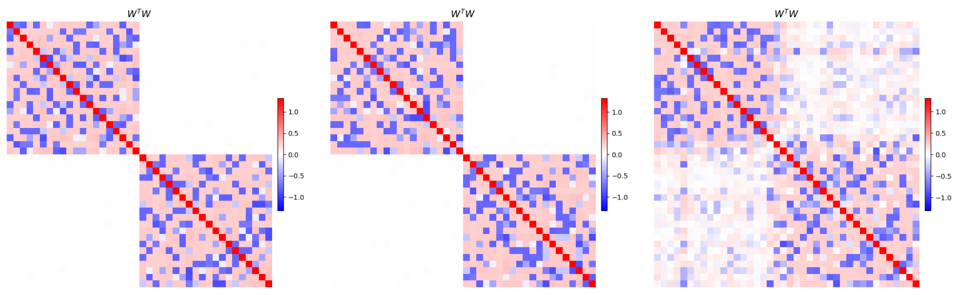

(a) $S = 0$ (b) $S = 0.5$ (c) $S = 0.75$

Figure 6: $\mathbf{W}^T\mathbf{W}$, $z = 40$, $d = 12$, group=(20, 20)

subspace a, b, c, if (a, b) is selected, (b, c) will not be selected. We merge at most $S/8$ pairs, where S is the number of subspaces. Note that merging does not change the weights of $\mathbf{R}$ (or just reordering), merging affects the training as we now search the nearest neighbor in the joint space and optimize the distance in the joint space. When we merge subspaces, the optimizer states (for the whole $\mathbf{R}$ are also re-initialized.

Note that although we have experimented with some alternatives, these specific details are not necessarily optimal, each part of the method can be studied and optimized more extensively in the future.

Lastly, to clarify which hyperparameters we refer to throughout the rest of the paper. We assign them the following names: the initial dimensionality for subspaces is referred as unit size (i.e. $d_1, \cdots d_S$ in Algorithm 1 which are equal at the beginning). We search the nearest neighbor among N activations (including the point itself, so only $N - 1$ candidates), we refer this as search number (i.e. equal to $n \times m$ in Algorithm 1). The orthogonal matrix is first trained for some steps, during this stage no merging happens, we call it merging start delay. After this stage, we measure MI and merge subspaces every t step, we call t merging interval. Lastly, the normalized MI threshold τ is called merging threshold.

C More Experiments in Toy Setting

C.1 Toy Model Feature Geometry

In this section, we extend the experiment in Sec 2 with more different configurations. We keep model the same, while changing the feature group structure and model dimensions to bring a more comprehensive view. We use group=(20, 20) to refer to 2 groups, each group has 20 features, other cases follow this pattern. All experiments in toy setting is done with batch size of 128, training steps of 10000, Adam optimizer, and linear learning rate scheduler which decrease learning rate from 0.003 to 0.0003. The trained model is tested on 12800 samples. Overall, we see strong orthogonal structure in all cases.

Group Sparsity We refer the probability for a whole feature group being not activating as group sparsity S. In Sec 2 we have experimented with $S = 0.25$. We keep other parameters the same ($z = 40$, $d = 12$, group=(20, 20)), but set $S = 0.0$ (Fig. 6a) $S = 0.5$ (Fig. 6b) and $S = 0.75$ (Fig. 6c). We train the model until convergence and final FVU is 0.028, 0.028 and 0.035 respectively. From the figures we can see as the S increases, features in different groups are less likely to co-occur, thus more similar to mutual exclusive condition, which encourages superposition. So we see weaker orthogonality (bottom left and top right submatrices are nonzero, though the absolute values are smaller) when $S = 0.75$.

More Groups and Different Hidden Dimension We also experiment with group=(5, 15, 5, 15), $z = 40$, $S = 0.25$, and $d = 10, 12, 16$, corresponding to 3 subfigures in Fig. 7. Final FVU are 0.166, 0.066, 0.016 for $d = 10, 12, 16$ respectively. We can still see similar orthogonal structure. When $d = 10$, the dimensionality is not enough to allocate orthogonal subspaces to each group, and the

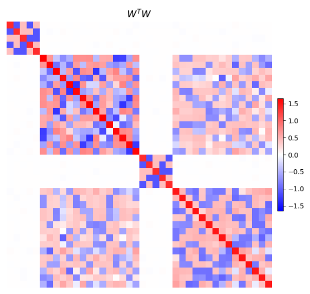

(a) $d = 10$

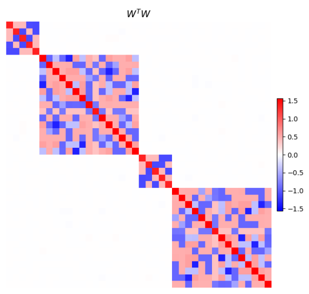

(b) $d = 12$

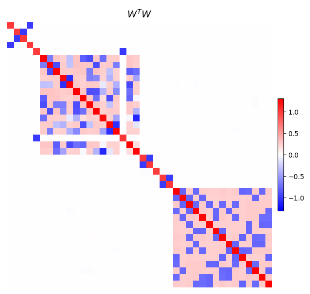

(c) $d = 16$

Figure 7: $\mathbf{W}^T\mathbf{W}$, $z = 40$, group=(5, 15, 5, 15), $S = 0.25$

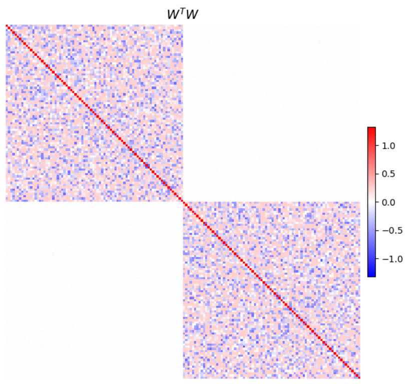

(a) $d = 32$, $z = 160$, $S = 0.25$, group=(80, 80)

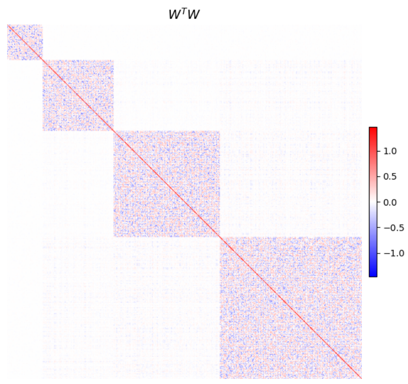

(b) $d = 64$, $z = 400$, $S = 0.25$, group=(40, 80, 120, 160)

Figure 8: $\mathbf{W}^T\mathbf{W}$

features from 2nd and 4th groups are superposed (as their frequency is lower than those from the other two groups), and the model cannot reconstruct $\boldsymbol{x}$ very well. When $d = 16$, as the dimensionality constraint becomes more relieved, orthogonality also occurs within groups.

More Features We increase the total number of features and experiment with 2 configurations. (a) $d = 32$, $z = 160$, $S = 0.25$, group=(80, 80), Fig. 8a, final FVU is 0.025. (b) $d = 64$, $z = 400$, $S = 0.25$, group=(40, 80, 120, 160), Fig. 8b, final FVU is 0.033. Again, the orthogonal structure is very obvious.

C.2 Toy Model Subspace Partitioning

In this section, we describe more experiments of NDM in toy setting. We apply it for toy models trained in previous section (Sec. C.1) whose orthogonal structure is clear.

Experimental Details For toy setting, we use a slightly different version from Algorithm 1. Specifically, we find it is not necessary to search over a huge amount of subspace activations, so we search for the nearest neighbor inside the batch (Eq. 3) thus simplify the algorithm. In addition, we find $\mathbf{R}$ usually get stuck at sub-optimal point. When observing $\mathbf{RW}$, we usually find one subspace is computed from two feature group, and this is usually accompanied with higher overall training loss, and more training steps and changing hyperparameters in Adam optimizer do not seem to help. We apply the following heuristics: we take the subspace with the largest loss and measure MI between this and all other subspaces, and multiply the MI values with loss of all other subspaces, then divide the resulting values (always > 0) by their sum as the probability by which we randomly choose the other subspace. This process selects two large loss subspaces which encodes similar information.

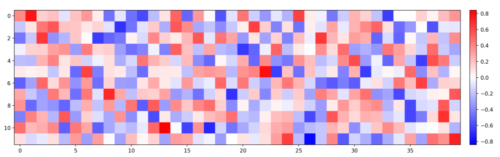
(a) $\mathbf{W}$ or $\mathbf{RW}$ before training. $\mathbf{R}$ is initialized as an identity matrix

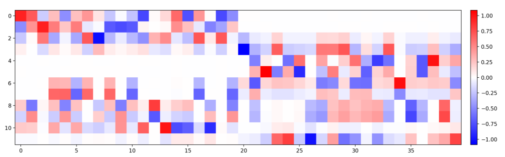
(b) $\mathbf{RW}$ after first 3k training step. Corresponding configuration $d_1 = 2, d_2 = 2, \cdots, d_6 = 2$

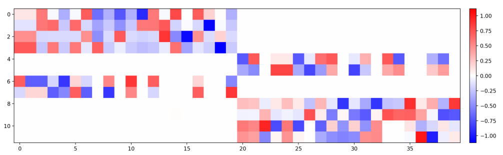
(c) $\mathbf{RW}$ after 60k training step before merging. Corresponding configuration $d_1 = 2, d_2 = 2, \cdots, d_6 = 2$

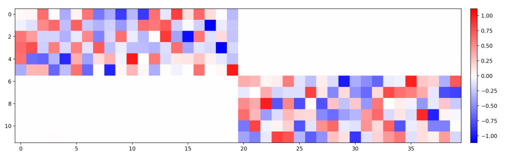
(d) $\mathbf{RW}$ after entire training procedure completes. Corresponding configuration $d_1 = 6, d_2 = 6$

Figure 9: $\mathbf{RW}$ at different stages of training. The toy model is the one from Fig. 1a, where $d = 12$ $z = 40$, group=(20, 20), $S = 0.25$

We multiply their corresponding rows in $\mathbf{R}$ with a random orthogonal matrix ($\in \mathbb{R}^{(d_1+d_2)\times(d_1+d_2)}$), thus re-initialize the weights for these two subspaces by mixing these two subspaces, while the whole matrix $\mathbf{R}$ remains orthogonal. We find that this technique helps R achieve lower training loss and produce a more ideal $\mathbf{RW}$. In other words, we have a better chance to find global minimum. But we also find this becomes less effective when number of features and dimension become larger. This also calls for more study on this atypical optimization problem, i.e., with orthogonality constraint and ignorance of distance change to all but the nearest neighbor when computing gradients.

For reproducibility we report the hyperparameters used as follows: We use euclidean distance as the optimization objective. We find 1 - cosine similarity leads to worse results, we also find taking the square or logarithm of the distance does not help. We use 2 as the unit size. We use search number $N = 4$. We find small search number is crucial, it can be much smaller than the number of features, but we are unclear about why small search number helps. For re-initialization of largest loss, we evaluate the loss (distance to nearest neighbor) on a much larger search number, $N = 1024$, which we find more accurate for selecting the correct subspace (subspace that contains more than 1 feature group). We use batch size of 128, learning rate of 0.001, and Adam optimizer. As we described previously, the training step is not fixed. Merge start delay is 60k steps, during this stage two subspaces are randomly re-initialized every 3k step. The optimizer states for the whole matrix are also re-initialized. After the 60k steps, we measure MI and merge subspaces with merge interval of 3k steps, and merge threshold of 0.04. Importantly, we use the same set of hyperparameters for all experiments in toy setting, regardless of the varying number of features and activation dimension.

Experimental Results We train $\mathbf{R}$ for toy models whose orthogonal structure is clear. Concretely, we present 4 experiments here, corresponding to toy models visualized in Fig. 1a, Fig. 7b, Fig. 8a and Fig. 8b. The results are shown in Fig. 9, 10, 11, 12. We can see the proposed method is quite effective. Before merging, each subspace gradually learns to encode only one feature group. For example, in Fig. 9c, each 2D subspace in $\hat{\boldsymbol{h}}$ is computed either from the first or the second feature group (e.g., the first 2 rows only have nonzero entries in first 20 columns, corresponding to the first group). In Fig. 10, at the beginning the third subspace encodes all 4 groups (a), then after 3k steps it only encodes the 1st and 3rd group (b), then later it encodes only the 1st group. We can clearly see how NDM training objective leads $\mathbf{R}$ to evolve towards the desirable direction. Loss values also confirm the alignment between neighbor distances and "purity" of subspace (encoding one group instead of a mixture of groups). We denote the loss when search number is 4 as $l_{N=4}$, and similarly $l_{N=1024}$. We take the mean of loss across subspaces instead of sum when reporting them. For example, Fig. 9b's loss values are: $l_{N=4} = 0.212$ and $l_{N=1024} = 0.011$. After more training when subspaces are "pure" (subfigure c), loss values are: $l_{N=4} = 0.194$ and $l_{N=1024} = 0.004$. Another example, Fig. 10 loss values are: $l_{N=4} = 0.340$ and $l_{N=1024} = 0.016$ for subfigure b, and $l_{N=4} = 0.322$ and $l_{N=1024} = 0.004$ for subfigure c. Importantly, we also see that $\mathbf{R}$ sometimes does not find global minimum. In Fig. 11 and 12, we see some sub-optimal subspaces, such as the 3rd subspace from the

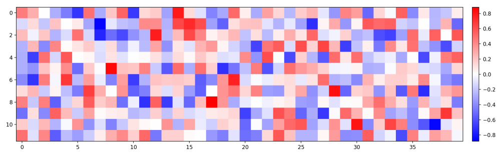
(a) **W** or **RW** before training. **R** is initialized as an identity matrix

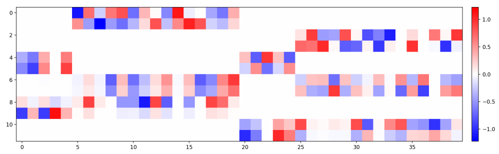
(b) **RW** after first 3k training step. Corresponding configuration $d_1 = 2, d_2 = 2, \cdots, d_6 = 2$

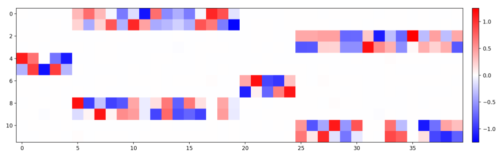
(c) **RW** after 60k training step before merging. Corresponding configuration $d_1 = 2, d_2 = 2, \cdots, d_6 = 2$

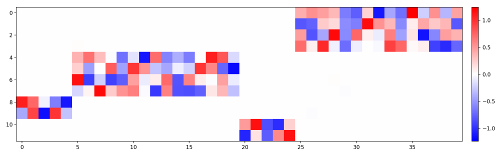
(d) **RW** after entire training procedure completes. Corresponding configuration $d_1 = 4, d_2 = 4, d_3 = 2, d_4 = 2$

Figure 10: **RW** at different stages of training. The toy model is the one from Fig. 7b, where $d = 12$ $z = 40$, group=(5, 15, 5, 15), $S = 0.25$

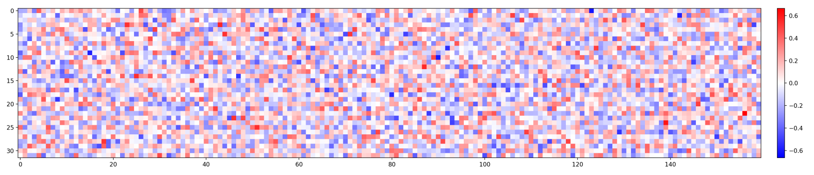
(a) **W** or **RW** before training. **R** is initialized as an identity matrix

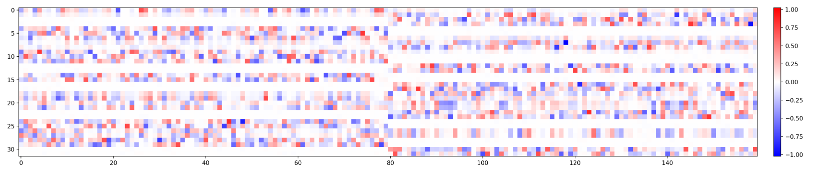
(b) **RW** after first 3k training step. Corresponding configuration $d_1 = 2, d_2 = 2, \cdots, d_{16} = 2$

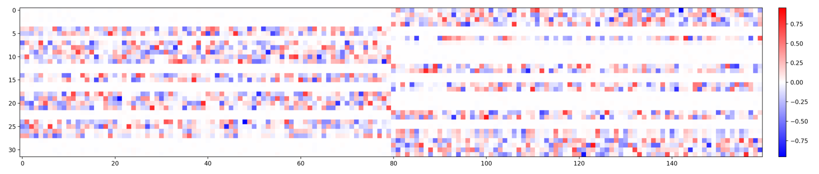
(c) **RW** after 60k training step before merging. Corresponding configuration $d_1 = 2, d_2 = 2, \cdots, d_{16} = 2$

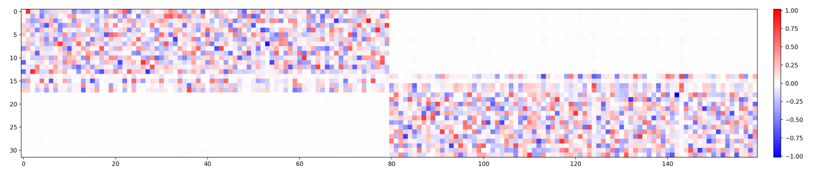
(d) **RW** after entire training procedure completes. Corresponding configuration $d_1 = 18, d_2 = 14$

Figure 11: **RW** at different stages of training. The toy model is the one from Fig. 8a, where $d = 32$ $z = 160$, group=(80, 80), $S = 0.25$

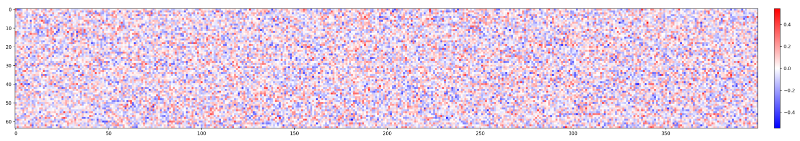

(a) **W** or **RW** before training. **R** is initialized as an identity matrix

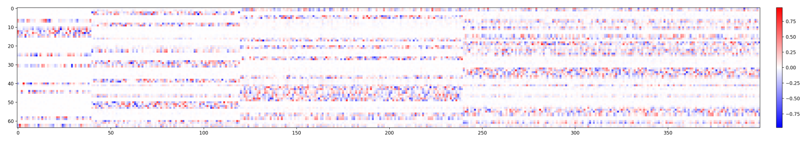

(b) **RW** after first 3k training step. Corresponding configuration $d_1 = 2, d_2 = 2, \cdots, d_{16} = 2$

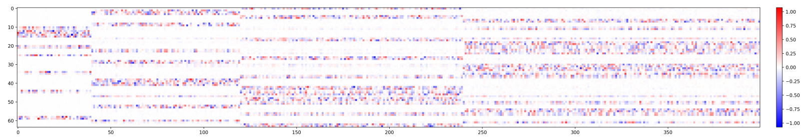

(c) **RW** after 60k training step before merging. Corresponding configuration $d_1 = 2, d_2 = 2, \cdots, d_{16} = 2$

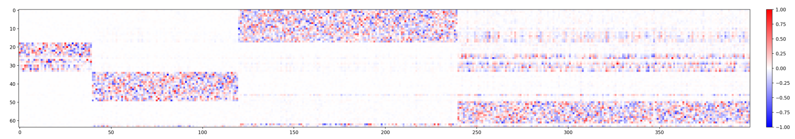

(d) **RW** after entire training procedure completes. Corresponding configuration $d_1 = 18, d_2 = 16, d_3 = 16, d_4 = 12, d_5 = 2$

Figure 12: **RW** at different stages of training. The toy model is the one from Fig. 8b, where $d = 32$ $z = 400$, group=(40, 80, 120, 160), $S = 0.25$

last in Fig. 11c, which is the reason for later imperfection of final $\mathbf{R}$. Moreover, we also see that the proposed MI-based merging works well. It correctly merges the subspaces encoding the same group. For example, in Fig. 10, normalized MI between 1st and 5th subspace is 0.55, and between 2nd and 6th is 0.49, normalized MI between all other pairs is below 0.03. In Fig. 9 and 10, we get the correct number of subspace and their dimension. In Fig. 11 and 12, the final configuration is imperfect but close to the ground truth. As mentioned before, we generally find the imperfection results from $\mathbf{R}$ being unable to find global minimum or disentangle feature groups for a few subspaces, the MI estimate usually works well.

In summary, we find the training objective of NDM indeed encourages subspaces to encode only one feature group. Together with MI based merging, the final subspace partition is close to the groundtruth, with each subspace encoding one feature group. While training objective aligns well with our goal, the orthogonal matrix sometimes gets stuck at local minimum of this objective, resulting in sub-optimal partition. Nevertheless, it might not be necessary to achieve perfect partition to make itself useful in practice. In subfigure b of Fig. 9-12, we observe that these sub-optimal points already have a good deal of disentanglement, which could potentially be very useful when using these subspaces as analyzing unit instead of random subspaces.

lastly, more experiments can be done in toy setting, we have not done extensive experiments exploring the effect of varying unit size and search number, much more feature groups, and many other aspects. More rigorous study can be done in this ideal testbed, but we would like to focus more on real world language models, in order to address more urgent concerns about whether the orthogonal structure even exists in real models.

D Quantitative Experiments on Language Models

D.1 Subspace Patching

Here we describe our method in detail. Formally, suppose $\boldsymbol{h}_{\text{cln}}$ and $\boldsymbol{h}_{\text{crp}}$ are the activations from clean and corrupt inputs respectively, at the same layer and token position. We patch subspace s as follows:

$$\hat{\boldsymbol{h}}_{\text{crp}} = \mathbf{R}\boldsymbol{h}_{\text{crp}} \tag{7}$$

$$\hat{\boldsymbol{h}}_{\text{cln}} = \mathbf{R}\boldsymbol{h}_{\text{cln}} \tag{8}$$

$$\hat{\boldsymbol{h}}_{\text{crp}} = \begin{bmatrix} \hat{\boldsymbol{h}}^{(1)}_{\text{crp}} \\ \vdots \\ \hat{\boldsymbol{h}}^{(s)}_{\text{crp}} \\ \vdots \\ \hat{\boldsymbol{h}}^{(S)}_{\text{crp}} \end{bmatrix}, \quad \hat{\boldsymbol{h}}_{\text{cln}} = \begin{bmatrix} \hat{\boldsymbol{h}}^{(1)}_{\text{cln}} \\ \vdots \\ \hat{\boldsymbol{h}}^{(s)}_{\text{cln}} \\ \vdots \\ \hat{\boldsymbol{h}}^{(S)}_{\text{cln}} \end{bmatrix} \tag{9}$$

$$\hat{\hat{\boldsymbol{h}}} = \begin{bmatrix} \hat{\boldsymbol{h}}^{(1)}_{\text{cln}} \\ \vdots \\ \hat{\boldsymbol{h}}^{(s)}_{\text{crp}} \\ \vdots \\ \hat{\boldsymbol{h}}^{(S)}_{\text{cln}} \end{bmatrix} \tag{10}$$

$$\bar{\boldsymbol{h}} = \mathbf{R}^T\hat{\hat{\boldsymbol{h}}} \tag{11}$$

after patching, the model uses $\bar{\boldsymbol{h}}$ to finish the rest of the forward pass on the clean input. To measure the patching effect, we first run the model on clean input, recording the original logits or probability, which we refer to as clean run. Then we run the model on corrupted input, to save the corrupted activations $\boldsymbol{h}_{\text{crp}}$, which we refer to as corrupted run. Finally we run the model on clean input, with certain subspace activation being patched with the value saved in corrupted run, and record the patched logits or probability, which we refer to as patched run. We compare the model output from clean run and patched run to measure the subspace patching effect.

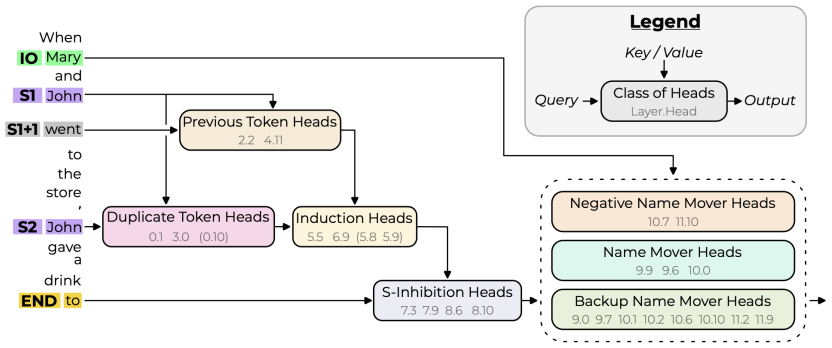

Figure 13: IOI circuit, Fig. 2 from (Wang et al., 2022). Attention heads in this figure is denoted as `layer_index.head_index`. E.g., The second previous token head, 4.11, refers to layer 4 and attention head 11 in that layer. Note that indices start from 0.

D.2 GPT-2 Small Test Suite

Tests based on IOI circuit The Indirect Object Identification (IOI) task consists of sentences like: “When Mary and John went to the store, John gave a drink to _”, which should be completed with “Mary”. (Wang et al., 2022) found a circuit in GPT-2 Small responsible for solving this task (Fig. 13). Besides computational graph, they also reveal the information moved between the nodes of the graph.

To understand our intervention, we briefly describe the information flow inside the circuit: At token S1+1 (see Fig. 13 for the notation), the model attends the previous token and moves the name from it, which will be used as key in later induction heads. *Right after layer 4, the model finishes moving previous token information, and this information is not yet used by downstream components.* At token S2, the induction heads attend to S1+1, moving the relative position of S1 (i.e., it occurs before or after IO, or equivalently, S1+1 is “and” or “went”). Meanwhile, Duplicate token heads attend to S1 from S2, moving S name and relative position of S1. Therefore, at S2’s residual stream, *right after layer 6 the model finishes moving position information of S1, and it is not yet moved by any downstream component*. Then at END token, S-Inhibition heads attend to S2 and move the position information of S1 and as well as the S name. *Right after layer 8, the model finishes moving position information of S1 and information of S name, and they are not yet used by any name mover heads.* Lastly, name mover heads avoid attending S1 by using those information and attend to IO to move IO name. Note that the claims about the moved information is supported by strong causal evidence from (Wang et al., 2022), and is confirmed again with a different method in (Huang et al., 2024b).

Importantly, we emphasize 3 key places in the circuit in our description (see the italics). Specifically, $\boldsymbol{h}_{\text{S1+1}}^{4,\text{post}}$, $\boldsymbol{h}_{\text{S2}}^{6,\text{post}}$, $\boldsymbol{h}_{\text{END}}^{8,\text{post}}$. They are ideal for causal intervention because in those places we know the existing information, and all heads that gather the information are before the place and all heads that use the information are after the place. In contrast, if we intervene on $\boldsymbol{h}_{\text{S1+1}}^{3,\text{post}}$ to change previous token information, the changed information might be overwritten by head 4.11, resulting in negligible effect even if we intervene on the right subspace. This is also the reason why we do not pick the layer after duplicate token heads, because similar information will be added later by induction heads. Moreover, if we intervene on $\boldsymbol{h}_{\text{S1+1}}^{5,\text{post}}$ to change previous token information, it will only affect induction head 6.9, while the original information was already moved by heads in layer 5. We do not select $\boldsymbol{h}_{\text{END}}^{11,\text{post}}$ because we suspect there is a big “output subspace” after the last layer and our method would not be very interesting there.

Based on the information used in the circuit, we design two kinds of counterfactual inputs. **(1) Position Swap**. We swap the position of the IO and S1 in the sub-clause at the beginning. For example, clean input: “When Mary and John went to the store, John gave a drink to”; corrupted input: “When John and Mary went to the store, John gave a drink to”. **(2) Name Swap**. We swap the names of IO and S (both S1 and S2). For example, clean input: “When Mary and John went to the store, John gave a drink to”; corrupted input: “When John and Mary went to the store, Mary gave a drink to”.

Finally, we design following tests:

1. Do subspace patching in residual stream $\boldsymbol{h}_{\text{S1+1}}^{4,\text{post}}$ and $\boldsymbol{h}_{\text{IO+1}}^{4,\text{post}}$ (IO+1 means the token following IO), using Position Swap. If the information about previous token is successfully changed, then in the patched run, induction heads would attend IO+1 instead of S1+1. Therefore, the induction heads would move the position of IO instead of S1, and pass the changed information to later components and cause name mover heads to avoid attending IO.
2. Do subspace patching in residual stream $\boldsymbol{h}_{\text{S2}}^{6,\text{post}}$ using Position Swap. If patching in the right subspace, corrupted activations should contain a different position of S1, thus cause the model to change towards an opposite prediction, similar to the explanation above.
3. Do subspace patching in residual stream $\boldsymbol{h}_{\text{END}}^{8,\text{post}}$ using Position Swap. This is to change the position of S1 in the residual stream of END.
4. Do subspace patching in residual stream $\boldsymbol{h}_{\text{END}}^{8,\text{post}}$ using Name Swap. This is to change the S name in the residual stream of END.

For all 4 tests in IOI circuit, we measure the drop in logit difference, we denote it as ΔLD. So $\Delta LD = (\text{logit}_{\text{cln}}^{\text{IO}} - \text{logit}_{\text{cln}}^{\text{S}}) - (\text{logit}_{\text{pch}}^{\text{IO}} - \text{logit}_{\text{pch}}^{\text{S}})$, where $\text{logit}_{\text{cln}}^{\text{IO}}$ is the logit value for IO name on the clean run, and $\text{logit}_{\text{pch}}^{\text{IO}}$ is the logit value for IO name on the patched run, and similarly for S. We use 1000 examples, which are clean inputs, and we construct counterfactual inputs on-the-fly. In these examples, the order of IO and S1 in the sub-clause is uniformly random. The names are picked randomly from a list of common one-token names. The template ("When ... went to the store, ... gave a drink to", "Then, ... had a long argument, and afterwards ... said to", etc.) is also picked randomly from a pre-defined list. The final reported effect ΔLD is averaged over the 1000 samples.

Test based on Greater-than circuit The Greater-than task (Hanna et al., 2023) consists of sentences in the form "The `<noun>` lasted from the year `XXYY` to the year `XX`", such as "The war lasted from the year 1732 to the year 17", the model should assign higher probability to years greater than 32, thus performing the simple greater-than math operation. (Hanna et al., 2023) revealed a circuit in GPT-2 Small responsible for solving this task. Briefly speaking, some attention heads between layer 5 to layer 9 (both inclusive) move `YY` to the last token's residual stream, and MLP layer 8 to 11 (both inclusive) specify which years are greater than `YY`. Therefore, *right after layer 9, the model finishes moving `YY` to the last token*, so we intervene at $\boldsymbol{h}_{\text{END}}^{9,\text{post}}$ to change the `YY`, where END denotes the last token.

Regarding counterfactual inputs, we use the same as the original paper: the `YY` in clean input is replaced by 01. For example, clean input: "The war lasted from the year 1732 to the year 17"; corrupted input: "The war lasted from the year 1701 to the year 17".

We do one test based on Greater-than circuit (continue the indexing from IOI tests):

5. Do subspace patching in residual stream $\boldsymbol{h}_{\text{END}}^{9,\text{post}}$, using 01 counterfactual input. If the information `YY` is successfully replaced with 01, the sum of the probability of years greater than `YY` will decrease.

Unlike IOI, we do not compare logits of two tokens as there are many possible answers. Instead, we compute the drop in sum of the probability of valid answers, we denote it as ΔP. In our running example where `YY`=32, it means $\Delta P = P_{\text{cln}}(\text{next token} \in \{33, 34, \cdots, 99\}) - P_{\text{pch}}(\text{next token} \in \{33, 34, \cdots, 99\})$, where P_{cln} and P_{pch} denotes probability in clean and patched run respectively.

Similar to IOI, the inputs for this task is also constructed from random nouns, years and random templates, while restricting years such that they are always 2-token long. The final reported effect ΔP is averaged over the 1000 samples.

Measuring target information inequality Therefore, we have 5 tests in total for GPT-2 Small, and 4 layers are involved. To test a training configuration of NDM, we apply the same procedure and hyperparameters to train 4 orthogonal matrices, for post MLP residual stream at layer 4, 6, 8, 9 respectively. Then apply the 5 aforementioned tests to each of the subspaces found in corresponding layer.

Each test changes one *type* of information. Analogously it means a fixed "variable", while the "variable" can take many different values. To measure if the target information (the "variable" we are interested in) only lives in one subspace, we quantify the inequality of patching effect across subspaces by calculating Gini coefficient. Same as before, s is subspace index, for the patching effect Δ_s (can be either ΔLD_s or ΔP_s), Gini coefficient is

$$G = \frac{\sum_{s_1=1}^{S} \sum_{s_2=1}^{S} |\Delta_{s_1} - \Delta_{s_2}|}{2S \sum_{s=1}^{S} \Delta_s} \tag{12}$$

A Gini coefficient of 0 means the effect is evenly distributed across all subspaces. If the effect is nonzero for only one subspace and zero elsewhere, the Gini coefficient will be close to 1.0 (the more subspaces there are, the closer it gets). If the effect is concentrated in about half of the subspaces, the Gini coefficient will fall somewhere in between. So by using Gini coefficient, the inequality of effects across subspaces or the inequality of the amount of target information across subspaces is summarized as one value, which makes our evaluation easier.

Importantly, there is one trivial way to get high value in this metric while not matching our expectation: there can be one big subspace and many tiny subspaces (e.g., one dimensional), the big one would presumably encode the target information, but as well as many other types of information. Therefore, we also calculate Gini coefficient after dividing the patching effect by the dimension of the subspace, which computes the "density" of target information in each subspace, or "amount of target information per dimension". Moreover, there can be another trivial way to get high value in the second metric: one can use PCA to concentrate variance or compress information into a few subspaces, thus these subspaces would have high "density" for all kinds of information. This again goes against our expectation, as we want subspaces to have high "density" for one or few kinds of information and low "density" for all others. Therefore, the third metric is to calculate Gini coefficient after dividing the patching effect by the sum of the variance of each axis in the subspace. We refer to this sum of variance as Var_s. We report all 3 variants (original effect, normalized by dimension, normalized by variance) in the results. Ideally, a good subspace partition should achieve high values in all 3 metrics.

D.3 NDM Training Details on GPT-2 Test Suite

We use the NDM algorithm described in Sec. 3 (with more details provided in App. B and Algorithm 1).

For reproducibility, we report the hyperparameters used as follows: We use euclidean distance as the optimization objective. We use 32 as the unit size. We try different search numbers $N = \{1 \times 2^{14}, 5 \times 2^{14}, 25 \times 2^{14}\}$. We do not do random re-initialization during the pre-merging stage like we did for the toy setting; preliminary results show this is not helpful for language models. We use batch size 128, learning rate 0.0003, and Adam optimizer. We try different merging intervals, 4k and 8k, and set the merging start delay as 2.5 times the merging interval. Longer merging intervals mean more training steps in general. We set 100k as the maximum training steps, which is usually not reached. We also try different merging threshold $\{0.02, 0.03, 0.04, 0.05\}$. We use MiniPile (Kaddour, 2023) as the data to run GPT-2 Small when collecting activations, instead of the OpenWebText dataset which is similar to GPT-2 pretraining data. Therefore, we do hyperparameter search over all the combinations of different search numbers, merging interval, and merging threshold, while other hyperparameters are always the same. For each hyperparameter configuration, we train 4 orthogonal matrices for post-MLP residual stream at layer 4, 6, 8, 9 respectively, as they are needed in the test suite.

As shown in later section, the best configuration is search number = $25 \times 2^{14}\}$, merging interval = 8k, merging threshold = 0.04. In Fig. 14, we show the MI after training, compared with the identity matrix, which is used to initialize $\mathbf{R}$.

In later section, we show ablation studies, and some of the hyperparameter choices will be justified by those results.

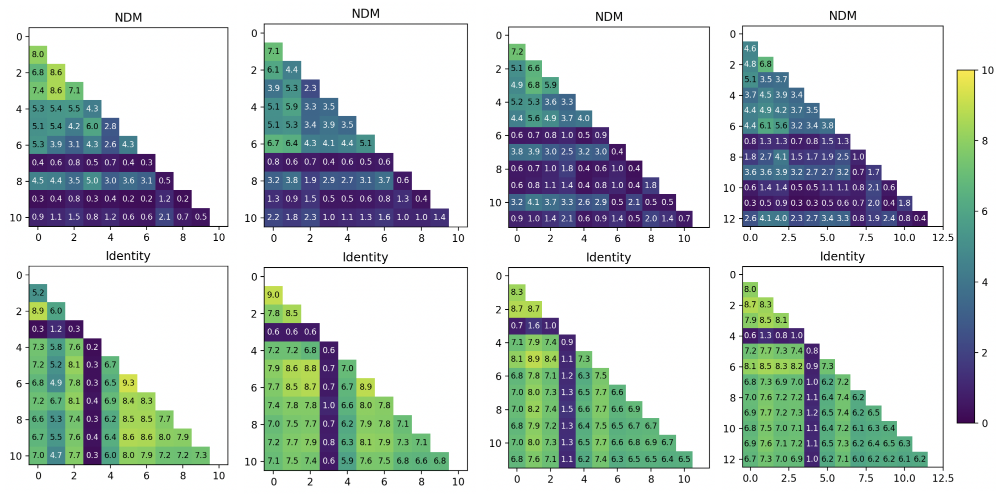

(a) $\boldsymbol{h}^{4,post}$ (b) $\boldsymbol{h}^{6,post}$ (c) $\boldsymbol{h}^{8,post}$ (d) $\boldsymbol{h}^{9,post}$

Figure 14: MI between each pair of subspaces. Top row: subspace partition given by NDM. Bottom row: subspace partition using the identity matrix and the dimensionality configuration given by NDM. Columns correspond to 4 layers in GPT-2 Small. We use the same MI estimation method as the one used during training. The MI values are not normalized. Bigger values in the top left corner are because subspaces are sorted in descending order according to dimensionality. We can see NDM produces more independent subspaces.

index s	0	1	2	3	4	5	6	7	8	9	10	11	12
d_s	128	96	96	64	64	64	64	32	32	32	32	32	32
Var_s $(\times 10^3)$	2.1	2.7	1.3	0.6	0.8	1.4	1.7	1.0	1.0	0.4	4.0	4.8	0.3
ΔP_s $(\times 10^{-2})$	5.4	0.7	1.8	1.9	29.7	0.6	0.6	0.3	0.6	0.8	1.2	0.7	0.7
$\frac{\Delta P_s}{d_s}$ $(\times 10^{-4})$	4.2	0.8	1.9	3.0	46.4	1.0	0.9	0.9	2.0	2.4	3.9	2.0	2.3
$\frac{\Delta P_s}{\text{Var}_s}$ $(\times 10^{-5})$	2.6	0.3	1.4	2.9	39.6	0.5	0.3	0.3	0.6	2.2	0.3	0.1	2.2

Table 2: Test 5 raw data for NDM results shown in main paper (Table 1). Gini coefficient for row ΔP_s is 0.72, for row $\frac{\Delta P_s}{d_s}$ is 0.67, and for row $\frac{\Delta P_s}{\text{Var}_s}$ is 0.78.

D.4 Representing Patching Effect Distribution with Gini Coefficient

We do not show the patching effect for each individual subspace, as there would be too many numbers, but rather summarize the degree of concentration using Gini coefficient. To provide a sense of how high the Gini coefficient should be for the partition to be considered good, we show some raw data in Table 2 - 4. We can see that, when the Gini coefficient is above 0.6 (Table 2), the distribution of the effect is quite satisfactory, as there is a single value much greater than all others. When Gini coefficient is around 0.5 (third and fifth row in Table 3), we do see some degree of concentration, but effect is concentrated in quite a few subspaces. Lastly, if Gini coefficient is lower than 0.3 (Table 4), we do not see any significant degree of concentration. Therefore, we can say that Gini coefficient should be greater than 0.6 to be considered "good", and the higher the better. In other sections of the paper, we only report Gini coefficients for the GPT-2 Small test suite.

D.5 Ablation Study on GPT-2 Test Suite

We also show hyperparameter searching results in Table 5, in order to provide information on how each factor affects the training result. First of all, we can see it is better to have larger merging interval, in other words, more training steps. Due to compute limits, we do not further experiment with more training steps, which would probably produce better results. Moreover, we show the same data in Fig. 15, using search number as the variable on x-axis. We can see that larger search number generally produces better results, though depending on merging threshold. However, considering both search

index s	0	1	2	3	4	5	6	7	8	9	10
d_s	192	128	64	64	64	64	64	32	32	32	32
Var_s $(\times 10^3)$	0.3	0.3	0.2	0.2	0.3	0.3	0.4	0.3	0.3	0.4	10.7
ΔLD_s $(\times 10^{-1})$	14.8	11.6	7.6	4.2	3.1	2.5	2.9	1.4	1.6	0.9	2.2
$\frac{\Delta LD_s}{d_s}$ $(\times 10^{-3})$	7.7	9.1	11.9	6.6	4.8	3.9	4.6	4.4	5.0	2.9	6.8
$\frac{\Delta LD_s}{\text{Var}_s}$ $(\times 10^{-4})$	49.5	37.6	38.5	18.1	11.0	7.5	7.1	5.5	5.2	2.2	0.2

Table 3: Test 2 raw data for PCA 1 baseline results shown in main paper (Table 1). Gini coefficient for row ΔLD_s is 0.46, for row $\frac{\Delta LD_s}{d_s}$ is 0.22, and for row $\frac{\Delta LD_s}{\text{Var}_s}$ is 0.52.

index s	0	1	2	3	4	5	6	7	8	9	10
d_s	128	128	96	96	64	64	64	32	32	32	32
Var_s $(\times 10^3)$	0.7	1.0	0.5	7.9	0.4	0.2	0.2	0.1	0.1	0.1	0.1
ΔLD_s $(\times 10^{-1})$	3.9	3.7	2.3	2.5	1.6	1.7	1.7	0.7	0.8	0.8	0.7
$\frac{\Delta LD_s}{d_s}$ $(\times 10^{-3})$	3.0	2.9	2.4	2.6	2.4	2.6	2.7	2.2	2.4	2.4	2.2
$\frac{\Delta LD_s}{\text{Var}_s}$ $(\times 10^{-4})$	5.5	3.6	4.7	0.3	4.0	8.1	9.1	5.2	8.0	7.7	7.0

Table 4: Test 1 raw data for identity baseline results shown in main paper (Table 1). Gini coefficient for row ΔLD_s is 0.33, for row $\frac{\Delta LD_s}{d_s}$ is 0.05, and for row $\frac{\Delta LD_s}{\text{Var}_s}$ is 0.23.

number and merging interval, when given fixed compute budget, it is a trade-off between searching among more activations per step and performing more training steps. Determining which side we should spend more compute on is an important question and should be explored more extensively in future work.

We also consider other alternatives for other hyperparameters. In Table 6 we compare different distance metric, under different condition. We use good hyperparameters for merging threshold (0.04 or 0.05) and merging interval (8000) based on our previous finding. When using cosine similarity as distance metric, losses (average distances) from different subspaces are weighted by the subspace dimensions. We found it important, because in some preliminary experiments where there is no such weights, the orthogonal matrix prioritizes maximizing cosine similarity for small subspaces while the big subspaces are somewhat ignored. From the results we can see that cosine similarity produces similar or worse results, which is consistent with our choice in toy setting.

In Table 7 we compare different data sources, i.e., the text data on which we run GPT-2 Small to collect activations. Again, we use merging threshold of 0.04 or 0.05, and merging interval of 8000. We can see that OpenWebText produces worse results in all cases, some of them are much worse. After checking Gini coefficient for individual tests, we found that using OpenWebText only hurts performance on test 2 - 5. We speculate that it is probably due to greater diversity in MiniPile.

A key hyperparameter is unit size, in the paper we normally use attention head dimension divided by 2. Though we think this is a very important aspect, we haven't done extensive testing on different

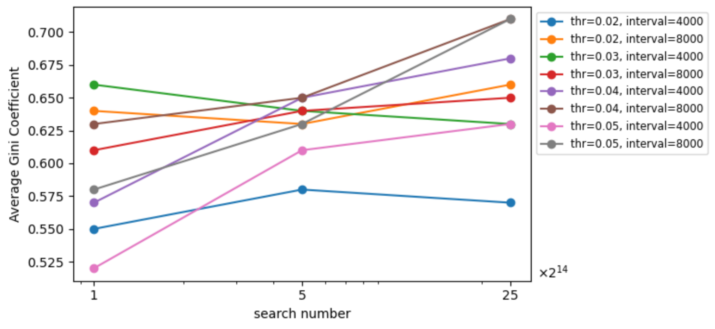

Figure 15: Average Gini coefficient on GPT2 test suite, as a function of search number, under different conditions. Same data as Table 5. X-axis is in log-scale.

search number ($\times 2^{14}$)	merging threshold	merging interval	number of subspaces	avg coefficient
1	0.02	4000	6,8,6,5	0.55
1	0.02	8000	9,9,9,9	0.64
1	0.03	4000	9,11,11,10	0.66
1	0.03	8000	9,11,11,10	0.61
1	0.04	4000	12,13,12,14	0.57
1	0.04	8000	12,12,13,14	0.63
1	0.05	4000	14,16,17,19	0.52
1	0.05	8000	13, 17,18,18	0.58
5	0.02	4000	5,8,7,6	0.58
5	0.02	8000	9,9,9,9	0.63
5	0.03	4000	8,8,9,10	0.64
5	0.03	8000	9,9,9,9	0.64
5	0.04	4000	11, 12, 14, 14	0.65
5	0.04	8000	10, 12, 13, 13	0.65
5	0.05	4000	12, 15, 16, 17	0.61
5	0.05	8000	12, 15, 16, 16	0.63
25	0.02	4000	5, 6, 5, 6	0.57
25	0.02	8000	9,9,9,9	0.66
25	0.03	4000	7, 9, 8, 10	0.63
25	0.03	8000	9, 9, 9, 10	0.65
25	0.04	4000	10, 10, 12, 13	0.68
25	0.04	8000	11, 11, 12, 13	0.71
25	0.05	4000	10, 13, 15, 16	0.63
25	0.05	8000	12, 15, 14, 15	0.71

Table 5: Combinations of different search number, merging threshold, and merging interval, and their resulting number of subspaces in the 4 layers used in the test (from low to high) and resulting average Gini coefficient on GPT-2 test suite. The one shown in Table 1 is the third row from the last, which is slightly better than the last row if we show more precision. Other hyperparameters are fixed, and described in D.3.

search number ($\times 2^{14}$)	merging threshold	avg coefficient	
		dist=1-cosine	dist=euclidean
1	0.04	0.62	0.63
1	0.05	0.58	0.58
5	0.04	0.64	0.65
5	0.05	0.64	0.63
25	0.04	0.65	0.71
25	0.05	0.68	0.71

Table 6: Average Gini coefficient on GPT2 test suite. We set merging interval as 8000. The last column comes from Table 5. Compared to euclidean distance, using cosine similarity produces in similar or slightly worse results

search number ($\times 2^{14}$)	merge threshold	avg coefficient	
		data=OpenWebText	data=MiniPile
1	0.04	0.54	0.63
1	0.05	0.54	0.58
5	0.04	0.59	0.65
5	0.05	0.58	0.63
25	0.04	0.61	0.71
25	0.05	0.60	0.71

Table 7: Average Gini coefficient on GPT2 test suite. We set merging interval as 8000. The last column comes from Table 5. Compared to MiniPile, using OpenWebText produces worse results. Closer look shows that, instead of degrading uniformly across all tests, using OpenWebText only hurts performance on test 2 - 5.

unit sizes as the search space is big and our compute budget is small. Moreover, the interaction of unit size and search number is also worth exploring, big search number might be less helpful when subspace dimension is small, thus we could spend compute on more training steps. More importantly, there could be many other changes, one could set search number depending on the dimension of the subspace instead of using the same search number for all subspaces throughout the whole training process, one could also do merging until a target number of subspaces is reached, instead of based on fixed threshold. In sum, we think there are many possibilities, we have only explored a small part of them, there is a lot of potential improvements for NDM.

D.6 Knowledge Conflict Experiment

Unlike the original purpose of RAVEL dataset, we do not aim to find separate subspaces for different types of attributes. Because we find many attributes given in RAVEL have high MI, e.g., the continent and country of a city, we think these attributes would not "naturally" been placed in separate subspaces, even if so, our method might merge them because of high MI. In contrast, we think there might be separate circuits routing context and parametric knowledge, and subspaces involved in these two circuits might be more separable.

We filter entities to make sure language models have parametric knowledge about them. Specifically, for each entity in RAVEL prize winner split, we prompt the model to complete "A. Michael Spence won the Nobel Prize in Economics. [target entity] won the Nobel Prize in", and only keep entities where model successfully predicts the ground truth. Moreover, we remove entities whose ground truth answer has more than one token. This includes "Linus Pauling" and "Marie Curie". This process produces 552 entities for Qwen2.5-1.5B and 719 for Gemma-2-2B after filtering, among total 927 entities in RAVEL's prize winner data split.

We only use Nobel prize winner data in RAVEL, because it satisfies several conditions: 1) Language models do not completely lean to one side. When there is no intervention, Original model choice should be ideally equally distributed between the context answer and parametric answer. Nobel prize winner data has a good distribution for both Qwen2.5-1.5B and Gemma-2-2B with this respect, make it possible to observe effect on both sides. 2) It should not be too hard for 2B models, such that we have enough instances to give a reliable result. 3) Answers are single tokens for the ease of implementation (not a real problem).

We patch subspace activations at all token positions together. In order to keep a simple one-to-one relationship between patching source and destination tokens, the made-up entity always has the same number of tokens as the target entity. We do so by prompting GPT-4o to generate random names that resemble real names, but are not associated with any well-known person. The length of generated names varies, ensuring that each target entity has at least one made-up name of the same number of tokens.

Hyperparameters for NDM are the same as those for GPT-2 (App. D.3), except for the following ones: We use 64 as the unit size for Qwen2.5-1.5B and 72 for Gemma-2-2B. We use $N = 25 \times 2^{14}$ as the search number. We set 150k as maximum training steps. We try different merging threshold $\{0.015, 0.02, 0.03, 0.04\}$ for Qwen and add one additional value 0.01 for Gemma. We try all these combinations and choose the best one. For Qwen2.5-1.5B, it is threshold = 0.02, merging interval = 8000; FOr Gemma-2-2B, it is threshold = 0.01, merging interval = 4000; We apply NDM to $\boldsymbol{h}^{11,mid}$ of Qwen2.5-1.5B (totally 28 layers) and $\boldsymbol{h}^{9,mid}$ of Gemma-2-2B (totally 26 layers). We choose the layer according to preliminary experiments where we patch the whole activation at the last token position of target entity.

After training the estimated MI decreases significantly, see Fig. 16 and 17. Interestingly, as we can see, the original basis of the representation space of Qwen2.5-1.5B is quite special, simply partition on standard basis can produce many independent subspaces.

We show baseline results in Fig. 18 and 19.

Some caveats for interpreting results We say the two mechanisms is mediated by different subspaces, instead of saying these subspaces encode contextual/parametric knowledge, as we do not know the underlying circuit, encoded information could also be others that support information routing, e.g., the value of target entity (as a key for retrieval), the fact that the entity is repeated in the

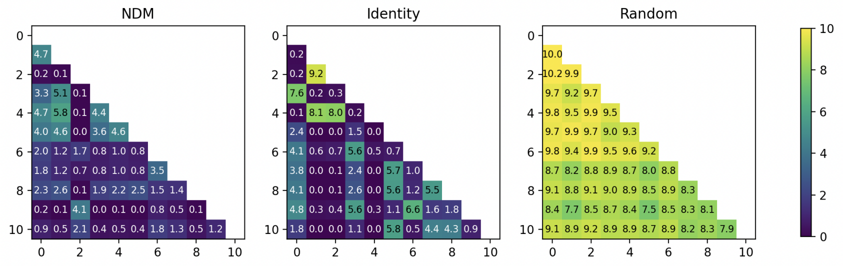

Figure 16: MI between each pair of subspaces. Activation site: $\boldsymbol{h}^{11,mid}$. NDM: subspaces given by NDM. Identity: subspaces given by the identity matrix and the dimensionality configuration from NDM. Random: subspaces given by the identity matrix and the dimensionality configuration from NDM. We use the same MI estimation method as the one used during training. The MI values are not normalized. We can see NDM produces more independent subspaces.

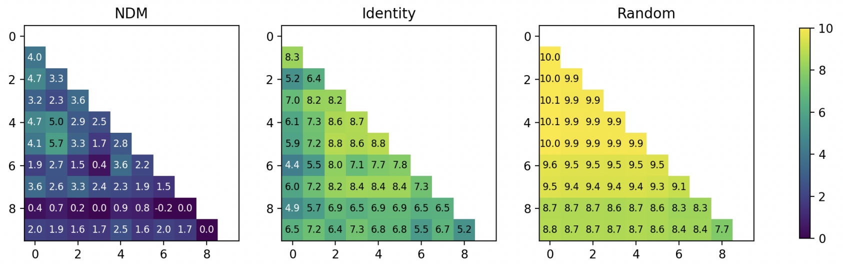

Figure 17: MI between each pair of subspaces. Activation site: $\boldsymbol{h}^{9,mid}$. See the previous Fig. 16 for explanation.

context (may trigger certain operation). They are different types of information and may be encoded in separate subspace, so effect does not have to be concentrated in one subspace. Moreover, it is also understandable if certain subspace is used in both mechanisms, thus having effect on both sides. So even if a subspace partition is perfect, it does not necessarily mean *all* subspaces only have effect on one side, but finding such subspaces is nevertheless a good sign. In addition, it is not necessarily the case that the two mechanism are using different subspaces in all layers. In early layers the current token subspace can affect both mechanism, while in later layers, the conflict may have been resolved and the final result is encoded in one subspace. The middle layer is likely the place where retrieval is already happened but one type of knowledge is not yet overwritten by the other.

E Qualitative Analysis Details

E.1 Building Activation Database

As we mentioned in main paper, we apply InversionView to subspaces and simply do vector search to find preimages. Here are the details: (1) The text data includes 2000 random sequences in MiniPile, 1000 IOI prompts and 1000 Greater-than prompts. We made IOI and Greater-than prompts using the same procedure as we did for clean inputs in patching experiments. We run GPT-2 Small on these text, producing 1178970 activations for each activation site (i.e., post MLP residual stream at layer 4, 6, 8, 9). Each activation has a corresponding token position from which it is collected. We maintain their correspondence such that we can always retrieve the input tokens that result in certain activation (i.e., all tokens in its previous context). (2) For a subspace partition trained for an activation site, i.e., orthogonal matrix $\mathbf{R}$ and configuration c, we make S (number of subspaces) databases by using FAISS (Douze et al., 2024) index. Activations in whole space are converted into subspace activations (multiplied by $\mathbf{R}$ and split according to c) and are added to each database respectively. Therefore, we make separate databases for each layer (activation site) and each subspace. (3) Then for any interested subspace activation (query activation), we search for other activations in corresponding subspace

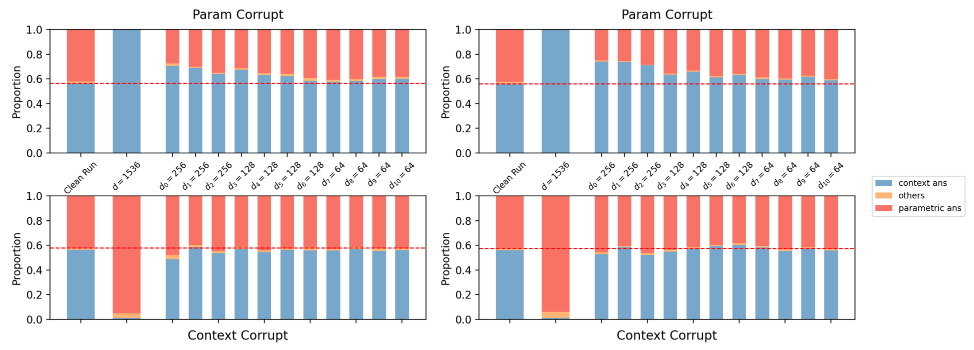

(a) Identity (b) Random

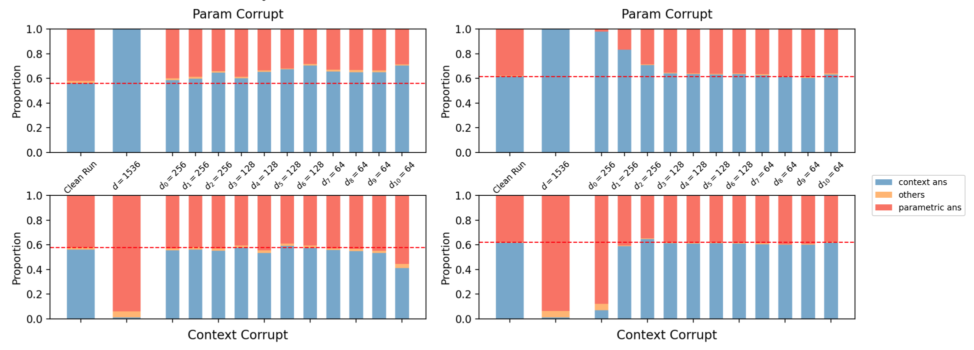

(c) PCA (d) PCA2

Figure 18: Subspace patching effect. Partition given by an identity matrix, a random orthogonal matrix, eigenvectors whose corresponding eigenvalues are in ascending order, eigenvectors whose corresponding eigenvalues are in descending order, on $\boldsymbol{h}^{11,mid}$ of Qwen2.5-1.5B. This figure supplements the main paper Fig. 4 (the right one) with baselines. We can see the effect under two types of counterfactual inputs tend to correlate.

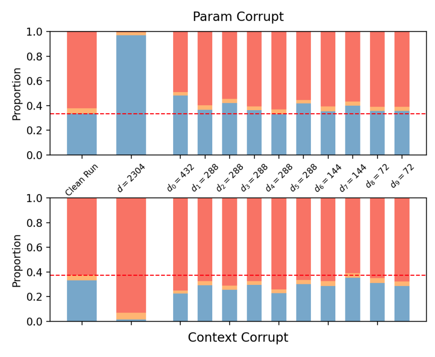

(a) Identity

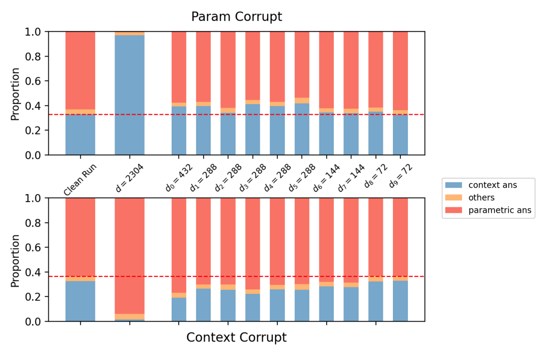

(b) Random

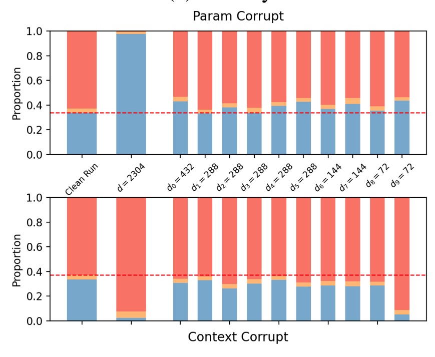

(c) PCA

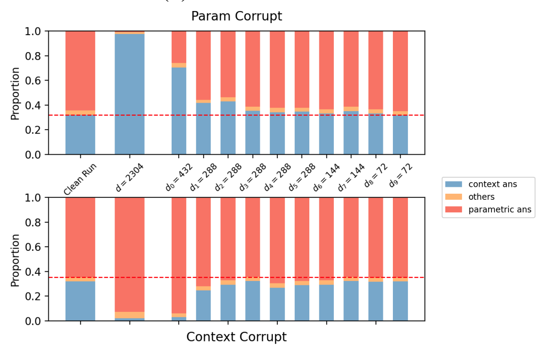

(d) PCA2

Figure 19: Subspace patching effect. Partition given by an identity matrix, a random matrix, eigenvectors whose corresponding eigenvalues are in ascending order, eigenvectors whose corresponding eigenvalues are in descending order, on $\boldsymbol{h}^{9,mid}$ of Gemma-2-2B. This figure supplements the main paper Fig. 4 (the right one) with baselines. We can see the effect under two types of counterfactual inputs tend to correlate.

database whose cosine similarity is above the threshold. We then show the inputs corresponding to query activation and searching results.

E.2 Input Attribution Details

As language model's representations are contextualized, sometimes activations encode information far from the token position it corresponds to, i.e., long-range dependency. This makes interpretation difficult, as we need to search commonality in a large context. We thus make use of input attribution method to highlight important tokens. We use integrated gradients with 10 interpolations. Specifically, given an query subspace activation and a sequence of tokens, we first obtain the initial residual stream activations from these tokens, and multiply them with $\alpha = 0.1, 0.2, \ldots, 1.0$ to create 10 interpolations. We continue the forward pass to get subspace activations. Importantly, we freeze all attention weights to the values they take when running on clean inputs ($\alpha = 1.0$) during the forward pass. We finally compute the cosine similarity between resulting subspace activation and the given query subspace activation. The gradient (not via attention weights) of the cosine similarity with respect to each interpolations are averaged and multiplied with residual stream activations to obtain the final token-level attribution score. The scores are normalized by the sum of scores of all tokens in the same input sequence before showing in the web application. So the scores sum to 1. But they usually spread somewhat evenly across many tokens, resulting in invisible highlights, so we also provide options in the web application to scale these scores together. Because it requires time to compute attribution scores, we pre-compute them for 50 random query activations and show them in a separate page in the application.

The reason for fixing attention weights is that, we empirically find it produces more plausible attribution. The idea behind it is to emphasize what is moved by the attention circuit, while ignoring how this circuit is formed. For example, for a induction head on input "A B ... A", it would only highlight "B" though all 3 tokens play a role. The same intuition is also used in other works (Ameisen et al., 2025). Importantly, we find the effectiveness of our attribution method is limited, as the scores are usually too concentrated at the most recent token, readers should be cautious when using them. This also highlights importance of better input attribution, as in larger and more capable models long-range dependency might be more prevalent.

E.3 More examples and Detailed Findings

Examples supplementing Fig. 2 Fig. 20 - 23 correspond to 4 subfigures in the main paper Fig. 2, in each of them we fix the subspace and vary inputs to observe the consistency.

Subspace interpretation is consistent while being dependent on the input When we say the subspace's interpretation or function is consistent, it does not mean it must align exactly with any human concept. For example, as shown in Fig. 24, subspace 0 encodes only the current token in first two subfigures, but it encodes 2 more previous token in the last subfigure. This does not contradict with our claim of consistency, as the 3 tokens form a frequent phrase, and can be regarded as one.

More importantly, as shown in Fig. 25, we found subspace interpretation can depend on input in an interesting and different way: the subspace encodes the occurrence of repetition if the current token is relatively less common and repeated, otherwise it "falls back" to encode the current token. This behavior is understandable, certain meaningful pattern does not always occur, the subspace might have an "default/empty state". When it occurs, it overwrites the information in the subspace. We also think the phenomenon for subspace 4 in Fig. 25 might be because the subspace partition is not done very well, so that it mixes "repetition subspace" with "current token subspace".

Several subspaces encode local context, while being slightly different We found that subspace 0, 1, 2, 3, 5 encode short-range local context, most of the time they only encode information about most recent 1-2 tokens. But they are slightly different. Fig. 26 shows an example, where subspace 0 encodes a more coarse-grained information for current token but a slightly longer context, and in contrast subspace 1 encodes a more fine-grained information for current token but shorter context. Among these subspaces, we found subspace 2 encodes mostly only the exact current token.

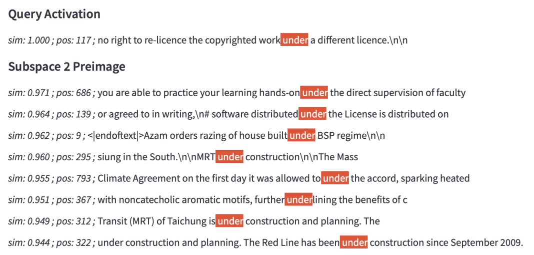

Query Activation

sim: 1.000 ; pos: 117 ; no right to re-licence the copyrighted work under a different licence.\n\n

Subspace 2 Preimage

sim: 0.971 ; pos: 686 ; you are able to practice your learning hands-on under the direct supervision of faculty
sim: 0.964 ; pos: 139 ; or agreed to in writing,\n# software distributed under the License is distributed on
sim: 0.962 ; pos: 9 ; <|endoftext|>Azam orders razing of house built under BSP regime\n\n
sim: 0.960 ; pos: 295 ; siung in the South.\n\nMRT under construction\n\nThe Mass
sim: 0.955 ; pos: 793 ; Climate Agreement on the first day it was allowed to under the accord, sparking heated
sim: 0.951 ; pos: 367 ; with noncatecholic aromatic motifs, further underlining the benefits of c
sim: 0.949 ; pos: 312 ; Transit (MRT) of Taichung is under construction and planning. The
sim: 0.944 ; pos: 322 ; under construction and planning. The Red Line has been under construction since September 2009.

(a)

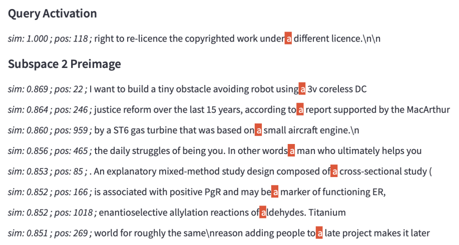

Query Activation

sim: 1.000 ; pos: 118 ; right to re-licence the copyrighted work under a different licence.\n\n

Subspace 2 Preimage

sim: 0.869 ; pos: 22 ; I want to build a tiny obstacle avoiding robot using a 3v coreless DC
sim: 0.864 ; pos: 246 ; justice reform over the last 15 years, according to a report supported by the MacArthur
sim: 0.860 ; pos: 959 ; by a ST6 gas turbine that was based on a small aircraft engine.\n
sim: 0.856 ; pos: 465 ; the daily struggles of being you. In other words a man who ultimately helps you
sim: 0.853 ; pos: 85 ; . An explanatory mixed-method study design composed of a cross-sectional study (
sim: 0.852 ; pos: 166 ; is associated with positive PgR and may be a marker of functioning ER,
sim: 0.852 ; pos: 1018 ; enantioselective allylation reactions of aldehydes. Titanium
sim: 0.851 ; pos: 269 ; world for roughly the same\nreason adding people to a late project makes it later

(b)

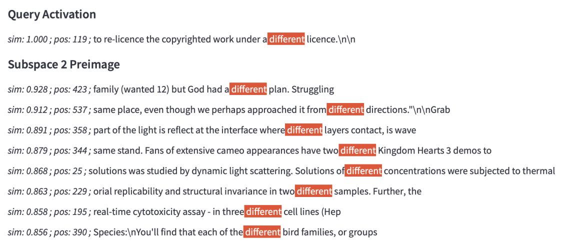

Query Activation

sim: 1.000 ; pos: 119 ; to re-licence the copyrighted work under a different licence.\n\n

Subspace 2 Preimage

sim: 0.928 ; pos: 423 ; family (wanted 12) but God had a different plan. Struggling
sim: 0.912 ; pos: 537 ; same place, even though we perhaps approached it from different directions."\n\nGrab
sim: 0.891 ; pos: 358 ; part of the light is reflect at the interface where different layers contact, is wave
sim: 0.879 ; pos: 344 ; same stand. Fans of extensive cameo appearances have two different Kingdom Hearts 3 demos to
sim: 0.868 ; pos: 25 ; solutions was studied by dynamic light scattering. Solutions of different concentrations were subjected to thermal
sim: 0.863 ; pos: 229 ; orial replicability and structural invariance in two different samples. Further, the
sim: 0.858 ; pos: 195 ; real-time cytotoxicity assay - in three different cell lines (Hep
sim: 0.856 ; pos: 390 ; Species:\nYou'll find that each of the different bird families, or groups

(c)

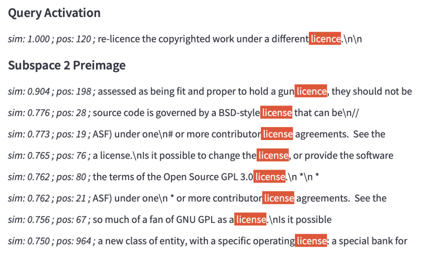

Query Activation

sim: 1.000 ; pos: 120 ; re-licence the copyrighted work under a different licence.\n\n

Subspace 2 Preimage

sim: 0.904 ; pos: 198 ; assessed as being fit and proper to hold a gun licence, they should not be
sim: 0.776 ; pos: 28 ; source code is governed by a BSD-style license that can be\n//
sim: 0.773 ; pos: 19 ; ASF) under one\n# or more contributor license agreements. See the
sim: 0.765 ; pos: 76 ; a license.\nIs it possible to change the license, or provide the software
sim: 0.762 ; pos: 80 ; the terms of the Open Source GPL 3.0 license.\n *\n *
sim: 0.762 ; pos: 21 ; ASF) under one\n * or more contributor license agreements. See the
sim: 0.756 ; pos: 67 ; so much of a fan of GNU GPL as a license.\nIs it possible
sim: 0.750 ; pos: 964 ; a new class of entity, with a specific operating license: a special bank for

(d)

Figure 20: Subspace 2 at $\boldsymbol{h}^{4,post}$: Preimages of the residual stream activation corresponding to a continuous span of tokens (“under”, “a”, “different”, “licence”) in the same subspace after the 5th layers in GPT-2 Small. Interpretation of encoded information: (a) the current token “under”. (b) the current token “a”. (c) the current token “different”. (d) the current token “license”. But there are not enough samples above cosine similarity of 0.85, we lower the threshold to 0.75 to check more samples. It is probably because it encodes more than just the current token.

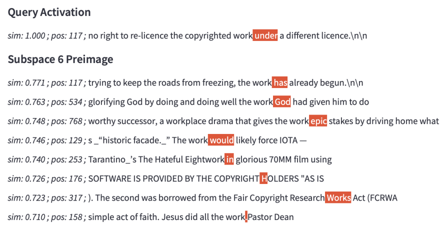

Query Activation

sim: 1.000 ; pos: 117 ; no right to re-licence the copyrighted work under a different licence.\n\n

Subspace 6 Preimage

sim: 0.771 ; pos: 117 ; trying to keep the roads from freezing, the work has already begun.\n\n
sim: 0.763 ; pos: 534 ; glorifying God by doing and doing well the work God had given him to do
sim: 0.748 ; pos: 768 ; worthy successor, a workplace drama that gives the work epic stakes by driving home what
sim: 0.746 ; pos: 129 ; s _“historic facade._” The work would likely force IOTA —
sim: 0.740 ; pos: 253 ; Tarantino_’s The Hateful Eightwork in glorious 70MM film using
sim: 0.726 ; pos: 176 ; SOFTWARE IS PROVIDED BY THE COPYRIGHT HOLDERS "AS IS
sim: 0.723 ; pos: 317 ;). The second was borrowed from the Fair Copyright Research Works Act (FCRWA
sim: 0.710 ; pos: 158 ; simple act of faith. Jesus did all the work.Pastor Dean

(a)

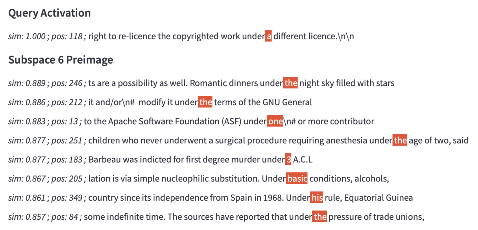

Query Activation

sim: 1.000 ; pos: 118 ; right to re-licence the copyrighted work under a different licence.\n\n

Subspace 6 Preimage

sim: 0.889 ; pos: 246 ; ts are a possibility as well. Romantic dinners under the night sky filled with stars
sim: 0.886 ; pos: 212 ; it and/or\n# modify it under the terms of the GNU General
sim: 0.883 ; pos: 13 ; to the Apache Software Foundation (ASF) under one\n# or more contributor
sim: 0.877 ; pos: 251 ; children who never underwent a surgical procedure requiring anesthesia under the age of two, said
sim: 0.877 ; pos: 183 ; Barbeau was indicted for first degree murder under 3 A.C.L
sim: 0.867 ; pos: 205 ; lation is via simple nucleophilic substitution. Under basic conditions, alcohols,
sim: 0.861 ; pos: 349 ; country since its independence from Spain in 1968. Under his rule, Equatorial Guinea
sim: 0.857 ; pos: 84 ; some indefinite time. The sources have reported that under the pressure of trade unions,

(b)

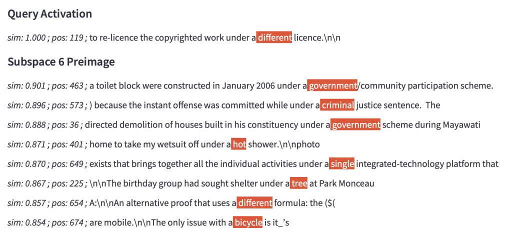

Query Activation

sim: 1.000 ; pos: 119 ; to re-licence the copyrighted work under a different licence.\n\n

Subspace 6 Preimage

sim: 0.901 ; pos: 463 ; a toilet block were constructed in January 2006 under a government/community participation scheme.
sim: 0.896 ; pos: 573 ;) because the instant offense was committed while under a criminal justice sentence. The
sim: 0.888 ; pos: 36 ; directed demolition of houses built in his constituency under a government scheme during Mayawati
sim: 0.871 ; pos: 401 ; home to take my wetsuit off under a hot shower.\n\nphoto
sim: 0.870 ; pos: 649 ; exists that brings together all the individual activities under a single integrated-technology platform that
sim: 0.867 ; pos: 225 ; \n\nThe birthday group had sought shelter under a tree at Park Monceau
sim: 0.857 ; pos: 654 ; A:\n\nAn alternative proof that uses a different formula: the ($(
sim: 0.854 ; pos: 674 ; are mobile.\n\nThe only issue with a bicycle is it_’s

(c)

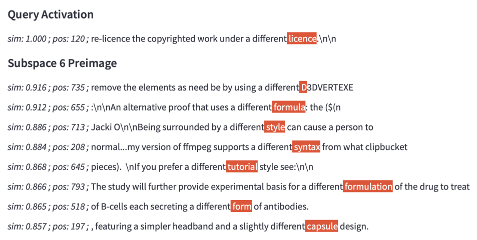

Query Activation

sim: 1.000 ; pos: 120 ; re-licence the copyrighted work under a different licence.\n\n

Subspace 6 Preimage

sim: 0.916 ; pos: 735 ; remove the elements as need be by using a different D3DVERTEXE
sim: 0.912 ; pos: 655 ; :\n\nAn alternative proof that uses a different formula: the ($(n
sim: 0.886 ; pos: 713 ; Jacki O\n\nBeing surrounded by a different style can cause a person to
sim: 0.884 ; pos: 208 ; normal...my version of ffmpeg supports a different syntax from what clipbucket
sim: 0.868 ; pos: 645 ; pieces). \nIf you prefer a different tutorial style see:\n\n
sim: 0.866 ; pos: 793 ; The study will further provide experimental basis for a different formulation of the drug to treat
sim: 0.865 ; pos: 518 ; of B-cells each secreting a different form of antibodies.
sim: 0.857 ; pos: 197 ; , featuring a simpler headband and a slightly different capsule design.

(d)

Figure 21: Subspace 6 at $\boldsymbol{h}^{4,post}$: Preimages of the residual stream activation corresponding to a continuous span of tokens (“under”, “a”, “different”, “licence”) in the same subspace after the 5th layers in GPT-2 Small. Interpretation of encoded information: (a) the previous two tokens “copyrighted” and “work”. We have to lower the threshold to 0.7 to have enough samples inside preimage. In those samples, we can see some contain “work” and others contain “COPYRIGHT” in previous tokens. We think that both tokens are encoded, that is why having only one of them cannot produce high similarity. (b) the previous token “under”. (c) the previous token “a”. (d) the previous token “different”. This subspace is the one with the largest patching effect in test 1. Its un-normalized effect is 3.60, much greater than the second largest value 0.03.

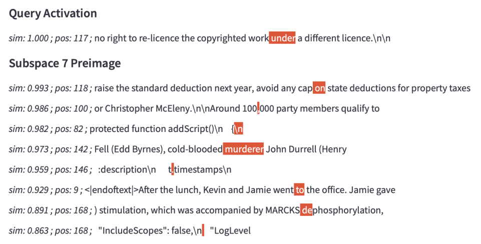

Query Activation

sim: 1.000 ; pos: 117 ; no right to re-licence the copyrighted work under a different licence.\n\n

Subspace 7 Preimage

sim: 0.993 ; pos: 118 ; raise the standard deduction next year, avoid any cap on state deductions for property taxes

sim: 0.986 ; pos: 100 ; or Christopher McEleny.\n\nAround 100,000 party members qualify to

sim: 0.982 ; pos: 82 ; protected function addScript()\n {\n

sim: 0.973 ; pos: 142 ; Fell (Edd Byrnes), cold-blooded murderer John Durrell (Henry

sim: 0.959 ; pos: 146 ; :description\n t.timestamps\n

sim: 0.929 ; pos: 9 ; <|endoftext|>After the lunch, Kevin and Jamie went to the office. Jamie gave

sim: 0.891 ; pos: 168 ;) stimulation, which was accompanied by MARCKS dephosphorylation,

sim: 0.863 ; pos: 168 ; "IncludeScopes": false,\n "LogLevel

(a)

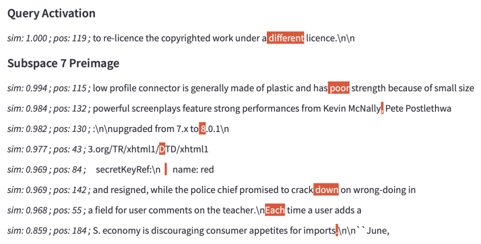

Query Activation

sim: 1.000 ; pos: 119 ; to re-licence the copyrighted work under a different licence.\n\n

Subspace 7 Preimage

sim: 0.994 ; pos: 115 ; low profile connector is generally made of plastic and has poor strength because of small size

sim: 0.984 ; pos: 132 ; powerful screenplays feature strong performances from Kevin McNally, Pete Postlethwa

sim: 0.982 ; pos: 130 ; :\n\nupgraded from 7.x to 8.0.1\n

sim: 0.977 ; pos: 43 ; 3.org/TR/xhtml1/DTD/xhtml1

sim: 0.969 ; pos: 84 ; secretKeyRef:\n name: red

sim: 0.969 ; pos: 142 ; and resigned, while the police chief promised to crack down on wrong-doing in

sim: 0.968 ; pos: 55 ; a field for user comments on the teacher.\nEach time a user adds a

sim: 0.859 ; pos: 184 ; S. economy is discouraging consumer appetites for imports.\n\n`` June,

(b)

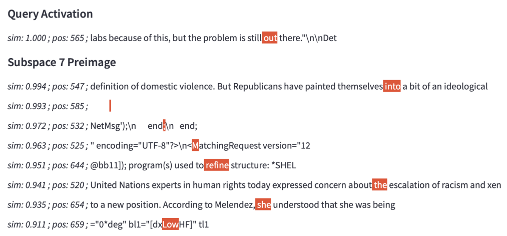

Query Activation

sim: 1.000 ; pos: 565 ; labs because of this, but the problem is still out there."\n\nDet

Subspace 7 Preimage

sim: 0.994 ; pos: 547 ; definition of domestic violence. But Republicans have painted themselves into a bit of an ideological

sim: 0.993 ; pos: 585 ;

sim: 0.972 ; pos: 532 ; NetMsg');\n end;\n end;

sim: 0.963 ; pos: 525 ; " encoding="UTF-8"?>\n<MatchingRequest version="12

sim: 0.951 ; pos: 644 ; @bb11]); program(s) used to refine structure: *SHEL

sim: 0.941 ; pos: 520 ; United Nations experts in human rights today expressed concern about the escalation of racism and xen

sim: 0.935 ; pos: 654 ; to a new position. According to Melendez, she understood that she was being

sim: 0.911 ; pos: 659 ; ="0*deg" bl1="[dxLowHF]" tl1

(c)

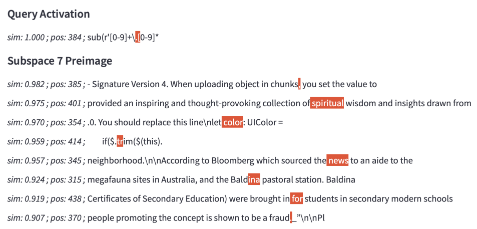

Query Activation

sim: 1.000 ; pos: 384 ; sub(r'[0-9]+\.[0-9]*

Subspace 7 Preimage

sim: 0.982 ; pos: 385 ; - Signature Version 4. When uploading object in chunks, you set the value to

sim: 0.975 ; pos: 401 ; provided an inspiring and thought-provoking collection of spiritual wisdom and insights drawn from

sim: 0.970 ; pos: 354 ; .0. You should replace this line\nlet color: UIColor =

sim: 0.959 ; pos: 414 ; if($.trim($(this).

sim: 0.957 ; pos: 345 ; neighborhood.\n\nAccording to Bloomberg which sourced the news to an aide to the

sim: 0.924 ; pos: 315 ; megafauna sites in Australia, and the Baldina pastoral station. Baldina

sim: 0.919 ; pos: 438 ; Certificates of Secondary Education) were brought in for students in secondary modern schools

sim: 0.907 ; pos: 370 ; people promoting the concept is shown to be a fraud._"\n\nPl

(d)

Figure 22: Subspace 7 at $\boldsymbol{h}^{4,post}$: Preimages of the residual stream activation corresponding to two tokens adjacent to the one in Fig. 2(c) ("under", "different"), and two tokens in very different positions (at position 565 and 384) in the same subspace after the 5th layers in GPT-2 Small. Interpretation of encoded information: (a) current position is around 117. (b) current position is around 119. (c) current position is around 565. (d) current position is around 384. For this subspace, one can increase the threshold and obtain samples of very similar positions as shown in Figure 30.

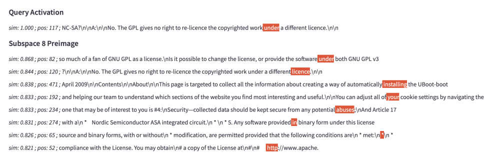

Query Activation

sim: 1.000 ; pos: 117 ; NC-SA?\n\nA:\n\nNo. The GPL gives no right to re-licence the copyrighted work under a different licence.\n\n

Subspace 8 Preimage

sim: 0.868 ; pos: 82 ; so much of a fan of GNU GPL as a license.\nIs it possible to change the license, or provide the software under both GNU GPL v3

sim: 0.844 ; pos: 120 ; ?\n\nA:\n\nNo. The GPL gives no right to re-licence the copyrighted work under a different licence.\n\n

sim: 0.838 ; pos: 471 ; April 2009\n\nContents\n\nAbout\n\nThis page is targeted to collect all the information about creating a way of automatically installing the UBoot-boot

sim: 0.833 ; pos: 192 ; and helping our team to understand which sections of the website you find most interesting and useful.\n\nYou can adjust all of your cookie settings by navigating the

sim: 0.833 ; pos: 234 ; one that may be of interest to you is #4:\nSecurity—collected data should be kept secure from any potential abuses;\nAnd Article 17

sim: 0.831 ; pos: 274 ; with a\n * Nordic Semiconductor ASA integrated circuit.\n * \n * 5. Any software provided in binary form under this license

sim: 0.826 ; pos: 65 ; source and binary forms, with or without\n * modification, are permitted provided that the following conditions are\n * met:\n *\n *

sim: 0.821 ; pos: 52 ; compliance with the License. You may obtain\n# a copy of the License at\n#\n# http://www.apache.

(a)

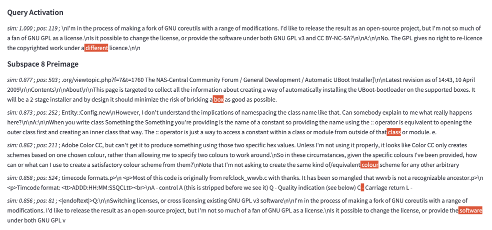

Query Activation

sim: 1.000 ; pos: 119 ; \nI'm in the process of making a fork of GNU coreutils with a range of modifications. I'd like to release the result as an open-source project, but I'm not so much of a fan of GNU GPL as a license.\nIs it possible to change the license, or provide the software under both GNU GPL v3 and CC BY-NC-SA?\n\nA:\n\nNo. The GPL gives no right to re-licence the copyrighted work under a different licence.\n\n

Subspace 8 Preimage

sim: 0.877 ; pos: 503 ; .org/viewtopic.php?f=7&t=1760 The NAS-Central Community Forum / General Development / Automatic UBoot Installer]\n\nLatest revision as of 14:43, 10 April 2009\n\nContents\n\nAbout\n\nThis page is targeted to collect all the information about creating a way of automatically installing the UBoot-bootloader on the supported boxes. It will be a 2-stage installer and by design it should minimize the risk of bricking a box as good as possible.

sim: 0.873 ; pos: 252 ; Entity::Config.new\nHowever, I don't understand the implications of namespacing the class name like that. Can somebody explain to me what really happens here?\n\nA:\n\nWhen you write class Something the Something you're providing is the name of a constant so providing the name using the :: operator is equivalent to opening the outer class first and creating an inner class that way. The :: operator is just a way to access a constant within a class or module from outside of that class or module. e.

sim: 0.862 ; pos: 211 ; Adobe Color CC, but can't get it to produce something using those two specific hex values. Unless I'm not using it properly, it looks like Color CC only creates schemes based on one chosen colour, rather than allowing me to specify two colours to work around.\nSo in these circumstances, given the specific colours I've been provided, how can or what can I use to create a satisfactory colour scheme from them?\nNote that I'm not asking to create the same kind of/equivalent colour scheme for any other arbitrary

sim: 0.858 ; pos: 524 ; timecode formats.p>\n <p>Most of this code is originally from refclock_wwvb.c with thanks. It has been so mangled that wwvb is not a recognizable ancestor.p>\n <p>Timcode format: <tt>ADDD:HH:MM:SSQCLtt>
\nA - control A (this is stripped before we see it) Q - Quality indication (see below) C - Carriage return L -

sim: 0.856 ; pos: 81 ; <|endoftext|>Q:\n\nSwitching licenses, or cross licensing existing GNU GPL v3 software\n\nI'm in the process of making a fork of GNU coreutils with a range of modifications. I'd like to release the result as an open-source project, but I'm not so much of a fan of GNU GPL as a license.\nIs it possible to change the license, or provide the software under both GNU GPL v

(b)

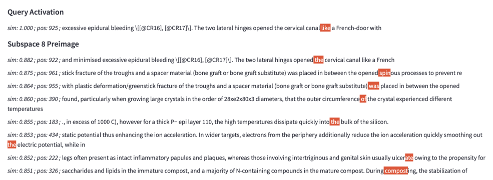

Query Activation

sim: 1.000 ; pos: 925 ; excessive epidural bleeding \[[@CR16], [@CR17]\]. The two lateral hinges opened the cervical canal like a French-door with

Subspace 8 Preimage

sim: 0.882 ; pos: 922 ; and minimised excessive epidural bleeding \[[@CR16], [@CR17]\]. The two lateral hinges opened the cervical canal like a French

sim: 0.875 ; pos: 961 ; stick fracture of the troughs and a spacer material (bone graft or bone graft substitute) was placed in between the opened spinous processes to prevent re

sim: 0.864 ; pos: 955 ; with plastic deformation/greenstick fracture of the troughs and a spacer material (bone graft or bone graft substitute) was placed in between the opened

sim: 0.860 ; pos: 390 ; found, particularly when growing large crystals in the order of 28xe2x80x3 diameters, that the outer circumference of the crystal experienced different temperatures

sim: 0.855 ; pos: 183 ; ., in excess of 1000 C), however for a thick P− epi layer 110, the high temperatures dissipate quickly into the bulk of the silicon.

sim: 0.853 ; pos: 434 ; static potential thus enhancing the ion acceleration. In wider targets, electrons from the periphery additionally reduce the ion acceleration quickly smoothing out the electric potential, while in

sim: 0.852 ; pos: 222 ; legs often present as intact inflammatory papules and plaques, whereas those involving intertriginous and genital skin usually ulcerate owing to the propensity for

sim: 0.851 ; pos: 326 ; saccharides and lipids in the immature compost, and a majority of N-containing compounds in the mature compost. During composting, the stabilization of

(c)

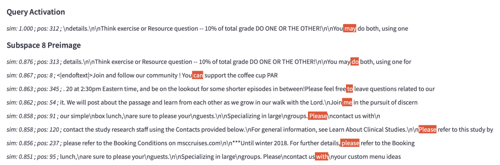

Query Activation

sim: 1.000 ; pos: 312 ; \ndetails.\n\nThink exercise or Resource question -- 10% of total grade DO ONE OR THE OTHER!\n\nYou may do both, using one

Subspace 8 Preimage

sim: 0.876 ; pos: 313 ; details.\n\nThink exercise or Resource question -- 10% of total grade DO ONE OR THE OTHER!\n\nYou may do both, using one for

sim: 0.867 ; pos: 8 ; <|endoftext|>Join and follow our community ! You can support the coffee cup PAR

sim: 0.863 ; pos: 345 ; . 20 at 2:30pm Eastern time, and be on the lookout for some shorter episodes in between!Please feel free to leave questions related to our

sim: 0.862 ; pos: 54 ; it. We will post about the passage and learn from each other as we grow in our walk with the Lord.\nJoin me in the pursuit of discern

sim: 0.858 ; pos: 91 ; our simple\nbox lunch,\nare sure to please your\nguests.\n\nSpecializing in large\ngroups. Please\ncontact us with\n

sim: 0.858 ; pos: 120 ; contact the study research staff using the Contacts provided below.\nFor general information, see Learn About Clinical Studies.\n\nPlease refer to this study by

sim: 0.856 ; pos: 237 ; please refer to the Booking Conditions on msccruises.com\n\n***Until winter 2018. For further details, please refer to the Booking

sim: 0.851 ; pos: 95 ; lunch,\nare sure to please your\nguests.\n\nSpecializing in large\ngroups. Please\ncontact us with\nyour custom menu ideas

(d)

Figure 23: Subspace 8 at $\boldsymbol{h}^{4,post}$: Preimages of the residual stream activation corresponding to two tokens adjacent to the one in Fig. 2(c) ("under", "different"), and two tokens in very different context in the same subspace after the 5th layers in GPT-2 Small. Interpretation of encoded information: (a) context is about software license/permission. (b) discussing software development. (c) describing detailed medical or physical processes in technical contexts. (d) online advertisements and announcements, more concretely, suggesting readers to do something. We can see as (a) and (b) are close, the topic information is also similar, while it is very different from (c) and (d)

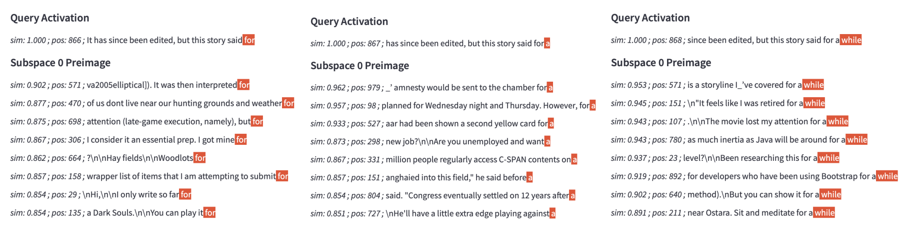

Query Activation

sim: 1.000 ; pos: 866 ; It has since been edited, but this story said for

Subspace 0 Preimage

sim: 0.902 ; pos: 571 ; va2005elliptical]). It was then interpreted for

sim: 0.877 ; pos: 470 ; of us dont live near our hunting grounds and weather for

sim: 0.875 ; pos: 698 ; attention (late-game execution, namely), but for

sim: 0.867 ; pos: 306 ; I consider it an essential prep. I got mine for

sim: 0.862 ; pos: 664 ; ?\n\nHay fields\n\nWoodlots for

sim: 0.857 ; pos: 158 ; wrapper list of items that I am attempting to submit for

sim: 0.854 ; pos: 29 ; \nHi,\n\nI only write so far for

sim: 0.854 ; pos: 135 ; a Dark Souls.\n\nYou can play it for

(a)

Query Activation

sim: 1.000 ; pos: 867 ; has since been edited, but this story said for a

Subspace 0 Preimage

sim: 0.962 ; pos: 979 ; _' amnesty would be sent to the chamber for a

sim: 0.957 ; pos: 98 ; planned for Wednesday night and Thursday. However, for a

sim: 0.933 ; pos: 527 ; aar had been shown a second yellow card for a

sim: 0.873 ; pos: 298 ; new job?\n\nAre you unemployed and want a

sim: 0.867 ; pos: 331 ; million people regularly access C-SPAN contents on a

sim: 0.857 ; pos: 151 ; anghaied into this field," he said before a

sim: 0.854 ; pos: 804 ; said. "Congress eventually settled on 12 years after a

sim: 0.851 ; pos: 727 ; \nHe'll have a little extra edge playing against a

(b)

Query Activation

sim: 1.000 ; pos: 868 ; since been edited, but this story said for a while

Subspace 0 Preimage

sim: 0.953 ; pos: 571 ; is a storyline I_'ve covered for a while

sim: 0.945 ; pos: 151 ; \n"It feels like I was retired for a while

sim: 0.943 ; pos: 107 ; .\n\nThe movie lost my attention for a while

sim: 0.943 ; pos: 780 ; as much inertia as Java will be around for a while

sim: 0.937 ; pos: 23 ; level?\n\nBeen researching this for a while

sim: 0.919 ; pos: 892 ; for developers who have been using Bootstrap for a while

sim: 0.902 ; pos: 640 ; method).\nBut you can show it for a while

sim: 0.891 ; pos: 211 ; near Ostara. Sit and meditate for a while

(c)

Figure 24: Subspace 0 at $\boldsymbol{h}^{4,post}$: Preimages of the residual stream activation corresponding to three tokens in a continuous span. While encoded information for (a) and (b) are the current token ("for", "a"), the encoded information for (c) is "for a while" instead of just "while" (we confirm this by checking more samples and varying threshold). So the high-level interpretation of the subspace is not current token, but more like current semantic unit. This also shows that sometimes several recent tokens are merged in representation, but sometimes they are not, indicating some kind of "internal tokenization".

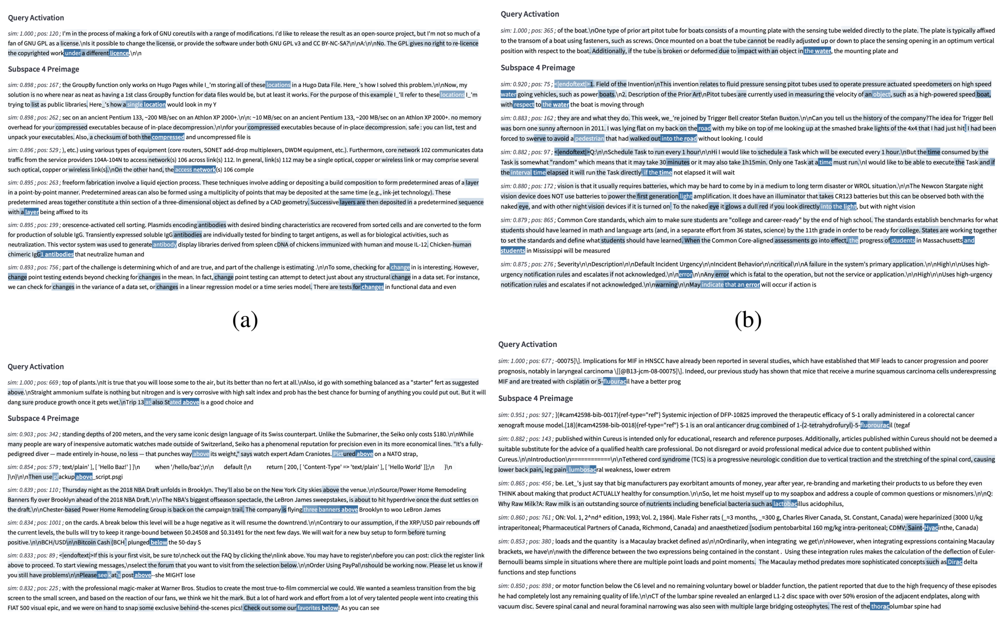

Query Activation

sim: 1.000 ; pos: 120 ; I'm in the process of making a fork of GNU coreutils with a range of modifications. I'd like to release the result as an open-source project, but I'm not so much of a fan of GNU GPL as a license.\nIs it possible to change the license, or provide the software under both GNU GPL v3 and CC BY-NC-SA?\n\nA:\n\nNo. The GPL gives no right to re-licence the copyrighted work under a different licence.\n\n

Subspace 4 Preimage

sim: 0.898 ; pos: 167 ; the GroupBy function only works on Hugo Pages while I_'m storing all of these locations in a Hugo Data File. Here_'s how I solved this problem.\n\nNow, my solution is no where near as neat as having a 1st class GroupBy function for data files would be, but at least it works. For the purpose of this example I_'ll refer to these locations I_'m trying to list as public libraries. Here_'s how a single location would look in my Y

sim: 0.898 ; pos: 262 ; sec on an ancient Pentium 133, ~200 MB/sec on an Athlon XP 2000+.\n\n: ~10 MB/sec on an ancient Pentium 133, ~200 MB/sec on an Athlon XP 2000+. no memory overhead for your compressed executables because of in-place decompression.\n\nfor your compressed executables because of in-place decompression. safe : you can list, test and unpack your executables. Also, a checksum of both the compressed and uncompressed file is

sim: 0.896 ; pos: 529 ;), etc.) using various types of equipment (core routers, SONET add-drop multiplexers, DWDM equipment, etc.). Furthermore, core network 102 communicates data traffic from the service providers 104A-104N to access network(s) 106 across link(s) 112. In general, link(s) 112 may be a single optical, copper or wireless link or may comprise several such optical, copper or wireless link(s).\nOn the other hand, the access network(s) 106 comple

sim: 0.895 ; pos: 263 ; freeform fabrication involve a liquid ejection process. These techniques involve adding or depositing a build composition to form predetermined areas of a layer in a point-by-point manner. Predetermined areas can also be formed using a multiplicity of points that may be deposited at the same time (e.g., ink-jet technology). These predetermined areas together constitute a thin section of a three-dimensional object as defined by a CAD geometry. Successive layers are then deposited in a predetermined sequence with a layer being affixed to its

sim: 0.895 ; pos: 199 ; orescence-activated cell sorting. Plasmids encoding antibodies with desired binding characteristics are recovered from sorted cells and are converted to the form for production of soluble IgG. Transiently expressed soluble IgG antibodies are individually tested for binding to target antigens, as well as for biological activities, such as neutralization. This vector system was used to generate antibody display libraries derived from spleen cDNA of chickens immunized with human and mouse IL-12. Chicken-human chimeric IgG1 antibodies that neutralize human and

sim: 0.893 ; pos: 756 ; part of the challenge is determining which of and are true, and part of the challenge is estimating .\n\nTo some, checking for a change in is interesting. However, change point testing extends beyond checking for changes in the mean. In fact, change point testing can attempt to detect just about any structural change in a data set. For instance, we can check for changes in the variance of a data set, or changes in a linear regression model or a time series model. There are tests for changes in functional data and even

(a)

Query Activation

sim: 1.000 ; pos: 365 ; of the boat.\nOne type of prior art pitot tube for boats consists of a mounting plate with the sensing tube welded directly to the plate. The plate is typically affixed to the transom of a boat using fasteners, such as screws. Once mounted on a boat the tube cannot be readily adjusted up or down to place the sensing opening in an optimum vertical position with respect to the boat. Additionally, if the tube is broken or deformed due to impact with an object in the water, the mounting plate and

Subspace 4 Preimage

sim: 0.920 ; pos: 75 ; <|endoftext|>1. Field of the Invention\nThis invention relates to fluid pressure sensing pitot tubes used to operate pressure actuated speedometers on high speed water going vehicles, such as power boats.\n2. Description of the Prior Art\nPitot tubes are currently used in measuring the velocity of an object, such as a high-powered speed boat, with respect to the water the boat is moving through

sim: 0.883 ; pos: 162 ; they are and what they do. This week, we_'re joined by Trigger Bell creator Stefan Buxton.\n\nCan you tell us the history of the company?The idea for Trigger Bell was born one sunny afternoon in 2011. I was lying flat on my back on the road with my bike on top of me looking up at the smashed brake lights of the 4x4 that I had just hit. I had been forced to swerve to avoid a pedestrian that had walked out into the road without looking. I could

sim: 0.882 ; pos: 97 ; <|endoftext|>Q:\n\nSchedule Task to run every 1 hour\n\nHi I would like to schedule a Task which will be executed every 1 hour.\nBut the time consumed by the Task is somewhat "random" which means that it may take 30 minutes or it may also take 1h15min. Only one Task at a time must run.\nI would like to be able to execute the Task and if the interval time elapsed it will run the Task directly, if the time not elapsed it will wait

sim: 0.880 ; pos: 172 ; vision is that it usually requires batteries, which may be hard to come by in a medium to long term disaster or WROL situation.\n\nThe Newcon Stargate night vision device does NOT use batteries to power the first generation light amplification. It does have an illuminator that takes CR123 batteries but this can be observed both with the naked eye, and with other night vision devices if it is turned on. To the naked eye it glows a dull red if you look directly into the light, but with night vision

sim: 0.879 ; pos: 865 ; Common Core standards, which aim to make sure students are "college and career-ready" by the end of high school. The standards establish benchmarks for what students should have learned in math and language arts (and, in a separate effort from 36 states, science) by the 11th grade in order to be ready for college. States are working together to set the standards and define what students should have learned. When the Common Core-aligned assessments go into effect, the progress of students in Massachusetts and students in Mississippi will be measured

sim: 0.875 ; pos: 276 ; Severity\n\nDescription\n\nDefault Incident Urgency\n\nIncident Behavior\n\ncritical\n\nA failure in the system's primary application.\n\nHigh\n\nUses high-urgency notification rules and escalates if not acknowledged.\n\nerror\n\nAny error which is fatal to the operation, but not the service or application.\n\nHigh\n\nUses high-urgency notification rules and escalates if not acknowledged.\n\nwarning\n\nMay indicate that an error will occur if action is

(b)

Query Activation

sim: 1.000 ; pos: 669 ; top of plants.\nIt is true that you will loose some to the air, but its better than no fert at all.\nAlso, id go with something balanced as a "starter" fert as suggested above.\nStraight ammonium sulfate is nothing but nitrogen and is very corrosive with high salt index and prob has the best chance for burning of anything you could put out. But it will dang sure produce growth once it gets wet.\nTrip 13 as also Stated above is a good choice and

Subspace 4 Preimage

sim: 0.903 ; pos: 342 ; standing depths of 200 meters, and the very same iconic design language of its Swiss counterpart. Unlike the Submariner, the Seiko only costs $180.\n\nWhile many people are wary of inexpensive automatic watches made outside of Switzerland, Seiko has a phenomenal reputation for precision even in its more economical lines. "It's a fully-pedigreed diver — made entirely in-house, no less — that punches way above its weight," says watch expert Adam Craniotes. Pictured above on a NATO strap,

sim: 0.854 ; pos: 579 ; text/plain'], ['Hello Baz!']]\n   when '/hello/baz';\n\n   default {\n   return [200, ['Content-Type' => 'text/plain'], ['Hello World']];\n   }\n }\n}\n\nThen use plackup above_script.psgi

sim: 0.839 ; pos: 110 ; Thursday night as the 2018 NBA Draft unfolds in Brooklyn. They'll also be on the New York City skies above the venue.\n\nSource/Power Home Remodeling Banners fly over Brooklyn ahead of the 2018 NBA Draft.\n\nThe NBA's biggest offseason spectacle, the LeBron James sweepstakes, is about to hit hyperdrive once the dust settles on the draft.\n\nChester-based Power Home Remodeling Group is back on the campaign trail. The company is flying three banners above Brooklyn to woo LeBron James

sim: 0.834 ; pos: 1001 ; on the cards. A break below this level will be a huge negative as it will resume the downtrend.\n\nContrary to our assumption, if the XRP/USD pair rebounds off the current levels, the bulls will try to keep it range-bound between $0.24508 and $0.31491 for the next few days. We will wait for a new buy setup to form before turning positive.\n\nBCH/USD\n\nBitcoin Cash (BCH) plunged below the 50-day S

sim: 0.833 ; pos: 89 ; <|endoftext|>If this is your first visit, be sure to\ncheck out the FAQ by clicking the\nlink above. You may have to register\nbefore you can post: click the register link above to proceed. To start viewing messages,\nselect the forum that you want to visit from the selection below.\n\nOrder Using PayPal\nshould be working now. Please let us know if you still have problems\n\nPlease see kat's post above--she MIGHT lose

sim: 0.832 ; pos: 225 ; with the professional magic-maker at Warner Bros. Studios to create the most true-to-film commercial we could. We wanted a seamless transition from the big screen to the small screen, and based on the reaction of our fans, we think we hit the mark. But a lot of hard work and effort from a lot of very talented people went into creating this FIAT 500 visual epic, and we were on hand to snap some exclusive behind-the-scenes pics! Check out some our favorites below! As you can see

(c)

Query Activation

sim: 1.000 ; pos: 677 ; -00075]\]. Implications for MIF in HNSCC have already been reported in several studies, which have established that MIF leads to cancer progression and poorer prognosis, notably in laryngeal carcinoma \[[@B13-jcm-08-00075]\]. Indeed, our previous study has shown that mice that receive a murine squamous carcinoma cells underexpressing MIF and are treated with cisplatin or 5-fluouracil have a better prog

Subspace 4 Preimage

sim: 0.951 ; pos: 927 ;](#cam42598-bib-0017){ref-type="ref"} Systemic injection of DFP-10825 improved the therapeutic efficacy of S-1 orally administered in a colorectal cancer xenograft mouse model.[18](#cam42598-bib-0018){ref-type="ref"} S-1 is an oral anticancer drug combined of 1-(2-tetrahydrofuryl)-5-fluorouracil (tegaf

sim: 0.882 ; pos: 143 ; published within Cureus is intended only for educational, research and reference purposes. Additionally, articles published within Cureus should not be deemed a suitable substitute for the advice of a qualified health care professional. Do not disregard or avoid professional medical advice due to content published within Cureus.\n\nIntroduction\n============\n\nTethered cord syndrome (TCS) is a progressive neurologic condition due to vertical traction and the stretching of the spinal cord, causing lower back pain, leg pain, lumbosacral weakness, lower extrem

sim: 0.865 ; pos: 456 ; be. Let_'s just say that big manufacturers pay exorbitant amounts of money, year after year, re-branding and marketing their products to us before they even THINK about making that product ACTUALLY healthy for consumption.\n\nSo, let me hoist myself up to my soapbox and address a couple of common questions or misnomers.\n\nQ: Why Raw Milk?A: Raw milk is an outstanding source of nutrients including beneficial bacteria such as lactobacillus acidophilus,

sim: 0.860 ; pos: 761 ; ON: Vol. 1, 2^nd^ edition, 1993; Vol. 2, 1984). Male Fisher rats (_≈3 months, _≈300 g, Charles River Canada, St. Constant, Canada) were heparinized (3000 U/kg intraperitoneal; Pharmaceutical Partners of Canada, Richmond, Canada) and anaesthetized (sodium pentobarbital 160 mg/kg intra-peritoneal; CDMV; Saint-Hyacinthe, Canada)

sim: 0.853 ; pos: 380 ; loads and the quantity is a Macaulay bracket defined as\n\nOrdinarily, when integrating we get\n\nHowever, when integrating expressions containing Macaulay brackets, we have\n\nwith the difference between the two expressions being contained in the constant . Using these integration rules makes the calculation of the deflection of Euler-Bernoulli beams simple in situations where there are multiple point loads and point moments. The Macaulay method predates more sophisticated concepts such as Dirac delta functions and step functions

sim: 0.850 ; pos: 898 ; or motor function below the C6 level and no remaining voluntary bowel or bladder function, the patient reported that due to the high frequency of these episodes he had completely lost any remaining quality of life.\n\nCT of the lumbar spine revealed an enlarged L1-2 disc space with over 50% erosion of the adjacent endplates, along with vacuum disc. Severe spinal canal and neural foraminal narrowing was also seen with multiple large bridging osteophytes. The rest of the thoracolumbar spine had

(d)

Figure 25: Subspace 4 at $\boldsymbol{h}^{4,post}$: Preimages of the residual stream activation. Different from other preimage figures, we show input attribution scores here, because the encoded information depends on long-range context, we need these hints to help us find commonality. The blue color represent the attribution score (see Sec. E.2 for details), they are amplified by a factor of 20 for visibility. The token where the activation is taken from is marked by bold and underscored font. Encoded information is: (a) the current token is repeated multiple times. (b) The current token is repeated multiple times. Note that we check the entire previous context of the query activation, and there are indeed more "water" tokens there. We don't show it due to space limit. (c) The current token "above" (if we only consider similarity > 0.85) (d) The current token "ac". We checked the entire context and found the token "ac" is not repeated. Overall, we found the following pattern: when the current token is relatively less frequent and is repeated, this subspace clusters together activations corresponding to different tokens, otherwise it clusters activations according to current token. The signal might be important to activate induction heads in later layers.

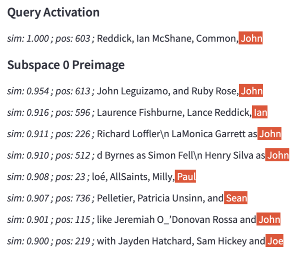

Query Activation

```
sim: 1.000 ; pos: 603 ; Reddick, Ian McShane, Common, John
```

Subspace 0 Preimage

```
sim: 0.954 ; pos: 613 ; John Leguizamo, and Ruby Rose, John
sim: 0.916 ; pos: 596 ; Laurence Fishburne, Lance Reddick, Ian
sim: 0.911 ; pos: 226 ; Richard Loffler\n LaMonica Garrett as John
sim: 0.910 ; pos: 512 ; d Byrnes as Simon Fell\n Henry Silva as John
sim: 0.908 ; pos: 23 ; loé, AllSaints, Milly, Paul
sim: 0.907 ; pos: 736 ; Pelletier, Patricia Unsinn, and Sean
sim: 0.901 ; pos: 115 ; like Jeremiah O_'Donovan Rossa and John
sim: 0.900 ; pos: 219 ; with Jayden Hatchard, Sam Hickey and Joe
```

(a)

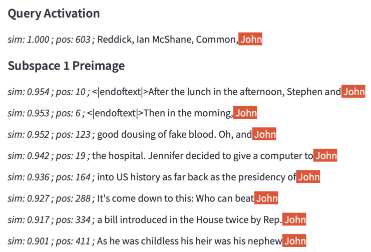

Query Activation

```
sim: 1.000 ; pos: 603 ; Reddick, Ian McShane, Common, John
```

Subspace 1 Preimage

```
sim: 0.954 ; pos: 10 ; <|endoftext|>After the lunch in the afternoon, Stephen and John
sim: 0.953 ; pos: 6 ; <|endoftext|>Then in the morning, John
sim: 0.952 ; pos: 123 ; good dousing of fake blood. Oh, and John
sim: 0.942 ; pos: 19 ; the hospital. Jennifer decided to give a computer to John
sim: 0.936 ; pos: 164 ; into US history as far back as the presidency of John
sim: 0.927 ; pos: 288 ; It's come down to this: Who can beat John
sim: 0.917 ; pos: 334 ; a bill introduced in the House twice by Rep. John
sim: 0.901 ; pos: 411 ; As he was childless his heir was his nephew John
```

(b)

Figure 26: Subspace 0 and subspace 1 at $\boldsymbol{h}^{4,post}$: Preimages of the residual stream activation corresponding to the same input. Both subspace 0 and 1 in this case encode local context, but they are slightly different: subspace 0 encodes a more coarse-grained information for current token (i.e., a first name) and encodes a slightly longer context (i.e., there are more than one name in context); subspace 1 encode shorter context (only the current token) but more fine-grained information (i.e., exactly "John").

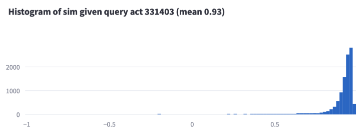

(a)

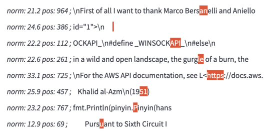

```
norm: 21.2 pos: 964 ; \nFirst of all I want to thank Marco Bersanelli and Aniello
norm: 24.6 pos: 386 ; id="1">\n
norm: 22.2 pos: 112 ; OCKAPI_\n#define _WINSOCKAPI_\n#else\n
norm: 22.6 pos: 261 ; in a wild and open landscape, the gurgle of a burn, the
norm: 33.1 pos: 725 ; \nFor the AWS API documentation, see L<https://docs.aws.
norm: 25.9 pos: 457 ;   Khalid al-Azm\n(1951)
norm: 23.2 pos: 767 ; fmt.Println(pinyin.Pinyin(hans
norm: 12.9 pos: 69 ;       Pursuant to Sixth Circuit I
```

(b)

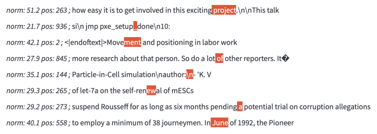

```
norm: 51.2 pos: 263 ; how easy it is to get involved in this exciting project.\n\nThis talk
norm: 21.7 pos: 936 ; si\n jmp pxe_setup_done\n10:
norm: 42.1 pos: 2 ; <|endoftext|>Movement and positioning in labor work
norm: 27.9 pos: 845 ; more research about that person. So do a lot of other reporters. It�
norm: 35.1 pos: 144 ; Particle-in-Cell simulation\nauthor:\n- 'K. V
norm: 29.3 pos: 265 ; of let-7a on the self-renewal of mESCs
norm: 29.2 pos: 273 ; suspend Rousseff for as long as six months pending a potential trial on corruption allegations
norm: 40.1 pos: 558 ; to employ a minimum of 38 journeymen. In June of 1992, the Pioneer
```

(c)

Figure 27: Subspace 9 at $\boldsymbol{h}^{4,post}$: (a) we show the histogram of cosine similarity between a activation and all other activations in the subspace. We can see all activations in the subspace are in similar direction. (b) (c) we show some examples inputs and the L2 norm of their corresponding activations in this subspace, we can see that while direction is similar, the norm can vary between 10-50.

Some subspaces are hard to explain We also find the remaining two subspaces 9 and 10 hard to explain. For subspace 9, we find that, somewhat surprisingly, almost all activations are in a similar direction, as shown in Fig. 27. We also find the norm of activations in this subspace varies, the main variance in this subspace is from this direction. If this is a single feature, what is the pattern that affect the magnitude in this direction? However, we do not have very confident conclusion for this question. We find that the norm is almost always small if the current token is in the middle of a multi-token word (e.g., Fig. 27(b)'s bottom row) and very big ≈ 2000 for "end of sequence" (EOS) token. One point we can believe is that, the information encoded in this direction is quite independent with the information in other subspaces. Interestingly, subspace 9 in $\boldsymbol{h}^{8,post}$ also shows this pattern, i.e., all activations point to similar direction and big norm for EOS. But subspace in that layer is the one with the highest effect in test 3 described in Sec. 5.1: it has an un-normalized effect of 2.31 ($d_9 = 32$), the second and third largest is 0.78 ($d_2 = 96$) and 0.30. This means such an subspace indeed encodes certain meaningful information. In IOI domain it is the position of the subject (outputs from S-Inhibition heads), but it might be part of a more general mechanism, like a signal to not attend to certain part of context. That explains why it is so hard to interpret.

Coming back to layer 4, for subspace 10, we also see many activations in the same direction, but not as often as subspace 9. For both 9 and 10, we do not have a clear conclusion for the information encoded by them. But we believe they are worth more extensive study, as it might reveal some unexpected features used by the model.

Summary of subspace interpretation for $\boldsymbol{h}^{4,post}$. So far we have described every subspace we found for one layer. Here is a brief overview:

- Subspace 0 ($d_0 = 128$), 1 ($d_1 = 128$), 2 ($d_2 = 96$), 3 ($d_3 = 96$), 5 ($d_5 = 64$): short-range local context, usually only most recent few tokens. They encode slightly different information.
- Subspace 4 ($d_4 = 64$): Repetition in the context.

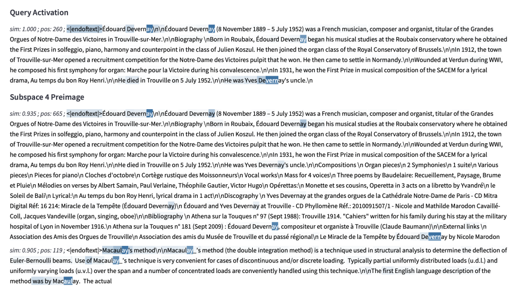

Query Activation

sim: 1.000 ; pos: 260 ; <|endoftext|>Édouard Devernay\n\nÉdouard Devernay (8 November 1889 – 5 July 1952) was a French musician, composer and organist, titular of the Grandes Orgues of Notre-Dame des Victoires in Trouville-sur-Mer.\n\nBiography \nBorn in Roubaix, Édouard Devernay began his musical studies at the Roubaix conservatory where he obtained the First Prizes in solfeggio, piano, harmony and counterpoint in the class of Julien Koszul. He then joined the organ class of the Royal Conservatory of Brussels.\n\nIn 1912, the town of Trouville-sur-Mer opened a recruitment competition for the Notre-Dame des Victoires pulpit that he won. He then came to settle in Normandy.\n\nWounded at Verdun during WWI, he composed his first symphony for organ: Marche pour la Victoire during his convalescence.\n\nIn 1931, he won the First Prize in musical composition of the SACEM for a lyrical drama, Au temps du bon Roy Henri.\n\nHe died in Trouville on 5 July 1952.\n\nHe was Yves Devernay's uncle.\n

Subspace 4 Preimage

sim: 0.935 ; pos: 665 ; <|endoftext|>Édouard Devernay\n\nÉdouard Devernay (8 November 1889 – 5 July 1952) was a French musician, composer and organist, titular of the Grandes Orgues of Notre-Dame des Victoires in Trouville-sur-Mer.\n\nBiography \nBorn in Roubaix, Édouard Devernay began his musical studies at the Roubaix conservatory where he obtained the First Prizes in solfeggio, piano, harmony and counterpoint in the class of Julien Koszul. He then joined the organ class of the Royal Conservatory of Brussels.\n\nIn 1912, the town of Trouville-sur-Mer opened a recruitment competition for the Notre-Dame des Victoires pulpit that he won. He then came to settle in Normandy.\n\nWounded at Verdun during WWI, he composed his first symphony for organ: Marche pour la Victoire during his convalescence.\n\nIn 1931, he won the First Prize in musical composition of the SACEM for a lyrical drama, Au temps du bon Roy Henri.\n\nHe died in Trouville on 5 July 1952.\n\nHe was Yves Devernay's uncle.\n\nCompositions \n Organ pieces\n 2 Symphonies\n 1 suite\n Various pieces\n Pieces for piano\n Cloches d'octobre\n Cortège rustique des Moissonneurs\n Vocal works\n Mass for 4 voices\n Three poems by Baudelaire: Recueillement, Paysage, Brume et Pluie\n Mélodies on verses by Albert Samain, Paul Verlaine, Théophile Gautier, Victor Hugo\n Opérettas:\n Monette et ses cousins, Operetta in 3 acts on a libretto by Yvandré\n le Soleil de Bali\n Lyrical:\n Au temps du bon Roy Henri, lyrical drama in 1 act\n\nDiscography \n Yves Devernay at the grandes orgues de la Cathédrale Notre-Dame de Paris - CD Mitra Digital Réf: 16 214: Miracle de la Tempête (Édouard Devernay)\n Édouard and Yves Devernay at Trouville - CD Phyllomène Réf.: 2010091507/1 - Nicole and Mathilde Marodon Cavaillé-Coll, Jacques Vandeville (organ, singing, oboe)\n\nBibliography \n Athena sur la Touques n° 97 (Sept 1988): Trouville 1914. "Cahiers" written for his family during his stay at the military hospital of Lyon in November 1916.\n Athena sur la Touques n° 181 (Sept 2009) : Édouard Devernay, compositeur et organiste à Trouville (Claude Baumann)\n\nExternal links \n Association des Amis des Orgues de Trouville\n Association des amis du Musée de Trouville et du passé régional\n Le Miracle de la Tempête by Édouard Devernay by Nicole Marodon

sim: 0.905 ; pos: 119 ; <|endoftext|>Macaulay's method\n\nMacaulay_'s method (the double integration method) is a technique used in structural analysis to determine the deflection of Euler-Bernoulli beams. Use of Macaulay_'s technique is very convenient for cases of discontinuous and/or discrete loading. Typically partial uniformly distributed loads (u.d.l.) and uniformly varying loads (u.v.l.) over the span and a number of concentrated loads are conveniently handled using this technique.\n\nThe first English language description of the method was by Macaulay. The actual

(a)

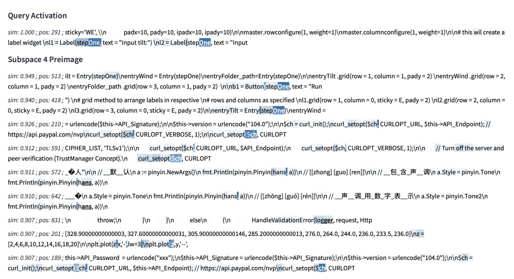

Query Activation

```
sim: 1.000 ; pos: 291 ; sticky='WE', \\n          padx=10, pady=10, ipadx=10, ipady=10)\n\nmaster.rowconfigure(1, weight=1)\nmaster.columnconfigure(1, weight=1)\n\n# this wil create a label widget \nl1 = Label(stepOne, text = "Input tilt:") \nl2 = Label(stepOne, text = "Input
```

Subspace 4 Preimage

```
sim: 0.949 ; pos: 513 ; ilt = Entry(stepOne)\nentryWind = Entry(stepOne)\nentryFolder_path=Entry(stepOne)\n\nentryTilt .grid(row = 1, column = 1, pady = 2) \nentryWind .grid(row = 2, column = 1, pady = 2) \nentryFolder_path .grid(row = 3, column = 1, pady = 2)  \n\nb1 = Button(stepOne, text = "Run

sim: 0.940 ; pos: 418 ; ") \n# grid method to arrange labels in respective \n# rows and columns as specified \nl1.grid(row = 1, column = 0, sticky = E, pady = 2) \nl2.grid(row = 2, column = 0, sticky = E, pady = 2) \nl3.grid(row = 3, column = 0, sticky = E, pady = 2)\n\nentryTilt = Entry(stepOne)\nentryWind =

sim: 0.926 ; pos: 210 ; = urlencode($this->API_Signature);\n\n$this->version = urlencode("104.0");\n\n$ch = curl_init();\ncurl_setopt($ch, CURLOPT_URL, $this->API_Endpoint); // https://api.paypal.com/nvp\ncurl_setopt($ch, CURLOPT_VERBOSE, 1);\n\ncurl_setopt($ch, CURLOPT

sim: 0.912 ; pos: 591 ; CIPHER_LIST, 'TLSv1');\n\n      curl_setopt($ch, CURLOPT_URL, $API_Endpoint);\n      curl_setopt($ch, CURLOPT_VERBOSE, 1);\n\n      // Turn off the server and peer verification (TrustManager Concept).\n      curl_setopt($ch, CURLOPT

sim: 0.911 ; pos: 572 ; _�人"\n\n // __默__认\n a := pinyin.NewArgs()\n fmt.Println(pinyin.Pinyin(hans, a))\n // [[zhong] [guo] [ren]]\n\n // __包_含_声__调\n a.Style = pinyin.Tone\n fmt.Println(pinyin.Pinyin(hans, a))\n

sim: 0.910 ; pos: 642 ; ___�\n a.Style = pinyin.Tone\n fmt.Println(pinyin.Pinyin(hans, a))\n // [[zhōng] [guó] [rén]]\n\n // __声__调_用_数_字_表__示\n a.Style = pinyin.Tone2\n fmt.Println(pinyin.Pinyin(hans, a))\n

sim: 0.907 ; pos: 831 ; \n          throw;\n          }\n        }\n      else\n      {\n          HandleValidationError(logger, request, Http

sim: 0.907 ; pos: 201 ; [328.90000000000003, 327.60000000000031, 305.90000000000146, 285.20000000000013, 276.0, 264.0, 244.0, 236.0, 233.5, 236.0]\nz = [2,4,6,8,10,12,14,16,18,20]\n\nplt.plot(z,x,'-',lw=3)\nplt.plot(z,y,'--',

sim: 0.907 ; pos: 189 ; this->API_Password  = urlencode("xxx");\n$this->API_Signature = urlencode($this->API_Signature);\n\n$this->version = urlencode("104.0");\n\n$ch = curl_init();\ncurl_setopt($ch, CURLOPT_URL, $this->API_Endpoint); // https://api.paypal.com/nvp\ncurl_setopt($ch, CURLOPT
```

(b)

Figure 28: Subspace 4 at $\boldsymbol{h}^{6,post}$: The subspace is the one with the highest patching effect in test 2 described in Sec. 5.1, so it should encode output of induction heads. (a) "ay" is moved by induction mechanism. We show the entire context for each input. (b) "," is moved by induction mechanism. We check the entire context and confirm that the first, second sample's context indeed contain a ("One", ",") combination, and the third from the last indeed contains a ("er", ",") combination. We scale attribution scores by 10 or so. Importantly, we *pick* these two on purpose, because in many case the induction mechanism is not "activated". In those cases the information is more about the current token. In many other cases there are simply not enough samples in preimage due to limited size of our activation database.

- Subspace 6 ($d_6 = 64$): Previous token, almost excluding the current token.
- Subspace 7 ($d_7 = 32$): Position information.
- Subspace 8 ($d_8 = 32$): Longer-range context, topic or the main described object.
- Subspace 9 ($d_9 = 32$), 10 ($d_{10} = 32$): No clear conclusion.

Subspaces in later layers After exhaustively exploring subspaces in the residual stream after layer 4 (the 5th layer), we move on to take a brief look at subspaces in later layers. We show some preimages in Fig. 28 and Fig. 29, which correspond to two subspaces with the highest patching effect in quantitative evaluation. The web application includes results for all 4 layers (4, 6, 8, 9) used in quantitative evaluation, we encourage readers to check our web application.

To check interpretability of subspaces in later layers, we also try to interpret every subspace of layer 9, and summarize our findings as follows:

- Subspace 0 ($d_0 = 128$), 1 ($d_1 = 96$), 2 ($d_2 = 96$), 3 ($d_3 = 64$), 8 ($d_8 = 32$): local context. Compared to layer 4, they tend to cover a longer span of context, such as a sub-clause. They encode slightly different information.
- Subspace 4 ($d_4 = 64$): Induction output.
- Subspace 5 ($d_5 = 64$): Longer-range context, topic or the main described object.
- Subspace 6 ($d_6 = 32$): Certain kind of syntactic role of the current token, not necessarily aligned with human definition, such as whether the current token is the subject, or starting/ending of a sub-clause/sentence.
- Subspace 7 ($d_7 = 32$): Position information.
- Subspace 9 ($d_9 = 32$), 10 ($d_{10} = 32$), 11 ($d_{11} = 32$), 12 ($d_{12} = 32$): No clear conclusion. Subspace 10 shows similar pattern as subspace 9 of layer 4 residual stream $\boldsymbol{h}^{4,post}$.

Again, we see some subspaces that are hard to interpret, they tend to be quite independent from other subspaces (Fig. 14(d)).

E.4 SUBSPACES FOR PARAMETRIC KNOWLEDGE ROUTING IN QWEN2.5-1.5B

In Fig. 4(a), we see that there are two subspaces, 2 and 6, playing important roles for parametric knowledge routing. We apply the same qualitative analysis to see what is the information encoded

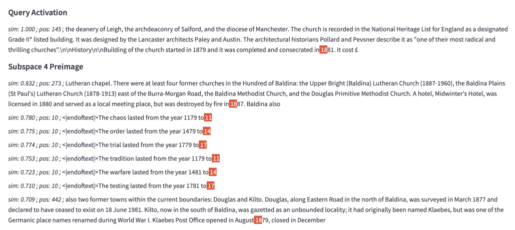
Query Activation

sim: 1.000 ; pos: 145 ; the deanery of Leigh, the archdeaconry of Salford, and the diocese of Manchester. The church is recorded in the National Heritage List for England as a designated Grade II* listed building. It was designed by the Lancaster architects Paley and Austin. The architectural historians Pollard and Pevsner describe it as "one of their most radical and thrilling churches".\n\nHistory\n\nBuilding of the church started in 1879 and it was completed and consecrated in 1881. It cost £

Subspace 4 Preimage

sim: 0.832 ; pos: 273 ; Lutheran chapel. There were at least four former churches in the Hundred of Baldina: the Upper Bright (Baldina) Lutheran Church (1887-1960), the Baldina Plains (St Paul's) Lutheran Church (1878-1913) east of the Burra-Morgan Road, the Baldina Methodist Church, and the Douglas Primitive Methodist Church. A hotel, Midwinter's Hotel, was licensed in 1880 and served as a local meeting place, but was destroyed by fire in 1887. Baldina also

sim: 0.780 ; pos: 10 ; <|endoftext|>The chaos lasted from the year 1179 to 11

sim: 0.775 ; pos: 10 ; <|endoftext|>The order lasted from the year 1479 to 14

sim: 0.774 ; pos: 10 ; <|endoftext|>The trial lasted from the year 1779 to 17

sim: 0.753 ; pos: 10 ; <|endoftext|>The tradition lasted from the year 1179 to 11

sim: 0.723 ; pos: 10 ; <|endoftext|>The warfare lasted from the year 1481 to 14

sim: 0.710 ; pos: 10 ; <|endoftext|>The testing lasted from the year 1781 to 17

sim: 0.709 ; pos: 442 ; also two former towns within the current boundaries: Douglas and Kilto. Douglas, along Eastern Road in the north of Baldina, was surveyed in March 1877 and declared to have ceased to exist on 18 June 1981. Kilto, now in the south of Baldina, was gazetted as an unbounded locality; it had originally been named Klaebes, but was one of the Germanic place names renamed during World War I. Klaebes Post Office opened in August 1879, closed in December

(a)

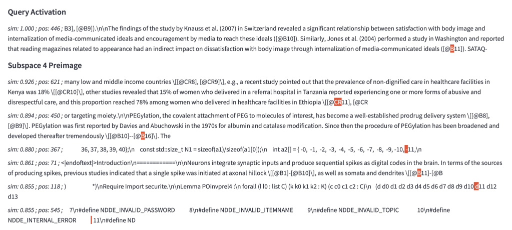
Query Activation

sim: 1.000 ; pos: 446 ; B3], [@B9]).\n\nThe findings of the study by Knauss et al. (2007) in Switzerland revealed a significant relationship between satisfaction with body image and internalization of media-communicated ideals and encouragement by media to reach these ideals ([@B10]). Similarly, Jones et al. (2004) performed a study in Washington and reported that reading magazines related to appearance had an indirect impact on dissatisfaction with body image through internalization of media-communicated ideals ([@B11]). SATAQ-

Subspace 4 Preimage

sim: 0.926 ; pos: 621 ; many low and middle income countries \[[@CR8], [@CR9]\], e.g., a recent study pointed out that the prevalence of non-dignified care in healthcare facilities in Kenya was 18% \[[@CR10]\], other studies revealed that 15% of women who delivered in a referral hospital in Tanzania reported experiencing one or more forms of abusive and disrespectful care, and this proportion reached 78% among women who delivered in healthcare facilities in Ethiopia \[[@CR11], [@CR

sim: 0.894 ; pos: 450 ; or targeting moiety.\n\nPEGylation, the covalent attachment of PEG to molecules of interest, has become a well-established prodrug delivery system \[[@B8], [@B9]\]. PEGylation was first reported by Davies and Abuchowski in the 1970s for albumin and catalase modification. Since then the procedure of PEGylation has been broadened and developed thereafter tremendously \[[@B10]--[@B16]\]. The

sim: 0.880 ; pos: 367 ;   36, 37, 38, 39, 40};\n   const std::size_t N1 = sizeof(a1)/sizeof(a1[0]);\n   int a2[] = { -0, -1, -2, -3, -4, -5, -6, -7, -8, -9, -10, -11,\n

sim: 0.861 ; pos: 71 ; <|endoftext|>Introduction\n============\n\nNeurons integrate synaptic inputs and produce sequential spikes as digital codes in the brain. In terms of the sources of producing spikes, previous studies indicated that a single spike was initiated at axonal hillock \[[@B1]-[@B10]\], as well as somata and dendrites \[[@B11]-[@B

sim: 0.855 ; pos: 118 ;)   *)\nRequire Import securite.\n\nLemma POinvprel4 :\n forall (l l0 : list C) (k k0 k1 k2 : K) (c c0 c1 c2 : C)\n   (d d0 d1 d2 d3 d4 d5 d6 d7 d8 d9 d10 d11 d12 d13

sim: 0.855 ; pos: 545 ;   7\n#define NDDE_INVALID_PASSWORD   8\n#define NDDE_INVALID_ITEMNAME   9\n#define NDDE_INVALID_TOPIC   10\n#define NDDE_INTERNAL_ERROR   11\n#define ND

(b)

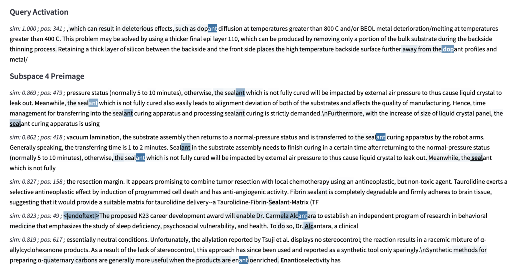
Query Activation

sim: 1.000 ; pos: 341 ; , which can result in deleterious effects, such as dopant diffusion at temperatures greater than 800 C and/or BEOL metal deterioration/melting at temperatures greater than 400 C. This problem may be solved by using a thicker final epi layer 110, which can be produced by removing only a portion of the bulk substrate during the backside thinning process. Retaining a thick layer of silicon between the backside and the front side places the high temperature backside surface further away from the dopant profiles and metal/

Subspace 4 Preimage

sim: 0.869 ; pos: 479 ; pressure status (normally 5 to 10 minutes), otherwise, the sealant which is not fully cured will be impacted by external air pressure to thus cause liquid crystal to leak out. Meanwhile, the sealant which is not fully cured also easily leads to alignment deviation of both of the substrates and affects the quality of manufacturing. Hence, time management for transferring into the sealant curing apparatus and processing sealant curing is strictly demanded.\nFurthermore, with the increase of size of liquid crystal panel, the sealant curing apparatus is using

sim: 0.862 ; pos: 418 ; vacuum lamination, the substrate assembly then returns to a normal-pressure status and is transferred to the sealant curing apparatus by the robot arms. Generally speaking, the transferring time is 1 to 2 minutes. Sealant in the substrate assembly needs to finish curing in a certain time after returning to the normal-pressure status (normally 5 to 10 minutes), otherwise, the sealant which is not fully cured will be impacted by external air pressure to thus cause liquid crystal to leak out. Meanwhile, the sealant which is not fully

sim: 0.827 ; pos: 158 ; the resection margin. It appears promising to combine tumor resection with local chemotherapy using an antineoplastic, but non-toxic agent. Taurolidine exerts a selective antineoplastic effect by induction of programmed cell death and has anti-angiogenic activity. Fibrin sealant is completely degradable and firmly adheres to brain tissue, suggesting that it would provide a suitable matrix for taurolidine delivery--a Taurolidine-Fibrin-Sealant-Matrix (TF

sim: 0.823 ; pos: 49 ; <|endoftext|>The proposed K23 career development award will enable Dr. Carmela Alcantara to establish an independent program of research in behavioral medicine that emphasizes the study of sleep deficiency, psychosocial vulnerability, and health. To do so, Dr. Alcantara, a clinical

sim: 0.819 ; pos: 617 ; essentially neutral conditions. Unfortunately, the allylation reported by Tsuji et al. displays no stereocontrol; the reaction results in a racemic mixture of α-allylcyclohexanone products. As a result of the lack of stereocontrol, this approach has since been used and reported as a synthetic tool only sparingly.\nSynthetic methods for preparing α-quaternary carbons are generally more useful when the products are enantioenriched. Enantioselectivity has

(c)

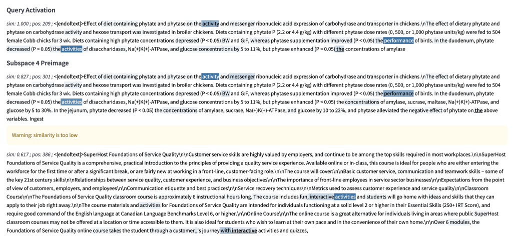
Query Activation

sim: 1.000 ; pos: 209 ; <|endoftext|>Effect of diet containing phytate and phytase on the activity and messenger ribonucleic acid expression of carbohydrase and transporter in chickens.\nThe effect of dietary phytate and phytase on carbohydrase activity and hexose transport was investigated in broiler chickens. Diets containing phytate P (2.2 or 4.4 g/kg) with different phytase dose rates (0, 500, or 1,000 phytase units/kg) were fed to 504 female Cobb chicks for 3 wk. Diets containing high phytate concentrations depressed (P < 0.05) BW and G:F, whereas phytase supplementation improved (P < 0.05) the performance of birds. In the duodenum, phytate decreased (P < 0.05) the activities of disaccharidases, Na(+)K(+)-ATPase, and glucose concentrations by 5 to 11%, but phytase enhanced (P < 0.05) the concentrations of amylase

Subspace 4 Preimage

sim: 0.827 ; pos: 301 ; <|endoftext|>Effect of diet containing phytate and phytase on the activity and messenger ribonucleic acid expression of carbohydrase and transporter in chickens.\nThe effect of dietary phytate and phytase on carbohydrase activity and hexose transport was investigated in broiler chickens. Diets containing phytate P (2.2 or 4.4 g/kg) with different phytase dose rates (0, 500, or 1,000 phytase units/kg) were fed to 504 female Cobb chicks for 3 wk. Diets containing high phytate concentrations depressed (P < 0.05) BW and G:F, whereas phytase supplementation improved (P < 0.05) the performance of birds. In the duodenum, phytate decreased (P < 0.05) the activities of disaccharidases, Na(+)K(+)-ATPase, and glucose concentrations by 5 to 11%, but phytase enhanced (P < 0.05) the concentrations of amylase, sucrase, maltase, Na(+)K(+)-ATPase, and glucose by 5 to 30%. In the jejunum, phytate decreased (P < 0.05) the concentrations of amylase, sucrase, Na(+)K(+)-ATPase, and glucose by 10 to 22%, and phytase alleviated the negative effect of phytate on the above variables. Ingest

Warning: similarity is too low

sim: 0.617 ; pos: 386 ; <|endoftext|>SuperHost Foundations of Service Quality\n\nCustomer service skills are highly valued by employers, and continue to be among the top skills required in most workplaces.\n\nSuperHost Foundations of Service Quality is a comprehensive, practical introduction to the principles of providing a quality service experience. Available online or in-class, this course is ideal for people who are either entering the workforce for the first time or after a significant break, or are fairly new at working in a front-line, customer-facing role.\n\nThe course will cover:\n\nBasic customer service, communication and teamwork skills – some of the key 21st century skills\n\nRelationships between service quality, customer experience, and business objectives\n\nThe importance of front-line employees in service sector businesses\n\nExpectations from the point of view of customers, employers, and employees\n\nCommunication etiquette and best practices\n\nService recovery techniques\n\nMetrics used to assess customer experience and service quality\n\nClassroom Course\n\nThe Foundations of Service Quality classroom course is approximately 6 instructional hours long. The course includes fun, interactive activities and students will go home with ideas and skills that they can apply to their job right away.\n\nThe course materials and activities for Foundations of Service Quality are intended for individuals functioning at a solid level 2 or higher in their Essential Skills (250+ IRT Score), and require good command of the English language at Canadian Language Benchmarks Level 6, or higher.\n\nOnline Course\n\nThe online course is a great alternative for individuals living in areas where public SuperHost classroom courses may not be offered at a location or time accessible to them. It is also ideal for students who wish to learn at their own pace and in the convenience of their own home.\n\nOver 6 modules, the Foundations of Service Quality online course takes the student through a customer_'s journey with interactive activities and quizzes,

(d)

Figure 29: Subspace 4 at $\boldsymbol{h}^{9,post}$: The subspace is the one with the highest patching effect in test 5 described in Sec. 5.1, the effect of all subspaces is shown in Table 2. So it should encode the starting year information in Greater-than prompts. (a) Encoded information is (approximately) "79". We can see how the same mechanism in Greater-than prompts is being used in more natural text. Note that we lower the threshold to 0.7 in order to include more samples. We can see though having the same starting year "79", the four Great-than prompts are not close enough to query activation, so some other context is also slightly encoded in this subspace. (b) Encoded information is "10". Here we can see how this circuit is useful in a broader domain. (c) Encoded information is "ant". We can see this subspace is essentially a induction output subspace. (d) It seems that the encoded information is a mixture of "activities" and "performance", having only one of them (like the last sample) is not enough to get close to the query activation. So the induction circuit is triggered quite often, it can be used to predict the noun after "the".

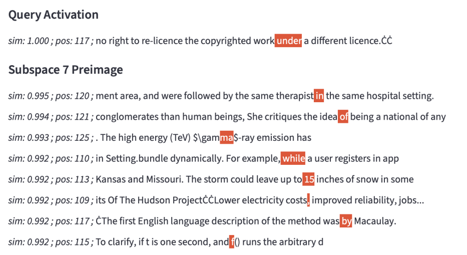
Query Activation

sim: 1.000 ; pos: 117 ; no right to re-licence the copyrighted work under a different licence.ĊĊ

Subspace 7 Preimage

sim: 0.995 ; pos: 120 ; ment area, and were followed by the same therapist in the same hospital setting.

sim: 0.994 ; pos: 121 ; conglomerates than human beings, She critiques the idea of being a national of any

sim: 0.993 ; pos: 125 ; . The high energy (TeV) γ-ray emission has

sim: 0.992 ; pos: 110 ; in Setting.bundle dynamically. For example, while a user registers in app

sim: 0.992 ; pos: 113 ; Kansas and Missouri. The storm could leave up to 15 inches of snow in some

sim: 0.992 ; pos: 109 ; its Of The Hudson ProjectĊĊLower electricity costs, improved reliability, jobs...

sim: 0.992 ; pos: 117 ; ĊThe first English language description of the method was by Macaulay.

sim: 0.992 ; pos: 115 ; To clarify, if t is one second, and f() runs the arbitrary d

(a)

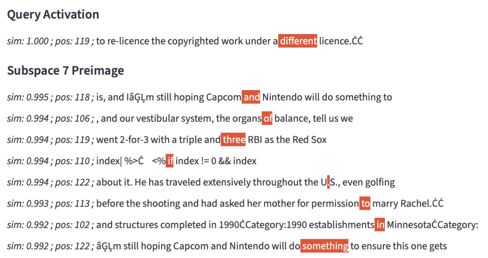
Query Activation

sim: 1.000 ; pos: 119 ; to re-licence the copyrighted work under a different licence.ĊĊ

Subspace 7 Preimage

sim: 0.995 ; pos: 118 ; is, and IâĢĻm still hoping Capcom and Nintendo will do something to

sim: 0.994 ; pos: 106 ; , and our vestibular system, the organs of balance, tell us we

sim: 0.994 ; pos: 119 ; went 2-for-3 with a triple and three RBI as the Red Sox

sim: 0.994 ; pos: 110 ; index| %>Ċ   <% if index != 0 && index

sim: 0.994 ; pos: 122 ; about it. He has traveled extensively throughout the U.S., even golfing

sim: 0.993 ; pos: 113 ; before the shooting and had asked her mother for permission to marry Rachel.ĊĊ

sim: 0.992 ; pos: 102 ; and structures completed in 1990ĊCategory:1990 establishments in MinnesotaĊCategory:

sim: 0.992 ; pos: 122 ; âĢĻm still hoping Capcom and Nintendo will do something to ensure this one gets

(b)

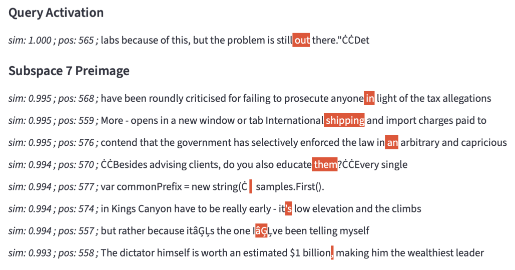
Query Activation

sim: 1.000 ; pos: 565 ; labs because of this, but the problem is still out there."ĊĊDet

Subspace 7 Preimage

sim: 0.995 ; pos: 568 ; have been roundly criticised for failing to prosecute anyone in light of the tax allegations

sim: 0.995 ; pos: 559 ; More - opens in a new window or tab International shipping and import charges paid to

sim: 0.995 ; pos: 576 ; contend that the government has selectively enforced the law in an arbitrary and capricious

sim: 0.994 ; pos: 570 ; ĊĊBesides advising clients, do you also educate them?ĊĊEvery single

sim: 0.994 ; pos: 577 ; var commonPrefix = new string(Ċ samples.First().

sim: 0.994 ; pos: 574 ; in Kings Canyon have to be really early - it's low elevation and the climbs

sim: 0.994 ; pos: 557 ; but rather because itâĢĻs the one IâĢĻve been telling myself

sim: 0.993 ; pos: 558 ; The dictator himself is worth an estimated $1 billion, making him the wealthiest leader

(c)

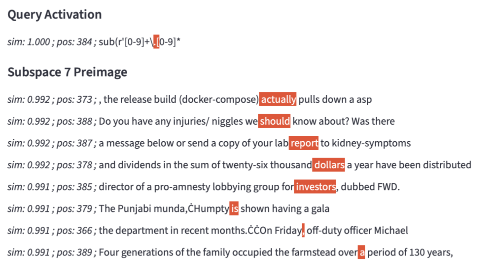
Query Activation

sim: 1.000 ; pos: 384 ; sub(r'[0-9]+\.[0-9]*

Subspace 7 Preimage

sim: 0.992 ; pos: 373 ; , the release build (docker-compose) actually pulls down a asp

sim: 0.992 ; pos: 388 ; Do you have any injuries/ niggles we should know about? Was there

sim: 0.992 ; pos: 387 ; a message below or send a copy of your lab report to kidney-symptoms

sim: 0.992 ; pos: 378 ; and dividends in the sum of twenty-six thousand dollars a year have been distributed

sim: 0.991 ; pos: 385 ; director of a pro-amnesty lobbying group for investors, dubbed FWD.

sim: 0.991 ; pos: 379 ; The Punjabi munda,ĊHumpty is shown having a gala

sim: 0.991 ; pos: 366 ; the department in recent months.ĊĊOn Friday, off-duty officer Michael

sim: 0.991 ; pos: 389 ; Four generations of the family occupied the farmstead over a period of 130 years,

(d)

Figure 30: Subspace 7 at $\boldsymbol{h}^{4,post}$: Same examples as Figure 22, but the threshold for cosine similarity is increased to 0.99, we obtain samples of very similar positions. Remaining error could be because the optimization is not optimal, or the model has forgotten the information a bit at this layer.

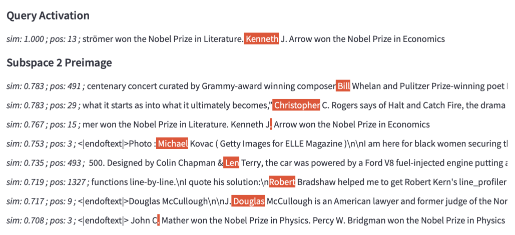

Query Activation

sim: 1.000 ; pos: 13 ; strömer won the Nobel Prize in Literature. Kenneth J. Arrow won the Nobel Prize in Economics

Subspace 2 Preimage

sim: 0.783 ; pos: 491 ; centenary concert curated by Grammy-award winning composer Bill Whelan and Pulitzer Prize-winning poet

sim: 0.783 ; pos: 29 ; what it starts as into what it ultimately becomes," Christopher C. Rogers says of Halt and Catch Fire, the drama

sim: 0.767 ; pos: 15 ; mer won the Nobel Prize in Literature. Kenneth J. Arrow won the Nobel Prize in Economics

sim: 0.753 ; pos: 3 ; <|endoftext|>Photo : Michael Kovac (Getty Images for ELLE Magazine)\n\nI am here for black women securing t

sim: 0.735 ; pos: 493 ; 500. Designed by Colin Chapman & Len Terry, the car was powered by a Ford V8 fuel-injected engine putting

sim: 0.719 ; pos: 1327 ; functions line-by-line.\nI quote his solution:\nRobert Bradshaw helped me to get Robert Kern's line_profiler

sim: 0.717 ; pos: 9 ; <|endoftext|>Douglas McCullough\n\nJ. Douglas McCullough is an American lawyer and former judge of the Nor

sim: 0.708 ; pos: 3 ; <|endoftext|> John C. Mather won the Nobel Prize in Physics. Percy W. Bridgman won the Nobel Prize in Physics

(a)

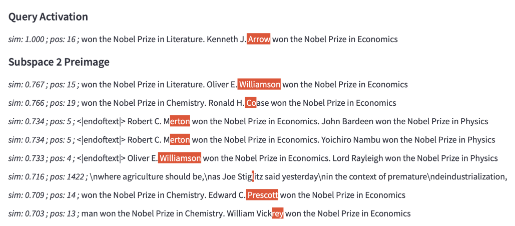

Query Activation

sim: 1.000 ; pos: 16 ; won the Nobel Prize in Literature. Kenneth J. Arrow won the Nobel Prize in Economics

Subspace 2 Preimage

sim: 0.767 ; pos: 15 ; won the Nobel Prize in Literature. Oliver E. Williamson won the Nobel Prize in Economics

sim: 0.766 ; pos: 19 ; won the Nobel Prize in Chemistry. Ronald H. Coase won the Nobel Prize in Economics

sim: 0.734 ; pos: 5 ; <|endoftext|> Robert C. Merton won the Nobel Prize in Economics. John Bardeen won the Nobel Prize in Physics

sim: 0.734 ; pos: 5 ; <|endoftext|> Robert C. Merton won the Nobel Prize in Economics. Yoichiro Nambu won the Nobel Prize in Physics

sim: 0.733 ; pos: 4 ; <|endoftext|> Oliver E. Williamson won the Nobel Prize in Economics. Lord Rayleigh won the Nobel Prize in Physics

sim: 0.716 ; pos: 1422 ; \nwhere agriculture should be,\nas Joe Stiglitz said yesterday\nin the context of premature\ndeindustrialization,

sim: 0.709 ; pos: 14 ; won the Nobel Prize in Chemistry. Edward C. Prescott won the Nobel Prize in Economics

sim: 0.703 ; pos: 13 ; man won the Nobel Prize in Chemistry. William Vickrey won the Nobel Prize in Economics

(b)

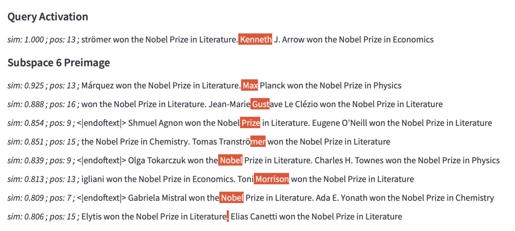

Query Activation

sim: 1.000 ; pos: 13 ; strömer won the Nobel Prize in Literature. Kenneth J. Arrow won the Nobel Prize in Economics

Subspace 6 Preimage

sim: 0.925 ; pos: 13 ; Márquez won the Nobel Prize in Literature. Max Planck won the Nobel Prize in Physics

sim: 0.888 ; pos: 16 ; won the Nobel Prize in Literature. Jean-Marie Gustave Le Clézio won the Nobel Prize in Literature

sim: 0.854 ; pos: 9 ; <|endoftext|> Shmuel Agnon won the Nobel Prize in Literature. Eugene O'Neill won the Nobel Prize in Literature

sim: 0.851 ; pos: 15 ; the Nobel Prize in Chemistry. Tomas Tranströmer won the Nobel Prize in Literature

sim: 0.839 ; pos: 9 ; <|endoftext|> Olga Tokarczuk won the Nobel Prize in Literature. Charles H. Townes won the Nobel Prize in Physics

sim: 0.813 ; pos: 13 ; igliani won the Nobel Prize in Economics. Toni Morrison won the Nobel Prize in Literature

sim: 0.809 ; pos: 7 ; <|endoftext|> Gabriela Mistral won the Nobel Prize in Literature. Ada E. Yonath won the Nobel Prize in Chemistry

sim: 0.806 ; pos: 15 ; Elytis won the Nobel Prize in Literature. Elias Canetti won the Nobel Prize in Literature

(c)

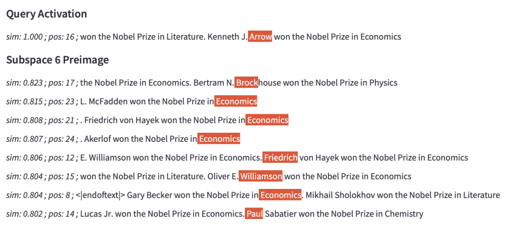

Query Activation

sim: 1.000 ; pos: 16 ; won the Nobel Prize in Literature. Kenneth J. Arrow won the Nobel Prize in Economics

Subspace 6 Preimage

sim: 0.823 ; pos: 17 ; the Nobel Prize in Economics. Bertram N. Brockhouse won the Nobel Prize in Physics

sim: 0.815 ; pos: 23 ; L. McFadden won the Nobel Prize in Economics

sim: 0.808 ; pos: 21 ; . Friedrich von Hayek won the Nobel Prize in Economics

sim: 0.807 ; pos: 24 ; . Akerlof won the Nobel Prize in Economics

sim: 0.806 ; pos: 12 ; E. Williamson won the Nobel Prize in Economics. Friedrich von Hayek won the Nobel Prize in Economics

sim: 0.804 ; pos: 15 ; won the Nobel Prize in Literature. Oliver E. Williamson won the Nobel Prize in Economics

sim: 0.804 ; pos: 8 ; <|endoftext|> Gary Becker won the Nobel Prize in Economics. Mikhail Sholokhov won the Nobel Prize in Literature

sim: 0.802 ; pos: 14 ; Lucas Jr. won the Nobel Prize in Economics. Paul Sabatier won the Nobel Prize in Chemistry

(d)

Figure 31: All statements shown are true, there is no made-up entity. **(a) & (b)**: Subspace 2 at $\boldsymbol{h}^{11,mid}$ in Qwen2.5-1.5B. The subspace is the one with the highest patching effect under `Param Corrupt` in shown in Fig. 4(a). So it should play an important role for routing parametric knowledge. Encoded information shown in (a) is simply "first name" or "partial person name", while information shown in (b) is the knowledge retrieved from model's parametric memory, "the person is economist". Therefore, we hypothesize that *this subspace receives knowledge retrieved from MLP layer*. When only part of the name is observed, the only "knowledge" is that "this is a first name", when enough tokens are observed (not necessarily the full name) to identify a memorized person, the subspace is filled with retrieved knowledge, like the field of work. Note that for this subspace we lower the threshold of cosine similarity to 0.7 in order to include enough samples. So it seems to also encode other kinds of information. Better training might help disentangle them. **(c) & (d)**: Subspace 6 at $\boldsymbol{h}^{11,mid}$ in Qwen2.5-1.5B. This is the one with the second highest effect under `Param Corrupt` in shown in Fig. 4(a). That means it also plays a non-trivial role for parametric knowledge. Encoded information shown in (c) is "Literature in the context", in (d) is "Economics in the context". From these two preiamges, we hypothesize that *this subspace receives knowledge broadcasted from the most recent recognized entity*. At first name token position, the current name "Kenneth" is not enough to identified any memorized person, so this subspace contains the previous entity's knowledge "Literature", other normal tokens such as "Prize", "Nobel", "." also receive this knowledge, and similarly for (d). Note that for this subspace we sometimes do not find clear interpretation for individual preimage. Possible reason could be that sometimes current entity is "half recognized" and its knowledge is mixed with previous entity.

in them, and if they differ in some way. Like in quantitative tests, we test and remove entities that model does not have knowledge for. We randomly sample 250 entity pairs from them, each is used to construct a 2-shot example. We then run Qwen2.5-1.5B on these examples, together with 2000 text sequences from MiniPile, and collect activations to build the database. Fig. 31 shows some examples. As we can see, they indeed differ. Though they both contain retrieved parametric knowledge, subspace 2 encodes the knowledge about the current n-gram, while subspace 6 encodes knowledge that does not depend on current token. We therefore have the following hypothesis: when enough tokens are observed and the name is identifiable, MLP retrieves knowledge and places it into subspace 2, this knowledge is then emitted by attention heads to many other tokens' residual stream (or in other words, attended by other tokens), this information arrives at certain subspace similar to subspace 6, but at later layers. This behavior is probably distributed and repeated across multiple middle layers, so subspace 6 in this layer receives information from certain subspaces in earlier layer that resemble subspace 2 of this layer. So the information transfer is not done all at once. To verify this hypothesis, more rigorous experiments should be done. We encourage readers to check more examples. Due to its large size and various limits we did not manage to deploy the database for Qwen2.5-1.5B on our web application. But we released all trained orthogonal matrices together with the code. Readers can follow the instructions in our repository and easily reproduce the database.

F COMPARISON TO SPARSE AUTOENCODERS (SAES)

Due to the popularity of SAEs, in this section, we explain the difference and connections between them and our method. Readers who are familiar with SAEs might find this section particularly helpful.

F.1 FAQ

(1) *Why not compare with SAEs?*

Quantitative evaluation In previous quantitative evaluations, we patch each subspace and see its average effect on the output. SAEs do not provide such subspaces directly. If we have to make a comparison, we can change the evaluation method to apply an analogous evaluation to SAEs. One way is to patch the basis elements that SAEs provide, the features. This means that we replace a feature's activation value with its value on the corrupted input. For example, in the clean input on the token after "John", a feature representing *"previous token is John"* is highly activated – while, in the same position in the corrupted input, a feature representing *"previous token is Mary"* is highly activated. If we patch the "prev-Mary" feature, the new activation would say *"previous token is both John and Mary"*. If we patch the "prev-John" feature, the new activation has no information about previous token. In other words, we need to add a feature while removing another one (and it's hard to select which one since there are multiple active features), which requires understanding of feature dependency that SAEs do not provide ("prev-Mary" and "prev-John" are mutually exclusive). More importantly, patching the "prev-John" feature would not have any real effect on inputs where the names are not John. In other words, conceptually, one would expect such patching to only have effect on a few specific inputs, and only to confuse the model. In contrast, patching subspace can be thought of patching meaningful feature *groups*. Moreover, applying such patching to SAEs requires running evaluation on each of the features, which is too computationally expensive due to the large amount of features.

Because of these fundamental difference, we do not compare with SAEs in the main paper. Nevertheless, readers might still wonder how would SAEs perform under the same evaluation used in the paper. For this, a better way is to derive subspaces from SAE features. We take this up in Section F.2.

Qualitative evaluation Our qualitative evaluation has two aspects: (i) interpretability of preimages for subspaces, (ii) consistency of the type of information encoded in a subspace across inputs (thus, interpretability of the overall subspace). Regarding (i), we think that a single SAE feature would have interpretability comparable to a single subspace preimage, as we know that they are interpretable most of the time but also some features do not have clear and easy interpretation. However, regarding (ii), this is not applicable to SAEs, as they provide no clear structure between features; rather, to find encodings of the same type of information requires inspecting each feature individually. In contrast, information in the same subspace found by NDM is of the same "type" across inputs most of the time. Inspecting some of the them can give an idea of the whole feature group, significantly reducing the amount of interpretation work needed.

(2) *What about training SAEs within subspaces?*

Conceptually, if one trained a top-1 SAE (top-k SAE with k=1) within each subspace, we expect that the features would be the cluster centers in the subspace. Inspecting a feature means to find inputs whose activation in the subspace is close to the feature. This is roughly the same as inspecting preimages in InversionView, with query activations taking the role of the "feature". Thus, InversionView can conceptually be thought of as a "parameter-free" top-1 SAE.

F.2 Quantitative Experiments on GPT2 Test Suite

In this section, we check whether we can obtain some meaningful subspaces from SAE features and evaluate them with our metrics.

Settings We use the method introduced in Engels et al. (2024) (Sec. 4), where the authors cluster feature vectors and find subspaces. Specifically, the method has three steps:

1. Cluster features by their pairwise cosine similarity. There are two clustering method, (a) `Graph`. It connects each feature with its top-k neighbors whose similarity is above a threshold, and form clusters by recursively searching for connected features. (b) `Spectral`. Spectral clustering.
2. For each cluster, run the SAE on model activations. When reconstructing activations, they only use features inside the cluster (i.e., activation value for other features are always zero), we refer them as cluster-specific reconstructions. They remove zero reconstructions from this collection, so that at least one feature in the cluster is activated.
3. Find the multi-dimensional subspaces spanned by these cluster-specific reconstructions. They apply PCA on these reconstructions and inspect the points in the subspaces spanned by pairs of principle components with large eigenvalues.

In our case, we aim to *extract subspaces* from clusters of features. Thus we slightly change their method for our purpose:

1. Cluster features. Same as above.
2. Sort clusters either by the average cosine similarity between features inside the cluster, or by the cluster size (number of features) in descending order.
   For each cluster (in this order), apply the next three steps. Overall, we iteratively build a matrix $C \in \mathbb{R}^{d\times m}$ of orthonormal where m is the number of dimensions selected so far. The columns of C are orthonormal columns, representing a basis for the subspaces constructed so far. for each cluster, we add another set of columns representing the subspace for that cluster.
   (a) Obtain cluster-specific reconstructions, using the same method as Step 2 above in the original method. Denote the reconstructions as $X \in \mathbb{R}^{d\times n}$, where n is the number of data points and d is model dimension.
   (b) Remove variance on previous selected directions (skip if no direction has been selected so far). Denote the directions selected so far as $C \in \mathbb{R}^{d\times m}$, where m is the number of selected directions. We then take
   $$\hat{X} \leftarrow X - CC^T X \tag{13}$$
   which removes variance on the directions selected so far, or – equivalently – projects on the orthogonal complement of the subspaces constructed so far.
   (c) Apply SVD on $\hat{X}$. We select all left singular vectors (i.e., the same same as the eigenvectors in PCA) whose corresponding singular values are above a threshold. The threshold is set by multiplying the maximum singular value with a hyperparameter `rtol`. The selected singular vectors, or directions, form a **new subspace** corresponding to this feature cluster. They are added as the new columns of C.

Cluster config	Extract config	# subspaces	test 1			test 2			test 3			test 4			test 5			**Avg**
			-	d_s	Var_s	-	d_s	Var_s	-	d_s	Var_s	-	d_s	Var_s	-	d_s	Var_s	
Spectral, num=10	avg-sim, rtol=0.1	7,8,9,7	0.60	0.44	0.60	0.61	0.41	0.67	0.73	0.39	0.54	0.74	0.31	0.54	0.71	0.56	0.61	**0.56**
Spectral, num=10	size, rtol=0.1	5,7,8,8	0.70	0.61	0.35	0.40	0.32	0.56	0.70	0.30	0.49	0.64	0.22	0.44	0.68	0.50	0.46	0.49
Spectral, num=25	avg-sim, rtol=0.03	6,7,7,7	0.78	0.72	0.72	0.42	0.16	0.36	0.48	0.24	0.33	0.35	0.20	0.30	0.48	0.33	0.41	0.42
Spectral, num=25	avg-sim, rtol=0.1	10,12,12,13	0.52	0.60	0.53	0.50	0.26	0.48	0.60	0.43	0.54	0.60	0.30	0.51	0.59	0.36	0.48	0.49
Spectral, num=25	size, rtol=0.1	9,9,8,7	0.81	0.67	0.36	0.53	0.48	0.52	0.55	0.38	0.33	0.49	0.44	0.42	0.59	0.51	0.42	0.50
Spectral, num=50	avg-sim, rtol=0.01	5,6,6,6	0.65	0.67	0.71	0.37	0.15	0.42	0.13	0.11	0.35	0.18	0.14	0.35	0.27	0.15	0.32	0.33
Spectral, num=50	avg-sim, rtol=0.03	7,8,9,8	0.77	0.69	0.73	0.45	0.21	0.41	0.43	0.19	0.36	0.39	0.18	0.34	0.43	0.25	0.46	0.42
Spectral, num=50	avg-sim, rtol=0.1	15,18,21,19	0.85	0.80	0.53	0.55	0.31	0.44	0.52	0.29	0.36	0.46	0.27	0.42	0.49	0.26	0.49	0.47
Spectral, num=50	size, rtol=0.1	7,8,8,7	0.63	0.62	0.68	0.45	0.29	0.35	0.52	0.43	0.49	0.46	0.35	0.38	0.64	0.48	0.50	0.48
Spectral, num=100	avg-sim, rtol=0.01	9,8,8,9	0.70	0.56	0.72	0.28	0.17	0.36	0.21	0.09	0.27	0.19	0.11	0.26	0.31	0.14	0.30	0.31
Spectral, num=100	avg-sim, rtol=0.03	13,12,11,12	0.84	0.70	0.81	0.45	0.21	0.47	0.34	0.16	0.32	0.33	0.18	0.33	0.34	0.18	0.36	0.40
Spectral, num=100	avg-sim, rtol=0.1	24,26,26,25	0.86	0.74	0.54	0.51	0.33	0.47	0.48	0.32	0.43	0.41	0.24	0.42	0.38	0.21	0.41	0.45
Spectral, num=100	size, rtol=0.1	9,12,12,11	0.76	0.74	0.66	0.54	0.49	0.57	0.63	0.59	0.60	0.51	0.33	0.29	0.69	0.59	0.40	**0.56**

Table 8: Results on GPT-2 Small test suite, higher is better. Refer to Table 1 for explanation of the metrics. We include hyperparameters and the number of subspaces produced for each layer used in the tests.

3. We stop once C becomes a full basis, i.e., $C \in \mathbb{R}^{d \times d}$, or the clusters are exhausted. In the latter case, we supplement C with remaining directions to make it an orthogonal matrix.

In sum, we follow the original method from Engels et al. (2024) as much as we can, while adapting it to construct a full orthogonal decomposition of the space. We test this method on the GPT-2 test suite, with many different hyperparameter configurations. Each configuration is a combination of the following hyperparameters: In step 1, use `Graph` or `Spectral`. For the former, there are two hyperparameters: the `k` used in defining top-k neighbors and the threshold `cutoff`. For the latter, `num` specifies how many cluster there should be. In step 2, sort the feature in two ways, `avg-sim` or `size`. In Step 5, `rtol` that filters out unimportant directions. We search `k` among [2, 3, 4, 5, 6, 8, 16, 32], search `cutoff` among [0.1, 0.11, 0.13, 0.14, 0.16, 0.18, 0.21, 0.23, 0.26, 0.3, 0.34, 0.38, 0.43, 0.48, 0.5, 0.55, 0.62, 0.7, 0.78, 0.89, 1.0], search `num` among [10, 25, 50, 100], search `rtol` among [0.01, 0.03, 0.1]. For `graph`, the resulting number of clusters varies a lot. We remove those configurations whose number of clusters in any layer is out of the range [5, 200]. This results in 16 configurations for `graph`. When extracting subspaces, we ignore clusters which contain ≤ 3 features (as the target information we are testing is not likely to be encoded in 3D or smaller subspaces), and further restrict the number of subspace to be inside [5, 50] in order to speed up the evaluation. Unexpectedly, none of the configuration using `graph` produced a partition satisfying the constraint. We find that this is mainly because it produces very uneven-sized clusters. There are usually a few big clusters, and many small clusters each of which has a few features. Some configurations that use `spectral` are end up being filtered out.

Results The results are shown in Table 8. We can see there are two best-performing configurations whose average Gini coefficient is 0.56; we put the first row in the main paper, Table 1. It shows that extracting subspaces from SAE feature clusters is significantly better than other baseline methods (0.21-0.38 in Table 1), probably producing somewhat meaningful partition. But there is still a significant gap between it and NDM's result (0.71). In addition, we can see that many configurations are somewhat successful in test 1, e.g., the third to last row (Spectral, num=100, avg-sim, rtol=0.03), but not very successful in other tests.

G Additional Discussion

G.1 Why is InversionView More Suitable in Subspaces

Compared to whole representation space, we argue that InversionView (Huang et al., 2024b) is more suitable to be applied to subspaces. For example, subspace 2 and subspace 7 in Fig. 2 encode current token and current position respectively. If we look for the preimage in the joint space of subspace 2 and 7, the inputs will need to have the same token at the same position to be inside the preimage. Thus when the query activation contains multiple pieces of information, or encode multiple aspects of the input, the samples in preimage should be the same in all these aspects, which makes it hard to find such samples. Even if we can find enough, they might simply have the same recent tokens, which does not give much insights.

Importantly, some subspaces might be dominating the joint space while some others are ignored. If the norm of the activations in subspace A is much bigger than those in subspace B, the cosine

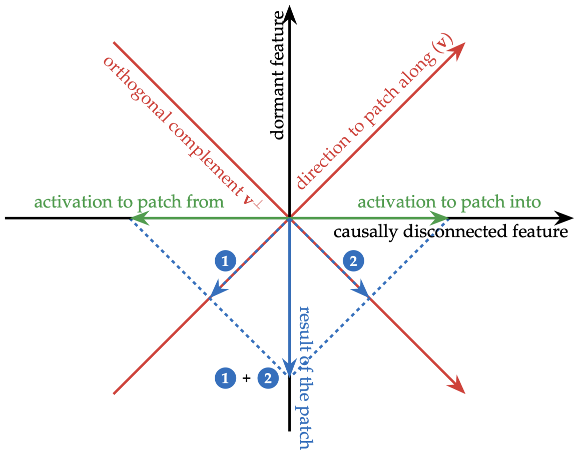
dormant feature
orthogonal complement $v_\perp$
direction to patch along $\langle v \rangle$
activation to patch from
activation to patch into
causally disconnected feature
1
2
1 + 2
result of the patch

Figure 32: An example illustrating subspace activation patching illusion. Fig. 1 from (Makelov et al., 2023). The 2D space is partitioned into two 1D space (red arrrows). Green arrows represent activations in the whole space. Subspace patching modify their projection along the red $\boldsymbol{v}$ direction, resulting a new activation (blue arrow). In this setting, suppose x-axis has variance but no downstream causal effect, while y-axis has no variance when running model on normal data but has causal effect if there is any nonzero value. In this setting, resulting new activation (blue arrow) is out-of-distribution and will have causal effect, suggesting $\boldsymbol{v}$ is a meaningful direction. However, this 2D space does not play a meaningful role in model's computation (suppose this 2D space is a subspace of a bigger space). In our case this does not raise a severe concern. When applying NDM in this 2D space, partitioning like red arrows in this figure is not likely to happen, because the resulting two 1D subspaces have very high MI. Partitioning like the x and y-axis is the optimal choice, thus resulting two unimportant 1D space.

similarity in the joint space of A and B will mainly depend on the cosine similarity in subspace A. In this case, the information read out in preimage of the joint space is only the information encoded in subspace A. In some cases this is fine, as the information in subspace A is much more prominent than the one in subspace B, and InversionView gives the right overall picture. But in some cases, e.g., in the residual stream of transformers, small subspaces might dominate certain attention heads, as attention heads usually operate in small subspaces (we do not think this only applies to attention heads).

G.2 On the Reliability of Subspace Activation Patching

Our quantitative experiments on language models relies on subspace activation patching. (Makelov et al., 2023) found cases where subspace activation patching produces illusory conclusion. Subspace intervention might change the model's output by activating a dormant pathway which does not have effect in normal computation, as illustrated in Fig. 32. Here we argue that our experiments are still reliable because of following reasons: (1) Our method finds subspace partition that reduces MI or dependency between subspaces, instead of partition that maximize patching effect. The partition shown in Fig. 32 that causes illusion has very high MI between subspaces, thus our method would not give such partition. In other words, we apply subspace patching on subspaces found by NDM, because of relatively good independency, so activations from different subspaces can be composed more or less freely, without causing out-of-distribution activations. (2) (Makelov et al., 2023) recommend doing subspace patching in activation bottlenecks, especially residual stream, to avoid such illusion. This is exactly what we did in experiments (3) We also provide validation by examining the subspaces qualitatively.

G.3 About Future Directions

So far we have provided various evidence supporting our claim that we can decompose representation space into smaller and meaningful subspaces, without any human supervision. These subspaces, being orthogonal to each other, can serve as new basic units or mediators for mechanistic interpretability. Compared to neurons, they capture the distributed nature of neural representations. Compared to sparse features, they provide more structure. Each subspace can be thought of as a group of infinitely many features sharing a certain higher-level concept, by interpreting some of them we can understand the whole group. Moreover, it enables us to understand the model by directly analyzing the model's weight matrices. For example, we can understand an attention head by checking which subspace its query, key, and value matrices read from and which subspace it writes to (Elhage et al., 2021). By doing so, we build connections between subspaces across layers, resulting in subspace circuits. We believe subspaces could be more "fundamental" than model components as they are designed to be as independent as possible. Moreover, subspace circuits would, like real transformers, operate in the same manner over the whole input sequence (uniform across token positions) as well as over different input sequences. Such circuits could be predecessors of source-code-like explanation of the model, since variables in RASP language (Weiss et al., 2021) can fundamentally be treated as subspaces of residual stream. To support this ambitious plan, the current version of subspace partition method might not be good enough. We believe there is plenty of room for further improvement. For example, allowing more flexible searching over dimension configurations (rather than having all dimensions as multiples of a fixed number). We also think a hierarchical structure of subspaces could also be helpful. For example, subspace A and B are very independent (e.g., current token and position), and A can be further partitioned into A1 and A2, which are less independent (e.g., the plain token and retrieved knowledge about it). More importantly, there could be potentially different ways achieving the same goal (e.g., by minimax approaches, see App. G.4). We also call for efforts from industry as this unsupervised method should benefit from more data and compute.

G.4 Possible Alternative Approaches

In this section, we describe some alternative approaches in order to inspire future research.

Split-based approach The high-level idea is as follows:

1. partition the space into two subspaces. We search over n possible configurations (for example, when d=100, we can have [$d_1 = 25, d_2 = 75$], [$d_1 = 50, d_2 = 50$], [$d_1 = 75, d_2 = 25$]), each configuration has a dedicated orthogonal matrix. It turns out that initialization matters a lot and standard basis is kind of special (Fig. 14), though they are symmetric, empirically we found [$d_1 = 25, d_2 = 75$] and [$d_1 = 75, d_2 = 25$] produces quite different results. After certain amount of steps, measure (normalized) MI for each configuration, select the one with the lowest MI.
2. Repeat step 1 for each subspaces already obtained, while restricting the rotation inside the already obtained subspace. For example, assume we have learned a matrix $\mathbf{R}^{\text{prev}}$ and configuration [$d_1^{\text{prev}} = 75, d_2^{\text{prev}} = 25$], we keep (previous) subspace 1 and 2 fixed. For subspace 1, we search over configurations [$d_1 = 18, d_2 = 57$], [$d_1 = 36, d_2 = 39$], [$d_1 = 54, d_2 = 21$], each associated with a separate $\mathbf{R}_1, \mathbf{R}_2, \mathbf{R}_3 \in \mathbb{R}^{75\times75}$. Similarly do this for subspace 2. Assume in this iteration, after training [$d_1 = 36, d_2 = 39$] has lowest MI for subspace 1, we then merge its orthogonal matrix $\mathbf{R}_2$ into $\mathbf{R}^{\text{prev}}$ by multiplying it with corresponding rows in $\mathbf{R}^{\text{prev}}$: $\mathbf{R}^{\text{prev}}_{[0:75]} \leftarrow \mathbf{R}_2\mathbf{R}^{\text{prev}}_{[0:75]}$. On the other hand, suppose none of the configuration for subspace 2 is lower than threshold, then we do not update that subspace. After this iteration, we have a new $\mathbf{R}^{\text{prev}}$, and new configuration [$d_1^{\text{prev}} = 36, d_2^{\text{prev}} = 39, d_3^{\text{prev}} = 25$]. Then keep repeating this loop until no subspace is separable (all configurations of all subspaces have MI greater than the threshold), or a pre-defined maximum iteration is reached.

This process increases the number of subspaces exponentially, if all subspace partition attempts are successful (MI below threshold). However, a disadvantage compared to merging-based approach in the main paper is increased compute cost, because we search over n configurations, training n $\mathbf{R}$s and select only one. An advantage is that it gives a tree structure, we can understand subspaces of different granularity. Our code link also contains code for this variant.

We did some preliminary experiments to test this approach, the results are not better than merging-based approach, while it takes longer to train. For example, Table 9 shows a partition learned for

index s	0	1	2	3	4	5	6	7	8	9	10	11
d_s	36	54	54	36	12	144	108	36	18	54	54	162
Var_s ($\times 10^3$)	0.4	1.0	0.5	0.4	0.8	2.7	8.3	0.6	0.4	0.6	0.6	5.8
ΔP_s ($\times 10^{-2}$)	0.3	1.3	1.1	0.3	0.3	2.8	2.3	0.6	0.4	1.9	0.6	40.7
$\frac{\Delta P_s}{d_s}$ ($\times 10^{-4}$)	0.9	2.5	2.0	0.8	2.1	1.9	2.2	1.6	2.3	3.5	1.1	25.1
$\frac{\Delta P_s}{\text{Var}_s}$ ($\times 10^{-5}$)	0.9	1.3	2.2	0.7	0.3	1.1	0.3	0.9	1.1	3.2	1.0	7.0

Table 9: Test 5 raw results for split-based NDM. Gini coefficient for row ΔP_s is 0.78, for row $\frac{\Delta P_s}{d_s}$ is 0.55, and for row $\frac{\Delta P_s}{\text{Var}_s}$ is 0.47.

layer 9 and tested on Test 5, it runs 4 outer iteration (each iteration splits subspaces), and each time 3 configuration are tested for each subspace. Search number is 5×2^{14}, totally 40k steps.

However, our negative results do no rule out its usefulness, it could be more computationally efficient if there's more flexible and efficient way to determine subspace dimensions, and might be suitable in some cases.

Minimax approach Mutual information can also be estimated by neural networks (Belghazi et al., 2018). The Mutual Information Neural Estimator (MINE) is as follows:

Let $\mathcal{F} = \{T_\theta\}_{\theta \in \Theta}$ be the set of functions parametrized by a neural network. MINE is defined as (we simplify the notation to avoid some details, please refer to (Belghazi et al., 2018) for the true definition):

$$I(X; Z) = \sup_{\theta \in \Theta} \mathbb{E}_{\mathbb{P}_{XZ}}[T_\theta] - \log \left(\mathbb{E}_{\mathbb{P}_X \otimes \mathbb{P}_Z}[e^{T_\theta}] \right). \tag{14}$$

Simply speaking, $\mathbb{P}_{XZ}$ means sampling vectors $\boldsymbol{x}$ and $\boldsymbol{z}$ from joint distribution, and $\mathbb{P}_X \otimes \mathbb{P}_Z$ means sampling them from their respective marginal distribution. The neural network T_θ takes both $\boldsymbol{x}$ and $\boldsymbol{z}$ as input and output a scalar, it is optimized with gradient ascent to approach the supremum.

Like split-based approach, we train an orthogonal matrix $\mathbb{R}$ to partition the space into two subspaces, given a fixed dimension configuration d_1, d_2. Assume X and Z represent random variables in the two subspaces. In order to find independent subspaces, we can optimize $\mathbf{R}$ to lower MI as follows:

$$\min_{\mathbf{R}} I(X; Z) = \min_{\mathbf{R}} \max_{\theta \in \Theta} \mathbb{E}_{\mathbb{P}_{XZ}}[T_\theta] - \log \left(\mathbb{E}_{\mathbb{P}_X \otimes \mathbb{P}_Z}[e^{T_\theta}] \right). \tag{15}$$

Empirically, $\mathbb{P}_{XZ}$ means that subspace activations are projected from the same activations, i.e., each pair $\boldsymbol{x}$ and $\boldsymbol{z}$ results from rotating and splitting a single activation vector into two parts. On the other hand, $\mathbb{P}_X \otimes \mathbb{P}_Z$ means each pair results from projecting two independently sampled activation vectors.

The intuition is that, if X and Z have high mutual information, knowing one can predict the other, the neural network can easily discriminate whether $\boldsymbol{x}$ and $\boldsymbol{z}$ are projected from the same activation, thus output high value when they "match" and low value when they do not, resulting high estimate of $I(X; Z)$. $\mathbf{R}$ rotates and reflects the space such that two subspace are as independent as possible, such that the neural network cannot easily discriminate, resulting low MI estimate. This is similar to Generative Adversarial Networks (Goodfellow et al., 2020).

However, empirically we do not find this approach is effective. We estimate MI with KSG estimator (so that comparable to our previous approaches) to evaluate performance during training, and found this does not produce significant decrease in MI.

In addition, based on the same intuition, we try another simpler approach: train two neural networks to reconstruct one subspace's activations based on the other's, and train $\mathbf{R}$ to make it hard to reconstruct.

$$\max_{\mathbf{R}} \min_{T_1, T_2} \mathbb{E}_{\mathbb{P}_{XZ}}[\text{MSE}(\boldsymbol{x}, T_1(\boldsymbol{z})) + \text{MSE}(T_2(\boldsymbol{x}), \boldsymbol{z})]. \tag{16}$$

where MSE denotes mean squared error, and T_1, T_2 are separate neural networks of different input-output dimension. We find this approach is more effective than the one based on MINE, but resulting final MI is still much higher than split-based NDM (and harder to train). Again, our negative results do not rule out its potential, the results might be because of the difficulties in optimization rather than training objective.

H COMPUTE USAGE

We run all experiments on H100s. We report the sources used when using 25×2^{14} as search number (largest option in our experiments). Train a subspace partition for one activation site in GPT-2 Small takes around 2 hours on a single H100 (stops at around 80k steps). Train a partition for one activation site in Qwen2.5-1.5B takes around 8 hours on a single H100 (stops at around 80k steps). For Gemma-2-2B, it takes around 8 hours on a single H100 (stops at around 50k steps). Experiments for subspace patching run quickly.

I LLMS USAGE

We used LLMs to polish the writing and rephrase some statements to improve the readability, while ensuring that the content continues to convey our intended meaning accurately. We also used them to identify related work and to generate code for producing figures.